The Influence of the Reaction Conditions on the

Synthesis of Vanadium Phosphate Catalyst for

Butane Oxidation to Maleic Anhydride

Thesis submitted in accordance with the requirements

of the Cardiff University for the degree of

Doctor of Philosophy

By

Umacaran Sithamparappillai

April 2008

UMI Number: U584268

UMI

Dissertation Publishing

UMI U584268

ProQuest

Acknowledgement

Table of contents

Abstract

Vanadium phosphate catalysts prepared by the reduction of $VOPO_4.2H_2O$ with 1-butanol are described and discussed. In particular, the effect of the addition of an alkane during the reflux stage of the preparation has been investigated. The materials were characterised using a combination of powder XRD, BET surface area measurement, laser Raman spectroscopy, scanning electron microscopy and transmission electron microscopy. The addition of $C_6 - C_{16}$ n-alkanes was studied and has been observed to significantly affect both the morphology and the structure of the vanadium phosphates. In the absence of an alkane $VOPO_4.2H_2O$ is reduced to $VOHPO_4.0.5H_2O$ with rosette morphology. Addition of low amounts of alkanes leads to a change in the crystallite morphology and platelet crystallites are preferentially formed. Decreasing the alcohol concentration further leads to the formation of $VO(H_2PO_4)_2$, with its characteristic block-shaped crystallites. The amount of alkane required to induce these changes decreased with increasing carbon number of the n-alkane. Furthermore, the different concentration of the alcohol results in a different reduction rate of V^{5+} to V^{4+} which changes the V: P ratio of the prepared materials. Therefore, different materials were obtained with respect to V: P ratio. Evaluation of the materials as catalysts for the oxidation of butane to maleic anhydride shows that the materials exhibit their characteristic activities and selectivities for this reaction.

A new synthesis route has been developed to prepare $(VO)_2P_2O_7$ directly from $VOPO_4.2H_2O$ using a reducing environment., Hydrogen (5% H_2/Argon 50 ml // min) was used for this transformation for 72 hours at temperature 550°C. The specific activity of these materials is higher than the conventional catalysts due to the low surface area.

Chapter 1

1.1 Introduction

Bergmann and Frish[1] disclosed in 1966 that selective oxidation of n-butane was catalysed by the VPO catalysts, and since 1974 n-butane has been increasingly used instead of benzene as the raw material for maleic anhydride production due to lower cost and high abundance in many places and low environmental effect (Scheme 1.1).
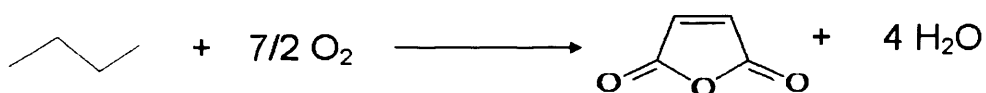
Scheme 1.1 The selective oxidation of n-butane to maleic anhydride

It is currently the only commercial catalytic oxidation process which uses an alkane as feedstock. The usage for maleic anhydride comes mainly from the manufacture of unsaturated polyester resins, agricultural chemicals, food additives, lubricating oil additives and pharmaceutical[2]. Production details and principal uses are presented in Table 1.1

Table 1.1 Annual production and principal uses of maleic anhydride [3]

Location	Production / ktonne yr^{-1}	Type of product	%
America	315	Unsaturated polyesters	63
Europe	100	Oil additives	12
Pacific	96	other	21
Total	500		

Different vanadium phosphate materials have been identified during the last four decades whose crystal structure and catalytic properties have been well published by many scientists. Some of the well known phases are the V^{5+} vanadyl orthophosphates (α-, β-, γ-, δ-, and ω-VOPO$_4$ and VOPO$_4$.2H$_2$O), and the V^{+4} vanadyl hydrogen phosphates [VOHPO$_4$.4H$_2$O, VOHPO$_4$.0.5H$_2$O, VO(H$_2$PO$_4$)$_2$)] ,vanadyl pyrophosphate (VO)$_2$P$_2$O$_7$ and vanadyl metaphosphate VO(PO$_3$)$_2$.

The main phase in the bulk of active and selective catalysts is (VO)$_2$P$_2$O$_7$, which is prepared by *in situ* activation of the precursor VOHPO$_4$.0.5H$_2$O. The catalyst is mostly used as an unsupported vanadium phosphorus oxide with a platelet type particle shape with small amount of V^{+5} phases such as α_I-VOPO$_4$ and α_{II}-VOPO$_4$,[4,5] which can be used in a variety of fixed and

mobile bed reactors. The reaction network involves the formation of butene, 1,3-butadiene and furan as intermediates. The active site for n- butane oxidation to maleic anhydride has been proposed as being the (200) plane of vanadyl pyrophosphate[6-8] and the yield of maleic anhydride improves when the active site of the (200) plane of $(VO)_2P_2O_7$ is maximized.[8]

For these reasons, the preparation of highly selective catalysts has been the focus of most VPO studies. Many properties of the final catalyst, such as crystalline behaviour and particle size, are established when precursor forms.[9] Hence, the preparation methods and reaction conditions during the preparation affect the morphology of $VOHPO_4.0.5H_2O$ and ultimately the catalyst performance.[10] Therefore, careful preparation of the precursor $VOHPO_4.0.5H_2O$ is the key to obtaining an effective catalyst.[11]

1.2 Proposed Active Sites and Mechanisms of n-Butane Oxidation

To date, many researchers have developed different models for n-butane oxidation on the VPO catalyst, which are based on the hypothetical sites present on the surface (200) plane[12]. Brønsted acid sites (-POH group), Lewis acid sites (V^{IV} and V^V), bridging oxygen (V-O-V, V-O-P or VO(P)V) and terminal oxygen (V^V=O, V^{IV}=O) are proposed active sites on the surface (200) plane.

Pepera et al.[13] reported that every two surface vanadium atoms are capable of activating one molecule of oxygen, while the bulk of the catalyst did not participate in n-butane oxidation.

n-Butane does not reversibly chemisorb onto the surface while maleic anhydride does. Although Pepera *et al.* did not report the mechanism of oxidation, but they proposed that V^{IV} on the surface of $(VO)_2P_2O_7$ may assist homolytic cleavage of the methylene C-H bond of *n*-butane. It is shown in Eq. 1.1

$$V^{IV} + 2RH \longrightarrow 2R^{\cdot} + V^{III} + 2H_2O \qquad\qquad Eq.\ 1.1$$
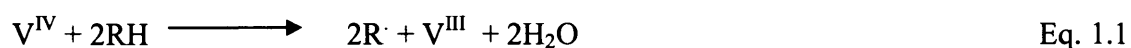
Centi *et al.* have calculated the rate constant for the theoretical dehydrogenation of light alkanes on a $(VO)_2P_2O_7$ catalyst with removal of two hydrogen atoms. They showed that the rate-determining step is the contemporaneous removal of two methylene hydrogen atoms from the carbon in the 2- and 3- positions in *n*-butane.

Centi *et al.*[6] also proposed that the Lewis acid site and the bridging oxygen abstract two hydrogen atoms from the two methylene groups of *n*-butane via a concerted mechanism shown in Scheme 1.2
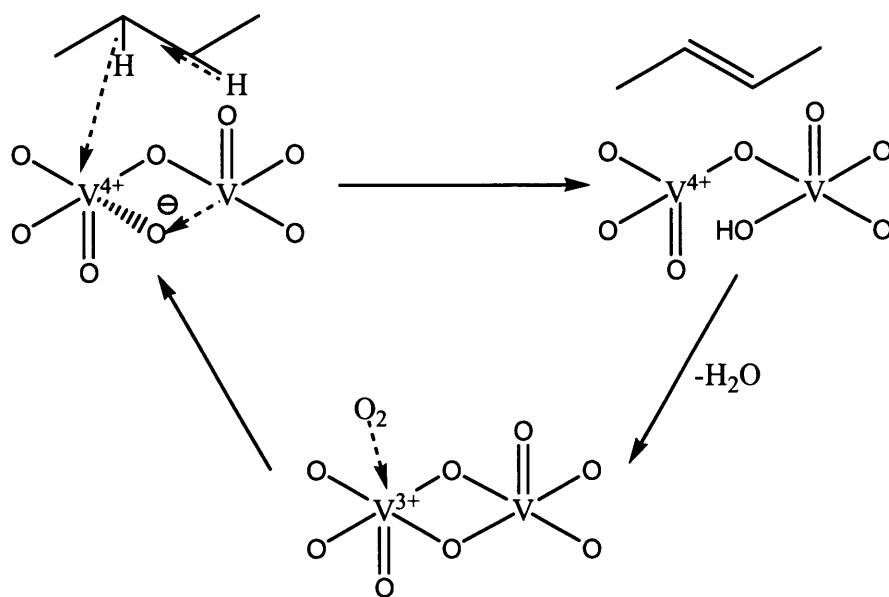
Scheme 1.2 Mechanism of *n*-butane activation on $(VO)_2P_2O_7$ proposed by Centi *et al.*[6]

Although Centi *et al.*[6] did not provide a complete mechanism of *n*-butane oxidation to maleic anhydride, they indicated that the Brønsted acid sites may be involved in the initial activation of *n*-butane. P-OH group involved for different functions such as to facilitate the removal of water formed during the partial oxidation, to stabilize the reaction intermediates, avoiding the desorption of these intermediates and to facilitate the desorption of maleic anhydride and preventing its over oxidation.

Bordes *et al.*[14] suggested that the active sites in *n*-butane oxidation to maleic anhydride are associated with coherent interfaces between slabs of the (100) planes of various $VOPO_4$ phases and the (200) planes of $(VO)_2P_2O_7$ along the (001) and (201) planes, respectively. However, the best $(VO)_2P_2O_7$ catalysts display the lack of other impurity $VOPO_4$ phases. Finally, Bordes explained the mechanism of *n*-butane to maleic anhydride based on the catalytic behavior of

non-equilibrated or over-oxidised VPO catalyst that contains different microcrystalline $VOPO_4$ phases.

Volta and co-workers,[15] on the contrary, believed that the active sites are not associated with interfaces between these crystalline phases. On the basis of comparison between XRD and radical electron distribution data they suggested that the active phase for selective oxidation of n-butane consists of a mixture of well- crystallized $(VO)_2P_2O_7$ and an amorphous $VOPO_4$ phase. This amorphous phase was identified as a precursor of β-$VOPO_4$, which formed at higher reaction temperatures. After four years, Volta et $al.$[15] suggested on the basis of kinetic data as well as XRD and ^{31}P MAS NMR results that domains of γ- $VOPO_4$ supported on a $(VO)_2P_2O_7$ mixture are necessary for selective n-butane oxidation. It is a better mechanism because it was based on the experimental data when compared with other theoretical mechanisms. Hutchings et $al.$[16] and Volta and co-workers.[17] suggested that the actives sites for n-butane oxidation to maleic anhydride comprise a V^{+4}/V^{+5} couple, well dispersed on the surface of a range of VPO phases.

Schiøtt and Jorgennson[18] applied the frontier orbital theory with Hückel calculation to explain the formation of 2,5-dihydrofuran from the butadiene intermediates and its vanadyl dimer present in the (200) plane of $(VO)_2P_2O_7$. Their calculations showed that $V^{4+} = O$ is involved in the (2 + 4) like cyclo addition of butadiene, which then rearranges to 2, 5- dihydrofuran. Molecular oxygen absorbed on the adjacent vanadium atom in the dimmer then activates the C-H bond in the 2-position of 2,5-dihydrofuran, leading to a hydrogen atom transfer to the peroxospecies to give a surface-bound hydroperoxide group. The O- H group in O- O – H then

transfers to the neighboring 2,5-dihydrofuran derivative yielding the 2- hydroxyl derivative. The asymmetric lactone (γ-butyrolactone) may be obtained by the hydrogen atom transfer to the adjacent radical oxovanadium site. The oxidation of the 5- position of γ-butyrolactone to maleic anhydride may take place in a similar fashion following the desorption of water and activation of another molecule of oxygen on the adjacent reduced vanadium site. There is no experimental evidence for this mechanism.

Guliants et al.[19] showed that the cis-dimeric site shown in Scheme 1.3, rather than the trans-oxovanadium (IV) dimer, may be involved in the C-H bond cleavage in n-butane and other C_4 molecules to maleic anhydride based on such dimeric peroxo site and V^{IV}-V^V redox couple. Some of the important observations made during oxidation of the probe molecules and proposed mechanism were explained based on the dimeric site. Further, the oxidation of a branched C_4 alkane, isobutane, was carried out to probe the mechanism of the C-H bond activation of alkanes on the VPO catalysts. Maleic anhydride was among the products of oxidation of this branched alkane. In the case of isobutane, the surface- bound peroxo radical would show discrimination in activating first the weaker tertiary C-H bond. The hydroxylation of the t-butyl radical would lead to t-butanol, it was an unselective path for maleic anhydride. On the other hand, he explained the selective path for maleic anhydride which involved the abstraction of the two hydrogen atoms in positions 1 and 3. Activation of the two methyl C-H bond may occur resulting in the formation of 1,3-diradical. Simple radical undergo skeletal rearrangement, leading to linear 1,2-diradical and butene. Finally formation of maleic anhydride during isobutane oxidation on the VPO catalyst suggests that such skeletal rearrangement does occur. On the other hand, it also indicates that the activation of n-butane on

the VPO catalysts may proceed via contemporaneous homolytic C-H bond cleavage and formation of a radical intermediate.

Reduced $V^{IV} - V^{IV}$ Site   Oxidised $V^{V} - V^{V}$ Site
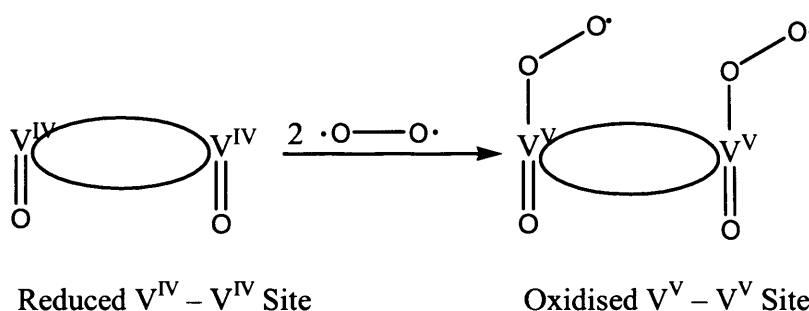
Scheme 1.3 Proposed cis-peroxo oxovanadium (V) dimeric active for n-butane oxidation to maleic anhydride on the surface (200) plane of $(VO)_2P_2O_7$ [19]

Shimizu et $al.$[20] investigated the mechanism of n-butane to maleic anhydride using density functional theory (DFT) method. They assumed that the monomeric complex is a fundamental structure and its two vanadium units were selected as two layer models of the catalyst. For these studies, the oxidation states of the inner vanadium atom and the influence of the presence or absence of lattice oxygen were analysed for this complex. The introduction of a phosphoric moiety on one of the hydroxy groups strongly stabilizes the lower oxidation states of the complexes. This result suggests that the surface vanadium species having the higher 5^+ oxidation state should possess stronger oxidation ability. The presence of the vanadium (4^+) atom at the lower layer relatively destabilizes the V^{3+} state of the upper vanadium complexes,

and stabilizes the peroxo-vanadium (4^+) complexes, which suggests that the lattice oxo-oxygen in vanadyl pyrophosphate may be involved in the activation of molecular oxygen. There is no experimental data used for analyzing this mechanism.

1.3 Influence of P: V ratio on catalyst performance

The commercial catalysts are prepared with a slight excess of phosphorus, typically with P: V close to 1.1:1.[8] Many studies reported that part of the phosphorus sublimes during normal operation and there are several reports that describe methods of replenishing the catalyst with phosphorus without significantly interfering with plant operation.[21] It is clear from a large number of studies that phosphorus in excess of the 1:1 stoichiometric ratio is important for the production of selective VPO catalysts prepared in aqueous media. Selectivity to maleic anhydride improves as the P:V ratio increases for catalysts prepared in aqueous media,[22] and this has been related to the role of excess phosphorous in these catalysts in stabilizing the 4^+ oxidation state of vanadium.

There is no clear evidence in the literature that catalysts prepared in organic media require a P:V ratio greatly in excess of the stoichiometric for optimum performance. Centi *et al.*[6] reported that yield-conversion plots for a number of VPO catalysts with different P:V ratios prepared in organic media. Clearly catalysts with P:V ratios less than 1:1 do not perform well, especially at high conversions, but neither is optimum performance achieved with catalysts with P:V ratios in excess of 1:1.

1.4 Preparation of vanadium phosphorus oxide (VPO) catalyst precursors

$VOHPO_4.0.5H_2O$ is the most important catalyst precursor for n-butane oxidation to maleic anhydride because thermal treatment of this $VOHPO_4.0.5H_2O$ precursor transforms it into vanadyl pyrophosphate catalyst which is highly active and selective for n-butane oxidation. Therefore, preparation of the catalyst precursor is a key factor in this research.

The structure of the precursor and catalyst were not discovered until 1980s, and then the precursor was called phase A, whereas the catalyst was referred as phase B.[23] Now, the structure of both is well documented. To date, many material scientists have reported different preparation methods for making catalyst precursors with or without mechanism of crystal growth. Commonly, three major preparation methods are used to make $VOHPO_4.0.5H_2O$ precursor and these are called VPA, VPO and VPD.[23,8]

Acid is used as the reducing agent in VPA method. In this method, V_2O_5 is refluxed with HCl, (Eq. 1.2) and then H_3PO_4 is added to this mixture (Eq. 1.3). Finally, the resulting solution is refluxed and filtered. This material has plate shaped morphology and its surface area was $3m^2/g$.[10] However, the obtained solid has more $VO(H_2PO_4)_2$ impurity as compared with other precursors obtained from VPO and VPD. Some vanadium phosphate phases and their unit cells are listed in Table 1.2.

$$V_2O_5 + 6HCl \rightarrow 2VOCl_2 + 3H_2O + Cl_2 \qquad \text{(Eq. 1.2)}$$

$$VOCl_2 + H_3PO_4 + 0.5H_2O \rightarrow VOHPO_4.0.5H_2O + 2HCl \qquad \text{(Eq. 1.3)}$$
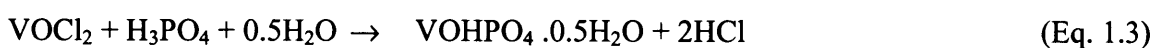
Table 1.2 Vanadium phosphate phases and their unit cells[14]

Phase	Unit cell	Cell parameters/nm
$VO(PO3)_2$	Tetragonal	a= 1.096, c= 0.425
$VOHPO_4.0.5H_2O$	Orthorhombic	a= 0.742, b= 0.960, c= 0.569
$(VO)_2P_2O_7$	Orthorhombic	a= 0.773, b= 1.658, c= 0.957
$VOPO_4.2H_2O$	Tetragonal	a= 0.620, c= 0.741
β- $VOPO_4$	Orthorhombic	a= 0.777, b= 0.614, c= 0.697
α_I- $VOPO_4$	Tetragonal	a= 0.620, c= 0.411
α_{II}- $VOPO_4$	Tetragonal	a= 0.601, c= 0.443
δ- $VOPO_4$	Orthorhombic	a= 0.642, b= 0.626, c= 0.909
γ- $VOPO_4$	Monoclinic	a= 0.964, b= 1.533, c= 1.662 and β= 93.04^0
$VO(H_2PO4)_2$	Tetragonal	a= 0.895, c= 0.797

The VPO and VPD preparation methods are carried out in organic solvent. In the VPO route, V_2O_5, phosphoric acid are refluxed (Eq.1.4), with an alcohol as solvent and reducing agent. The recovered solid has a platelet morphology and its surface area was between 10-18 m^2/g. $VOPO_4.2H_2O$ (Eq.1.5) is directly reduced by alcohols in VPD route (Eq.1.6). The morphology of these materials is varied depending on the alcohol used to reduce $VOPO_4.2H_2O$. Primary alcohols give a rosette structure while secondary alcohols give platelet morphology. Rosette structure materials exhibited higher surface area than other materials, which was 32 m^2/g.[24] XRD and SEM of platelet and rosette structure materials are shown in Figure 1.1 and 1.2 respectively.

VPO

$$V_2O_5 + R\text{-}CH_2\text{-}OH + 2H_3PO_4 \rightarrow 2VOHPO_4 \cdot 0.5H_2O + R\text{-}CH{=}O + 2H_2O \qquad \text{(Eq. 1.4)}$$

VPD

$$V_2O_5 + 2H_3PO_4 + 2H_2O \rightarrow 2VOPO_4.2H_2O \qquad \text{(Eq. 1.5)}$$

$$2VOPO_4.2H_2O + R\text{-}CH_2\text{-}OH \rightarrow 2VOHPO_4 \cdot 0.5H_2O + R\text{-}CH{=}O + 3H_2O \qquad \text{(Eq. 1.6)}$$
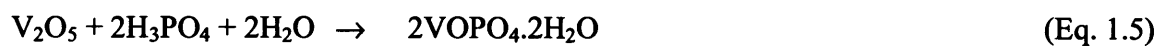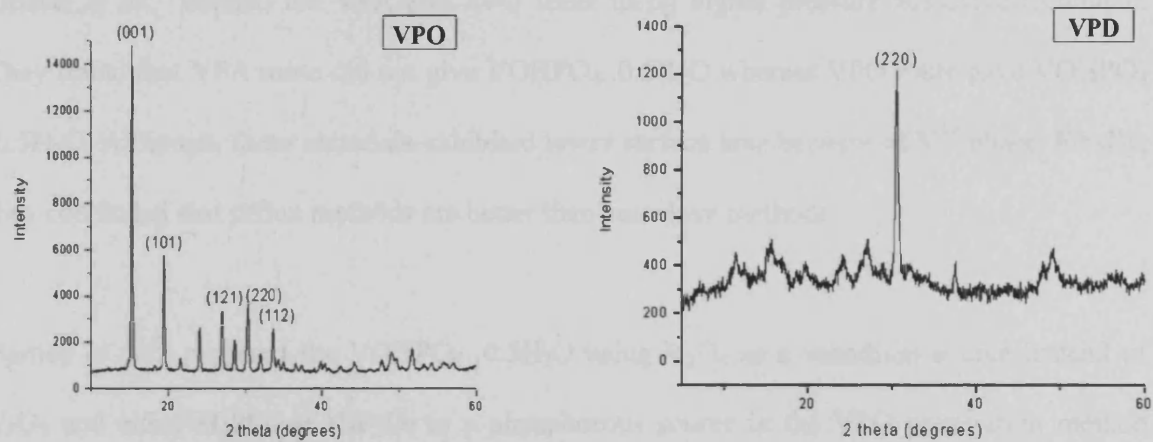
Fig. 1.1 X-ray diffraction patterns of standard VOHPO$_4$.0.5H$_2$O

Fig. 1.2 SEM of standard VOHPO$_4$.0.5H$_2$O

Griesel *et al.*[25] studied the VPA and VPO route using higher pressure autoclave technique. They found that VPA route did not give $VOHPO_4$ $.0.5H_2O$ whereas VPO route gave $VOHPO_4$ $.0.5H_2O$. Although, these materials exhibited lower surface area because of V^{5+} phase. Finally, they concluded that reflux methods are better than autoclave methods.

Bartley *et al.*[26] prepared the $VOHPO_4$ $.0.5H_2O$ using V_2O_4 as a vanadium source instead of V_2O_5 and either H_3PO_4 or $H_4P_2O_7$ as a phosphorous source in the VPO preparation method using autoclave method with or without water. However, that materials prepared using water as a solvent gave higher surface area than in the absence of water.

Connor *et al.*[27] investigated the organic route using mixture of *iso*-butanol and benzyl alcohol. Here, V_2O_5 is refluxed in the alcohol for an hour before H_3PO_4 is added, and the mixture refluxed for a further hour.

Griesel *et al.*[28] also reported that method of preparation of $VOPO_4.2H_2O$ and its morphology are very important factors in the preparation of $VOHPO_4$ $.0.5H_2O$ precursor. For these investigations, $VOPO_4.2H_2O$ was prepared using different techniques such as using different phosphoric acids and ageing time. Finally, these materials were converted to $VOHPO_4$ $.0.5H_2O$ precursor and they found that evaluation of these precursors for *n*-butane oxidation depends on the morphology of $VOPO_4.2H_2O$. The catalyst with rosette morphology were exhibited to have a considerably higher activity than the platelets because of higher surface area and all the $VOHPO_4$ $.0.5H_2O$ catalysts are reported to have similar specific activities.

Mahony *et al.*[29] investigated the crystallization of $VOHPO_4.0.5H_2O$ using VPO route. For this study, initially, V_2O_5 and alcohol were refluxed then phosphoric acid was added. They found that $VOPO_4.2H_2O$ was rapidly formed. After 15 minutes, d-spacing shifted from 7.5 to 6.7 Å, by this time, (001) phase of $VOHPO_4$.$0.5H_2O$ precursor forms at 5.7 Å with a maximum intensity at 60 minutes.

These observations lead to the first key point with respect to vanadium phosphate catalysts, namely that the surface area is the factor that controls the activity of catalysts prepared using $VOHPO_4$.$0.5H_2O$ as the precursor.

1.5 Preparation of other VPO phases for *n*-butane oxidation

It is very important to understand how other phases can be synthesised or enhance their formation in $VOHPO_4.0.5H_2O$ preparation.

$VOPO_4$ phases

α_I-$VOPO_4$, α_{II}-$VOPO_4$, γ-$VOPO_4$, δ-$VOPO_4$ and β-$VOPO_4$ can be prepared by calcination of $VOPO_4.2H_2O$ and $VOHPO_4.0.5H_2O$ in air[30]. It has shown in scheme 1.4

$VOHPO_4.0.5H_2O$ $\qquad$ $VOPO_42H_2O$ $\qquad$ $(NH_4)_2[(VO)_2C_2O_4(HPO_4)].5H_2O$

| 400 to 650°C | 400 to 600°C | 550°C |

$\delta\text{-VOPO}_4$ $\qquad\qquad$ $\alpha_I\text{-VOPO}_4$ $\qquad$ $\beta\text{-VOPO}_4$

| 740 to 780°C | 750°C | 600°C |

780°C

$\gamma\text{-VOPO}_4 \longleftarrow \alpha_{II}\text{-VOPO}_4$ $\qquad$ $(NH_4)_2(VO)_2PO_4$
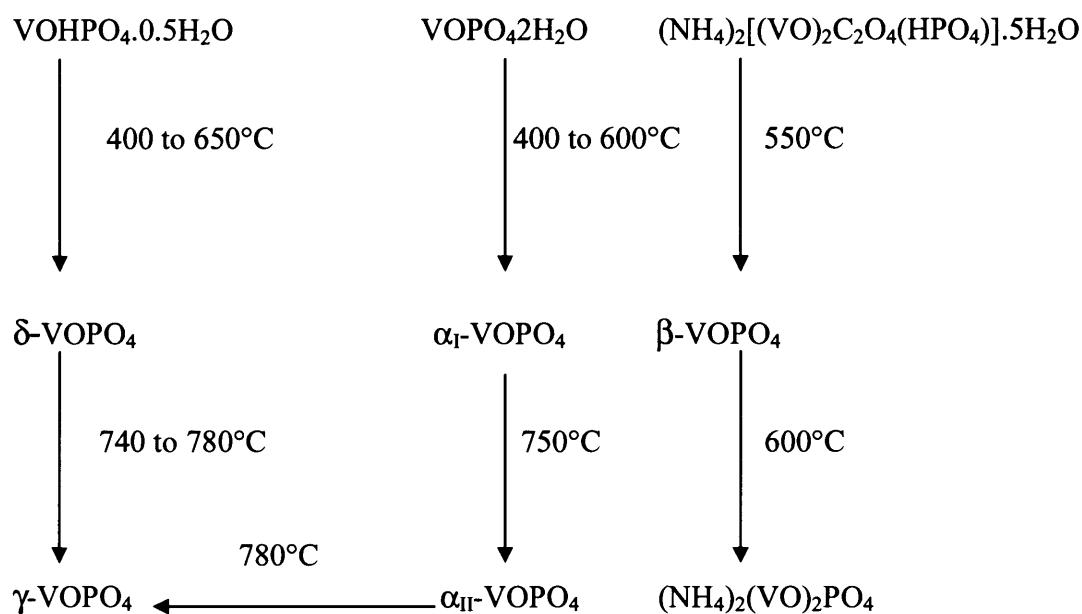
Scheme 1.4 preparation routes for $VOPO_4$ phases in static air environment[30]

Bordes et al.[14,31] reported that $VOPO_4$ phases can be prepared via dehydration of $VOPO_4.2H_2O$ in air, which is shown in Eq. 1.7

$$VOPO_4.2H_2O \xrightarrow{400°C} \alpha_I\text{-VOPO}_4 \xrightarrow{720°C} \alpha_{II}\text{-VOPO}_4 \xrightarrow{750°C} \beta\text{-VOPO}_4 \qquad Eq.1.7$$
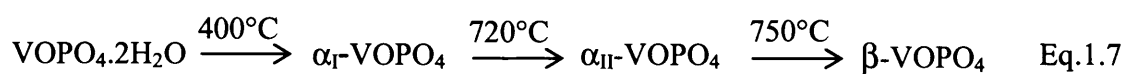
$VO(H_2PO_4)_2$

$VO(H_2PO_4)_2$ can be synthesized from reduction of $VOPO_4.2H_2O$ with 3-octanol.[22] Bartley et al.[32,33] also reported that $VO(H_2PO_4)_2$ can be synthesised by the reaction of V_2O_5, H_3PO_4 with aldehyde or ketone .

VOHPO₃.1.5H₂O

Guliants *et al.*[36] showed that $VOHPO_3.1.5H_2O$ can be synthesized by the reaction of V_2O_5, alcohol (isopropyl or isobutyl) and H_3PO_3 using reflux stage method. Hutchings and co-workers[34] prepared the vanadyl hydrogen phosphite, $VOHPO_3.1.5H_2O$ hydrate by the reaction of V_2O_5, H_3PO_4 and 1-proponal in the absence of water at 150°C using autoclave method. Whereas, $VOHPO_3.H_2O$ can be obtained in the presence of water.

Different vanadium phosphate phases can be synthesized using various experimental techniques. Some of these phases are active for butane oxidation.

1.6 Intercalation, exfoliation and reduction of VOPO₄·2H₂O with different solvents

Intercalation of organic molecules is widely used for modifying the chemical and physical properties of inorganic layered materials.[35] The intercalation compounds of layered vanadium phosphate dihydrates ($VOPO_4.2H_2O$) are of tremendous interest not only as fundamental examples of V-O-P nano-composites but also as intermediates for constructing novel V-P-O nanostructures of catalytic performance.[36] Due to the weak interlayer binding in $VOPO_4.2H_2O$, these materials can act as host to different guest molecules. Further, $VOPO_4.2H_2O$ can be intercalated by alcohols, aliphatic amines, acetone, pyridine, organometallic compounds, glycols and amides.[37,38]

Melánová *et al.*[39] reported that mixed intercalates can be prepared by reaction of polycrystalline vanadyl phosphate dihydrate with liquid mixtures of the primary alcohols in a microwave field. They found the same mixed layer- type complexes can be obtained as intermediary products of exchange reactions consisting of substitution of one alcohol bound in the solid intercalate by another alcohol introduced in the form of vapor.

Melánová *et al.*[40] also reported that aliphatic aldehydes can not be used for the preparation of intercalation compounds because the guests undergo aldol condensation and oxidation so these intercalates are unstable. Beneš *et al.*[41] investigated some intercalates of vanadyl phosphate with branched alcohols. They found that these alcohols were directly intercalated into vanadyl phosphate dihydrate and formed intercalates compounds. However, in neither of these studies did report any data for *n*-butane oxidation.

Yamamoto *et al.*[42] showed that $VOPO_4 \cdot 2H_2O$ can be intercalated using acrylamide then it was exfoliated by primary or secondary butanol and these compounds were reconstructed by removal of solvent. These materials consisted of aggregated small flakes which were morphologically very different from relatively large square platelets observed for both the starting $VOPO_4 \cdot 2H_2O$ and the initial intercalation compound.

Yamamoto *et al.*[43] reported that thin – layered sheets of $VOHPO_4 \cdot 0.5H_2O$ can be prepared from $VOPO_4 \cdot 2H_2O$ by intercalation, exfoliation and reduction in alcohol. Further, Kamiya *et al.*[44] reported that catalyst precursors ($VOHPO_4 \cdot 0.5H_2O$) can be prepared using exfoliation and reduction of $VOPO_4 \cdot 2H_2O$ in primary alcohol. $VOHPO_4 \cdot 0.5H_2O$ prepared with different

morphologies using exfoliation and reduction process is shown in Scheme1.5. Furthermore, the

obtained $(VO)_2P_2O_7$ through the exfoliation – reduction was well crystallized and consisted of

thin flaky crystallites. Finally, Okuhara and co-workers[44,45] found that $(VO)_2P_2O_7$ prepared

through the exfoliation – reduction was highly active and selective for oxidation of n-butane.
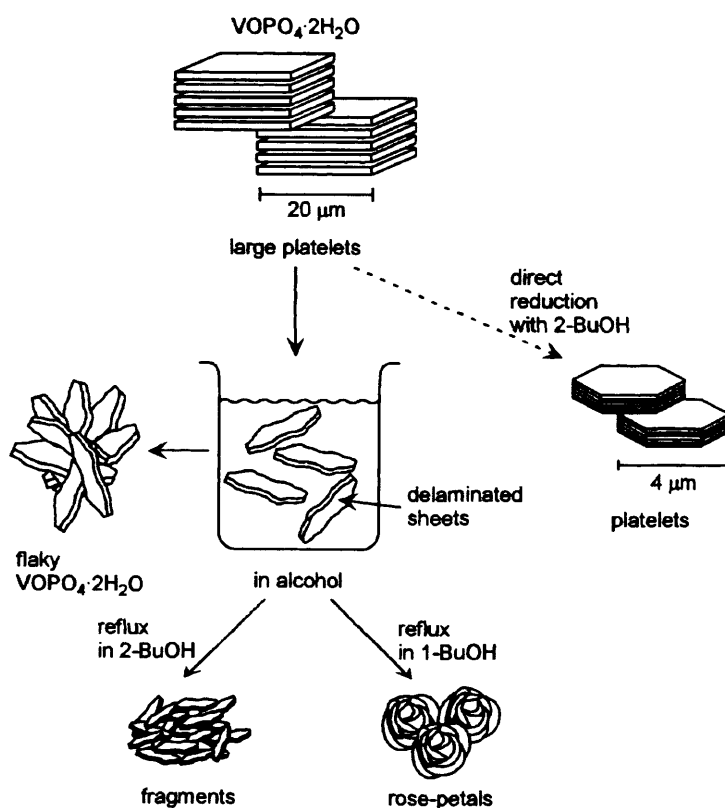
Scheme 1.5 $VOHPO_4 \cdot 0.5H_2O$ prepared using exfoliation and reduction process[43]

Beneš et al.[46] analysed the intercalation of $VOPO_4 \cdot 2H_2O$ with branched alcohols. They found

that with increasing length of the main chain the basal spacing of the intercalates of the C_3, C_4

and C_5 isoalcohols changes linearly, increasing by one carbon atom (1.51Å) at a time.

Trchová et al.[47] investigated the mechanism of intercalation for vanadium phosphate materials using infrared and Raman spectroscopy techniques. They proposed the mechanism based on these measurements that the vanadyl stretching band appears to be especially sensitive to atoms coordinated to the vanadium within an octahedral arrangement in the host lattice structure, during the intercalation its position at 1035 cm^{-1} in the anhydrous form changes to 995 cm^{-1}, typical for mono and dihydrates and they found that no formation of vanadyl phosphate monohydrate was observed during hydration of the anhydrous form under ambient conditions.

Beneš et al.[48] explained the possible mechanisms of intercalation reactions for vanadium phosphates materials on the basis of intercalation reactions of water and ethanol into anhydrous vanadyl phosphate and redox intercalation of alkali metal cations into vanadyl phosphate dihydrate. They found three possible mechanisms of intercalation for vanadium phosphate materials, which are based on (1) a concept of exfoliation of layers (2) the formation of stages and randomly stacked layers (3) co-existence of intercalated parts of crystals of the host separated by an advancing phase boundary. Further, it was reported that in the crystal of the cost, intercalated and non-intercalated parts of the crystal coexist. A two phase system is formed which is a transition area which has been designed as an advancing phase boundary.

The catalytic activity and selectivity of $(VO)_2P_2O_7$ are greatly dependent on the microstructure of the crystallites, control of the microstructure is critical for improvement of the catalytic performance. So, intercalation is the one of the key method for obtaining the different crystallites.

1.7 Effect of promoters on n- butane oxidation over VPO catalysts

The activity of vanadium phosphates is often enhanced by the addition of low concentrations of metal cations known as promoters. For this reason, many industries have been using promoted VPO catalysts for n-butane oxidation to maleic anhydride since last two decades.[49] Bi, Co, U, Fe, Nb, Zn, Ce, La, Cu, Ti, Mo, Ca, Si, and Zr have been tried as promoters for the preparation of $VOHPO_4.0.5H_2O$ precursors.[50]

Zazhigalov et al.[51] modified the redox properties of the VPO catalysts by incorporating metallic Co in the catalyst precursors, which improved the desorption of maleic anhydride and increased the selectivity to maleic anhydride.

Cornaglia et al.[52, 53] analysed the effect of Co cations on the activity and selectivity of n-butane oxidation to maleic anhydride over VPO catalysts prepared impregnation of $VOHPO_4.0.5H_2O$ with cobalt acetate and acetyl acetonate. They found that Co added at 1-6 weight % significantly improved the catalytic activity while slightly decreasing the maleic anhydride selectivity. The best catalyst can be obtained using Co acetyl acetonate for impregnation of the $VOHPO_4.0.5H_2O$ precursor. This catalyst exhibited an optimum concentration of very strong Lewis acid sites, very low concentration of isolated V(V) centers, and no V(V) phases.

Sajip et al.[54] investigated the effect of Co and Fe ions added during the $VOHPO_4.0.5H_2O$ precursor preparation using VPO route on n-butane oxidation to maleic anhydride. At low levels, both Co and Fe significantly enhanced the intrinsic activity and selectivity to maleic

anhydride. They suggested that Co was insoluble in the $(VO)_2P_2O_7$ phase, which transformed to a disordered V^{4+}-V^{5+} phosphate phase during the activation of $VOHPO_4.0.5H_2O$. Whereas, Fe may be soluble in the $(VO)_2P_2O_7$ structure and, therefore, function as an electronic promoter for this phase.

Shen et al.[55] investigated Ce-Fe promoted VPO catalysts for n-butane oxidation to maleic anhydride in the absence of gas-phase oxygen. They found that promoted catalysts exhibited higher conversion and selectivity to maleic anhydride than the conventional catalyst. Finally, they defined that the introduction of Ce-Fe complex oxides improved the redox performance of VPO catalysts by increasing the lattice oxygen activity.

Hutchings and co-workers[56] analysed the n-butane oxidation to maleic anhydride over vanadium phosphate catalysts using group 13 elements as promoters. For this investigation, two different types of $VOHPO_4.0.5H_2O$ were used, one is platelet morphology, and other one is rosette structure. They also showed that these promoters can be switched from platelet-like to rosette morphology. Although, all of these promoters functioned as modifiers of the VPO crystal morphology, the In and Ga-promoted materials exhibited improved catalyst performance in n-butane oxidation to maleic anhydride.

VPO catalysts promoted with a mixture of Mo, Zr and Zn ions were investigated by Xu et al.[57] The combination of these three cations created a synergistic effect that increased the performance of the promoted VPO catalysts. They found that these promoted VPO catalysts exhibited high selectivity and conversion for n-butane oxidation to maleic anhydride. However,

they did not report any comparison between promoted and un-promoted VPO catalysts for their investigations. Xu *et al.* suggested that these three cations were incorporated in the vacant surface sites as well as the bulk VPO structure.

Bismuth is the one of the important promoters for *n*-butane oxidation. These promoted VPO catalyst increased the selectivity to maleic anhydride in *n*-butane oxidation.[58,59] Recently, promoted VPO catalyst prepared using Pt and La-Bi as the promoters.[60,61] Pt was incorporated as H_2PtCl_6 into the layered $VOHPO_4.0.5H_2O$ precursor during its synthesis using VPO route. However, Pt-VPO catalysts did not apply for *n*-butane oxidation to maleic anhydride, but catalytic performance of these promoted catalysts was reported only for the hydrogenation of nitrobenzene and the oxidation of tetrahydrofuran.

1.8 Crystal structures of vanadium phosphate phases

$VOPO_4.2H_2O$

$VOPO_4.2H_2O$ consists of layered VO_6 octahedra of which the equatorial oxygen atoms are linked to PO_4 groups. Above and below the equatorial plane is a short V=O and long V-O bond respectively, forming chains of VO_6 octahedra. A specific layer consists of two sheets, an upper and lower floor. In $VOPO_4.2H_2O$ the V=O bonds in the same floor are cis orientated towards each other, and trans oriented towards the V=O bonds in the other floor within the same layer. Two water molecules are coordinated to vanadium in trans position to V=O and the remaining two are isolated in the channels formed by the hydrogen bonding network[1]. It is shown in Figure 1.3
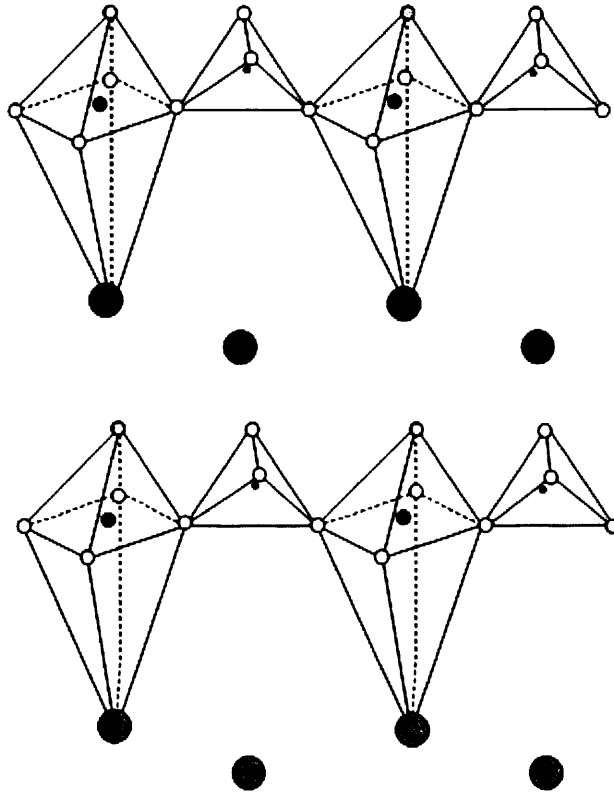
Fig 1.3 Schematic representation of layered VOPO$_4$.2H$_2$O structure[14]

Water molecules remove from the between the layers to form VOPO$_4$ phases. ● = H$_2$O

molecules, ○ = oxygen atoms

VOPO$_4$ phases

α_I-, α_{II}- and β-VOPO$_4$ are made up of PO$_4$ tetrahedra and distorted VO$_6$ octahedra. Both α_I-VOPO$_4$ and α_{II}-VOPO$_4$ have similar structure where oxygen atoms from every tetrahedron are shared with octahedral belonging to four different chains. These structures are shown in Figure 1.4 and 1.5.

(a)   (b)

☑ PO_4 tetrahedra

▣ VO_6 octahedran with V=O facing upwards

▣ VO_6 octahedran with V=O facing downwards

Fig 1.4 (a) A layer in the α_I-$VOPO_4$ structure. Dashed lines represent the short vanadyl bond

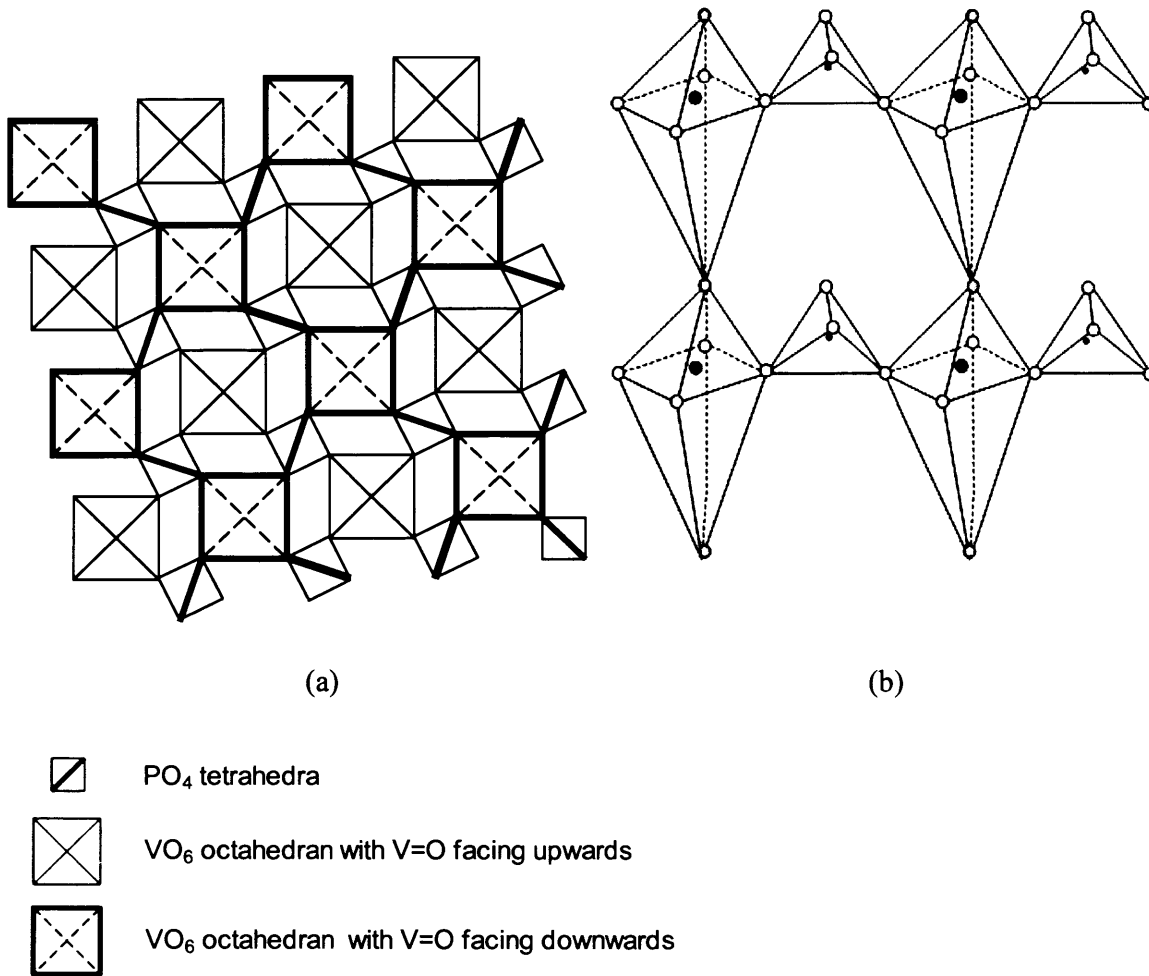facing downwards. Bold lines represent the upper layer [30] (b) Stacked octahedral in α_I-$VOPO_4$

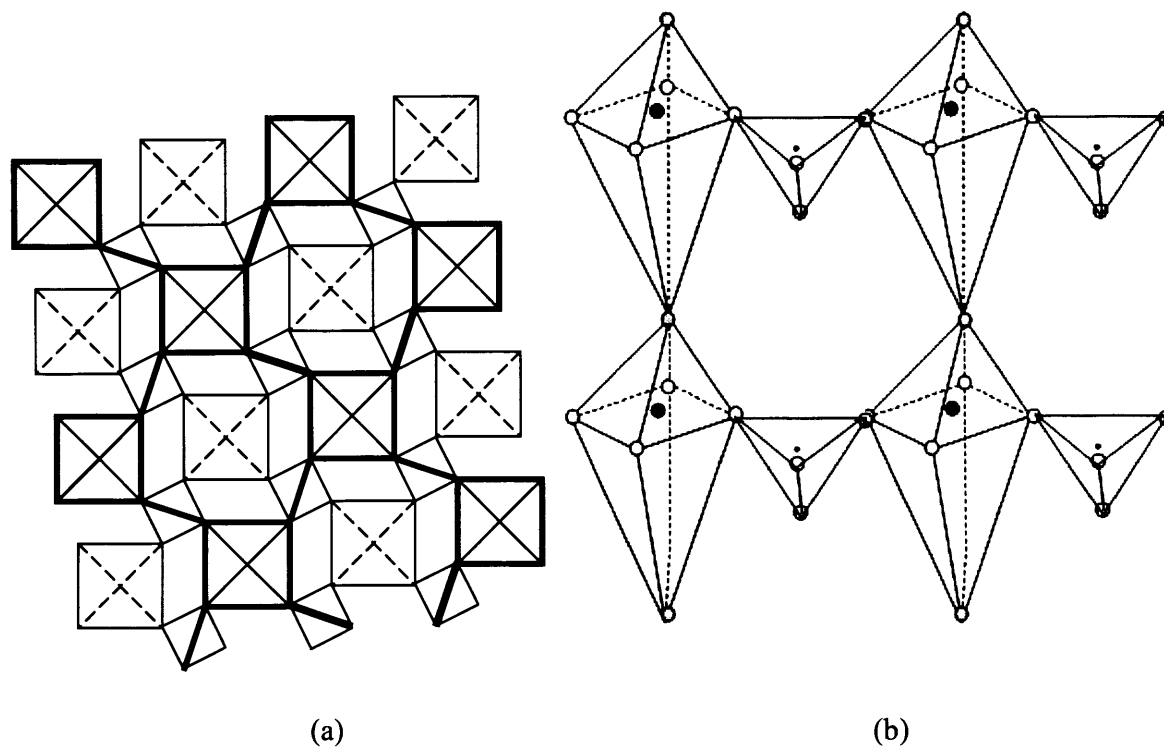linked with PO_4 tetrahedra. Open circles represent oxygen atoms.

(a)   (b)

Figure 1.5 (a) Schematic layer in α_{II}-VOPO$_4$ [30] (b) stacked VO$_6$ octahedra, with PO$_4$ tetrahedra orientated differently than in α_I-VOPO$_4$. Same legend as in Figure 1.4

The main difference between these two structures is the different positions of vanadium and phosphorus atoms relative to the equatorial plane of the octahedra. In α_I-VOPO$_4$, vanadium and phosphorous atoms are on the same side of the equatorial oxygen atom plane whereas in the α_{II}-VOPO$_4$ structure they are on opposite sides.

Benabdelouahab et al. proposed the structure of δ- VOPO$_4$ (Figure 1.6). The VO$_6$ octahedra are linked by the oxygens of PO$_4$ tetrahedra as in α_I- VOPO$_4$ and α_{II}- VOPO$_4$, but the V=O bonds of the linked octahedral sharing a floor are trans orientated towards each other.
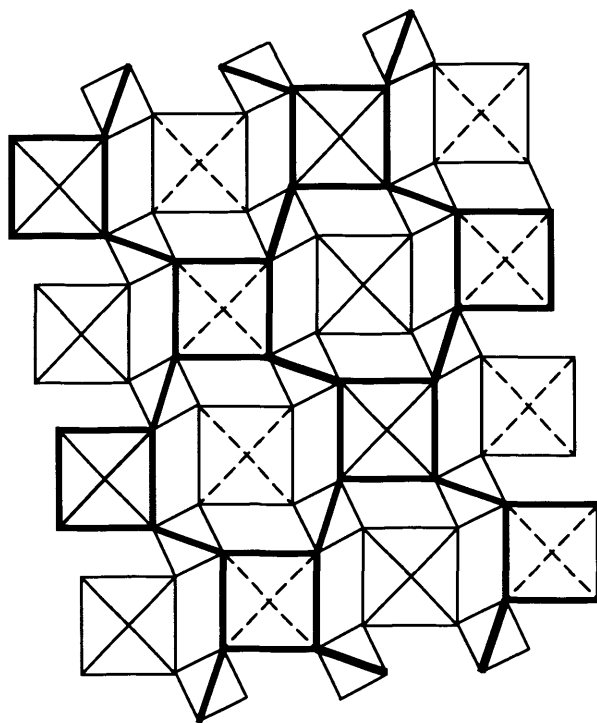
Fig 1.6 Proposed presentation of a layer in δ-VOPO$_4$.[30] Same legend as in Figure 1.4

The structure of γ-VOPO$_4$ is similar to that of δ-VOPO$_4$, but whereas the V=O bonds in of δ-VOPO$_4$ are trans oriented in the same floor, the V=O bonds in γ-VOPO$_4$ point in the same direction (Figure 1.7). The direction is the same for the upper and lower layers.
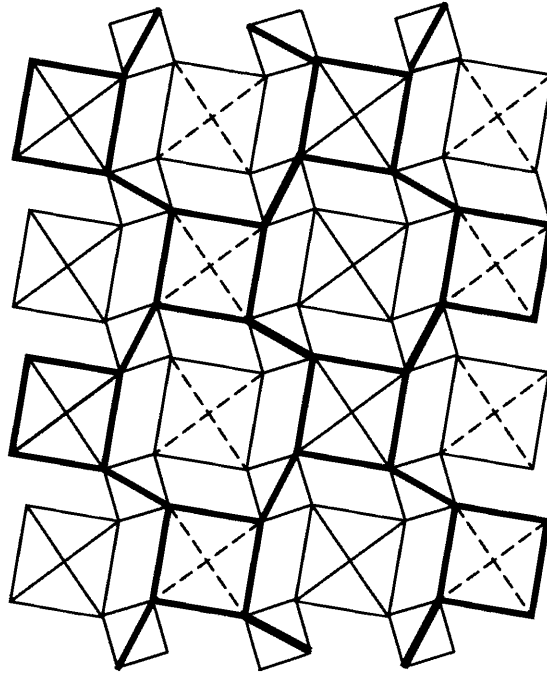
Fig 1.7 Proposed presentation of a layer in γ-VOPO$_4$.[30] Same legend as in Figure 1.4

1.9 Transformation of $VOHPO_4.0.5H_2O$ precursor to $(VO)_2P_2O_7$

$(VO)_2P_2O_7$ is obtained when vanadium phosphate hemihydrate,$VOHPO_4.0.5H_2O$ precursor is heated to about 400°C in 1.5% butane/air. The trapped solvent molecules are removed, when $VOHPO_4.0.5H_2O$ precursor is heated, which makes structural defects, microcracks and increase the surface area, here the precursor first transforms into an amorphous phase, then dehydrates to crystalline $(VO)_2P_2O_7$ and partially oxidized to V^{+5} orthophosphates when the reactant mixture is introduced.[62] The transformation of $VOHPO_4.0.5H_2O$ to $(VO)_2P_2O_7$ is topotactic.[23] Hence, morphology of the final catalyst depends on the morphology of the precursor.

Different crystalline final catalysts were obtained during the transformation of $VOHPO_4.0.5H_2O$ to $(VO)_2P_2O_7$ depending on the morphology of the precursor, the presence of defects in the structure, the activation temperature and time and the P/V ratio in the precursor. This transformation has been investigated widely.

Hutchings and co-workers[63] studied the transformation of the $VOHPO_4.0.5H_2O$ into $(VO)_2P_2O_7$ by *in situ* laser Raman spectroscopy and showed the morphology of the final catalyst remains unchanged. For these studies, three different $VOHPO_4.0.5H_2O$ precursors were converted to $(VO)_2P_2O_7$ under the same reaction conditions. The three final catalysts gave different Raman spectrum due to the P-O-P stretching. They also reported that the reactivity of all these catalysts with oxygen was different because the variation in reactivity could be related

to differences in the nature of the anion defects associated with the PO_4 units in these materials which would be reflected in the differences of the P-O-P stretching region of the spectrum.

Guliants et al.[64] also investigated the transformation of the $VOHPO_4.0.5H_2O$ into $(VO)_2P_2O_7$ by in situ laser Raman spectroscopy and X-ray diffraction techniques. They found that the $VOHPO_4.0.5H_2O$ is firstly transformed into disordered nanocrystalline $(VO)_2P_2O_7$ with V^{+5} phase , then it was converted to well-crystallised $(VO)_2P_2O_7$ in the equilibrated catalysts. Finally, they concluded that the (200) planes of $(VO)_2P_2O_7$ is a key factor for high activity and selectivity for n-butane oxidation.

Torardi et al.[65] studied the transformation of the $VOHPO_4.0.5H_2O$ into γ-$(VO)_2P_2O_7$ using electron microscopy and X-ray diffraction. For these investigations, single crystal and powder form of the vanadyl hydrogen phosphate precursors were converted to pseudomorphs. They found that size and shape of the catalyst are unchanged with respect to the starting materials.

Mahony et al.[66] reported the morphology changes of the $VOHPO_4.0.5H_2O$ to $(VO)_2P_2O_7$ during the two type of transformations. They showed that first way is heated with air and second one is heated with butane diluted with air. In the case of air, firstly, amorphous solid formed when precursor is heated at above 270°C whereas, crystalline V^{+5} formed when $VOHPO_4.0.5H_2O$ is heated at above 350°C. They also showed that second way is completely different results from the first one, where crystalline $(VO)_2P_2O_7$ was obtained without any intermediate amorphous phase.

Sajip *et al.*[67] analysed the structural transformation of a cobalt-doped vanadium phosphate hemihydrate to final catalyst using characterisation techniques. They prepared the cobalt-doped catalyst precursor via organic route and it has a rhomboidal plate-like morphology. They also applied the different activation times for the preparation of final catalyst. Finally, they found that the morphology of the activated materials is unchanged with respect to original precursor.

Koyano *et al.*[68] investigated the surface structure of vanadyl pyrophosphate $(VO)_2P_2O_7$ using different characterisation techniques. They found that the X_1 phase was obtained as a thin surface layer on $(VO)_2P_2O_7$ when crystalline $(VO)_2P_2O_7$ is reacted with oxygen molecule at 460°C. They also reported that $(VO)_2P_2O_7$ can be obtained when X_1 phase (δ-$VOPO_4$) is reacted with *n*-butane. Based on these observations, they defined that the reversible redox reactions between X_1 phase and $(VO)_2P_2O_7$ occur by the reactions with butane and oxygen.

Ryumon *et al.*[69] investigated the transformation of $VOHPO_4.0.5H_2O$ to $(VO)_2P_2O_7$ using water vapour. For these investigations, they used small and large crystallites with presence and absence of water vapour. They found that a single- phase of well crystallised $(VO)_2P_2O_7$ can be obtained within a short reaction time under a reactant gas (0.9% *n*-butane, 10% O_2) containing 40% water vapour using small crystallities. Whereas, the transformation took a longer period (100h) without water vapour. In the large crystallites, $(VO)_2P_2O_7$ was the main phase with water vapour, whereas α_{II}-$VOPO_4$ was obtained without water vapour. Therefore, water vapour can accelerate the transformation of $VOHPO_4.0.5H_2O$ to $(VO)_2P_2O_7$.

1.10 Conclusions

Selective oxidation of n-butane to maleic anhydride is a commercial process which depends for its operation on the structure of active sites located on the basal plane of $(VO)_2P_2O_7$. (200) plane of crystalline $(VO)_2P_2O_7$ is considered as the most active and selective for n-butane oxidation. Different crystalline vanadium phosphorous oxide phases were obtained during the transformation of the $VOHPO_4.0.5H_2O$ precursors to the final catalyst, $(VO)_2P_2O_7$ depending on

- the temperature, time and atmosphere of activation

- the morphology of the precursors

- P/V ratio in the precursors and

- the presence defects in the structure

Therefore, numbers of new preparation routes have been concentrated for obtaining the good materials. However, most of these methods have focused on the preparation of $VOHPO_4.0.5H_2O$ with differing morphologies and surface area.

1.11 Aim of this work

The catalytic performance of the VPO catalysts depends on (i) the method of $VOHPO_4.0.5H_2O$ preparation (ii) the procedures of activation and conditioning of the precursor at high temperature and (iii) the nature of metal promoters.

The preparation of $VOHPO_4.0.5H_2O$ depends on several factors such as types and concentration of reagents, reducing agents and solvents, the reduction temperature and synthesis duration. Here, types of alcohols (C_4 and $\geq C_8$) and various reduction temperatures were used for this investigation in VPD route.

Firstly, the addition of alkane in VPD method was studied. Different morphology materials were obtained when different amount of alkane solvent used and this led to a study into the different factors that influence the morphology of vanadium phosphate phase formed under different conditions.

The second aim of this project was to synthesis new materials as catalysts for butane oxidation. The first synthetic route studied was gas phase reduction of $VOPO_4.2H_2O$. Traditionally the reduction is carried out with either an aqueous reducing agent or an alcohol as the reducing agent. In this study we investigated using gas phase reductions at higher temperatures.

1.12 References

(1)   R. L. Bergmann and N. W. Frisch, US Patent 3293268, 1966, assigned to Princeton Chemical Research

(2)   Culbertson BM, *Catal. Today*, 1987, **1**, 609

(3)   Chemical week, 1997

(4)   G. Centi, *Catal. Today*, 1993, **16**, 1

(5)   V. V. Guliants, J. B. Benziger, S. Sundaresan, I. E. Wachs, J- M. Jehng, J. E. Roberts, *Catal. Today*, 1996, **28**, 275

(6)   G. Centi, F. TrifirÒ, J. R. Ebner, V. M. Franchetti, *Chem. Rev.* 1988, **88**, 55

(7)   J. R. Ebner, M. R. Thompson, *Catal. Today*, 1993, **16**, 51

(8)   H. S. Horowitz, C. M. Blackstone, A. W. Sleight, G. Teufer, Appl. Catal, 1998, **38**, 193

(9)   E. Bordes, *Catal. Today*, 1993, **16**, 27

(10)   C. J. Kiely, A Burrows, S. Sajip, G. J. Hutchings, M. T. Sananés, A. Tuel and J. C. Volta, *J. Catal*, 1996, **162**, 31

(11)   G. Centi, Catal. *Today*, 1993, **16**, 5

(12)   F. Cavani, F. TrifirÒ, Catalysis, 1994, **11**, 246

(13)   M. A. Pepera, J. L. Callahan, M. J. Desmond, E. C. Milberger, P. R. Blum and N. J. Bremer, *J. Am. Chem. Soc*, 1985, **107(17)**, 4883

(14)   E. Bordes, *Catal. Today*, 1987, **1**, 499

(15)   G. Bergeret, M. David, J. P. Broyer, J. C. Volta, G. Hecquet, *Catal. Today* 1987, **1**, 37

(16)   G. J. Hutchings, C. J. Kiely,   M. T. Sananés-Schulz, A. Burrows and J. C. Volta. *Catal Today*, 1996, **28**, 275

(17)   M. T. Sananés-Schulz, A. Tuel, G. J. Hutchings, J. C. Volta. *J. Catal*, 1997, **166, 2**, 388

(18)   B. SchiØtt, K. A. JØrgensen, *Catal. Today* 1993, **16**, 79

(19)   V. V. Guliants, S. A. Holmes, *J. Mol. Catal*, 2001, **175,1-2**, 227

(20)   R. Shimizu and T. Fuchikami, *Catalysis Today*, 2001, **71**, 137

(21)   B. K. Hodnett, *Catal. Lett*, 1985, **27**, 373

(22)   B. K. Hodnett, Ph. Permanne and B. Delmon, *Appl. Catal*, 1983, **6**, 231

(23)   J. W. Johnson, D. C. Johnston, A. J. Jacobson and J. F. Brody, *J. Am. Chem. Soc*, 1984, **106**, 8123

(24)   I. J. Ellison, G. J. Hutchings, M. T. Sananes and J. C. Volta, *J. Chem. Soc. Commun*, 1994, 1093

(25)   L. Griesel, J. K. Bartley, R. P.K. Wells and G. J. Hutchings, *Catalysis Toady*, 2005, **99**, 131

(26)   J. K. Bartley, J.A. Lopez-Sanchez and G. J. Hutchings, *Catalysis Toady*, 2003, **81**, 197

(27)   M. O. Conner, F. Dason and B. K. Hodnett, *Appl. Catal.*, 1990, **64**, 161

(28)   L. Griesel, J. K. Bartley, R. P.K. Wells and G. J. Hutchings, *Journal of Molecular Catalysis*, 2004, **220**, 113

(29)   L. O'Mahony, D. Sutton and B. K. Hodnett, *Catalysis Today*, 2004, **91-92**, 185

(30)   F. Benabdelouahab, J. Claude Volta and R. Oliver, *Journal of Catalysis*, 1994, **148**, 334

(31)   E. Bordes and P. Courtine, *J. Catal*, 1979, **57**, 236

(32)   J. K. Bartley, R. P. K. Wells and G. J. Hutchings, *Journal of Catalysis*, 2000, **195**, 423

(33)   J. K. Bartley, C. Rhodes, C. J. Kiely, A. F. Carley and G. J. Hutchings, *Phys. Chem. Chem. Phys.*, 2000, **2**, 4999

(34)   Wen-Sheng Dong, J. K. Bartley, Nian-Xue Song and G. J. Hutchings, *Chem. Mater*, 2005

(35)   M.S. Whittingham, A. J. Jacobson, *Intercalation Chemistry, Academic Press,* New York, 1982

(36)   V. V. Guliants, J. B. Benziger, S. Sundaresan, *Chem. Mater,* 1995, **7**, 1485

(37)   S. Okuna, G. Matsubayashi, J. Chem. Soc. Dalton Trans. 1992, 2441

(38)   P. Čapková, M. Trchová, V. Zima and H. Schenk, *Journal of Solid State Chemistry,* 2000, **150**, 356

(39)   K. Melánová, L. Beneš and V. Zima, *Journal of Inclusion and Macrocyclic Chemistry,* 1999, **33**, 391

(40)   K. Melánová, L. Beneš and V. Zima, *Journal of Solid State Chemistry*, 2001, **157**, 50

(41)   L. Beneš, V. Zima and K. Melánová, *Eur. J. Inorg. Chem,* 2001, 1883

(42)   N. Yamamoto, T. Okuhara and T. Nakato, *J. Mater. Chem.*, 2001, **11**, 1858

(43)   N. Yamamoto, N. Hiyoshi and T. Okuhara *Chem. Mater.*, 2002, **14**, 3882

(44)   Y. Kamiya, S. Ueki, N. Hiyoshi, N. Yamamoto and T. Okuhara, *Catalysis Today*, 2003, **78**, 281

(45)   Y. Kamiya, N. Hiyoshi, N. Hiyoshi and T. Okuhara, *Catalysis Today*, 2003, **78**, 281

(46)   L. Beneš, V. Zima and K. Melánová, *Eur. J. Inorg. Chem,* 2001, 1883

(47)   M. Trchová, P. Čapková, P. Matějka, K. Melánová, L. Beneš and E. Uhliřová, *Journal of Solid State Chemistry*, 1999, **148**, 197

(48)   L. Beneš, K. Melánová and V. Zima, *Journal of Inclusion Phenomena and Molecular Recognition in Chemistry*, 1998, **31**, 275

(49)   G. J. Hutchings, *Appl. Catal,* 1991, **72**, 1

(50)   G. J. Hutchings and R. Higgins, *J. Catal,* 1996, **162**, 153

(51)   V. A. Zazhigalov, J. Haber, J. Stoch, A. I. Pyatnitzkaya, G. A. Komashko, V.M. Belousov, *Appl. Catal. A* 1993, **96**, 135

(52)   L. M. Cornaglia, S. Irusta, E . A. Lombardo, M. C. Durupty, J. C. Volta *Catal.Today.* 2003, **78**, 291

(53)   L. M. Cornaglia, C. R. Carrara, J. O. Petunchi, E . A. Lombardo, *Catal. Today.* 2000, **57**, 313

(54)   S. Sajip, J. K. Bartley, A. Burrows, M. T. Sananés, A. Tuel, J. C. Volta, C. J. Kiely and G. J. Hutchings, *New J. Chem.,* 2001, **25**, 125

(55)   S. Shen, J. Zhou, F. Zhang, L. Zhou, R. Li, *Catal. Today*, 2002, **74**, 37

(56)   F. Javier Cabello Sanchez, J.A. Lopez-Sanchez, R P. K. Wells, Colin Rhodes, and G. J. Hutchings, *New. J. Chem.,* 2001, **25**, 1528

(57)   L. Xu, X. Chen, W. Ji, Q. Jan, Y. Chen, *React. Kinetics. Catal. Lett.,* 2002, **76**, **2**, 335

(58)   N. Yamazoe , H. Morishige, J. Tamaki, N. Miura, *Stud. Surf. Sci. Catal.* 1993, **75**,1989

(59)   P. Ruiz, Ph. Bastians, L. Caussin, R. Reuse, L. Dasa, D. Acosta, B. Delmon,Catal. Today, 1993, **16**, 99

(60)   A. Datta , M. Agarwal , S. Dasgupta, R. Y. Kelkar, *J. Mol. Catal. A,* 2003, **198**, 205

(61)   B.Solsona, V. A. Zazhigalov, J. M. Lopez Nieto, I. V. Bacherikova, E. A. Diyuk, *Appl. Catal. A.,* 2003, **249**, 81

(62)   L. M. Cornaglia, C. A. Sanchez, E . A. Lombardo, *Appl. Catal.* 1993, **95**, 117

(63)   F. Javier Cabello Sanchez, R P. K. Wells, Colin Rhodes, J. K. Bartley, C. J.Kiely and G. J. Hutchings, *Phys. Chem. Chem. Phys.,* 2001, **3**, 4122

(64)   V. V. Guliants, S. A. Holmes, J. B. Benziger, P. Heaney, D. Yates and I. E. Wachs, *J. Mol. Catal,* 2001, **172**, 265

(65)   C. C. Torardi, Z. G. Li and H. S. Horowitz, *J. of. Solid State Chemistry,* 1995, **119**, 349

(66)   L. O. Mahony, T. Curtin, J. Henry, D. Zemlyanov, M. Mihov and B. K. Hodnet, *Applied Catalysis A: General,* 2005, **285**, 36

(67)   S. Sajip, J. K. Bartley, A. Burrows, C. Rhodes, J. C. Volta, C. J. Kiely and G. J. Hutchings, *Phys. Chem. Chem. Phys.,* 2001, **3**, 2143

(68)   G. Koyano, T. Okuhara and M. Misono, *J. Am. Chem. Soc,* 1998, **120**, 767

(69)   N. Ryumon, H. Imai, Y. Kamiya and T. Okuhara, *Applied Catalysis A,* 2006, **297**, 73

Chapter 2

Experimental Details

2.1 V-P-O materials Preparation

Pure vanadium phosphate materials were prepared via new preparation routes. Firstly, $VOPO_4 \cdot 2H_2O$ was prepared using different vanadium sources and phosphoric acids based on the standard preparation method and some of these $VOPO_4 \cdot 2H_2O$ were transformed to final catalyst under the reducing environment (chapter 4).Secondly, different morphology VPO materials were synthesised using alkane solvent via standard VPD route (chapter 3). These materials were characterized by combination of XRD, laser Raman spectroscopy, SEM, TEM and BET surface area measurements. These characterized materials were compared with previous results and materials were evaluated for the selective oxidation of n-butane to maleic anhydride.

2.1.1 Materials

Details of materials used are shown in Table 2.1

Table 2.1 Materials used

Material name	Source and Purity
V_2O_5	Aldrich - 98% , Riedel-de Haën - 99%
Ortho-phosphoric acid	Aldrich - 85%
pyro-phosphoric acid	Aldrich - 99%
isobutanol	Aldrich - 99%
1-butanol	Aldrich - 99%
1-octanol	Aldrich - 99%
octane	Aldrich - 99%
heptane	Aldrich - 99%
dodecane	Aldrich - 99%
hexadecane	Aldrich - 99%

2.1.1.1 Standard $VOPO_4 \cdot 2H_2O$ preparation

Vanadium phosphate dihydrate ($VOPO_4 \cdot 2H_2O$) was prepared by VPO method. This method was described by Jonhson *et al.*[1]

V_2O_5 (10.00 g, Aldrich) and H_3PO_4 (60 ml, Aldrich) were refluxed in water (120 ml) under reflux conditions for 24 hours using a hot plate as heating source. The yellow solid was recovered immediately by vacuum filtration, washed with cold water (100 ml) and acetone (100 ml) and dried in air for 24 hours.

2.1.1.2 Using *pyro*-phosphoric acid

This method was very similar to that described above except for the use of *pyro*-phosphoric acid instead of *ortho*-phosphoric acid (chapter 4)

V_2O_5 (10.00 g, Aldrich or Riedel-de Haën) and $H_4P_2O_7$ (40.00 g, Aldrich) were refluxed in water (120 ml) under reflux conditions for 24 hours using a hot plate as heating source. The yellow solids was recovered immediately by vacuum filtration, washed with cold water (100 ml) and acetone (100 ml) and dried in air at 110°C for 24 hours.

2.1.1.3 Using organic solvent

V_2O_5 (5.90g, Aldrich) and isobutanol (125 ml, Aldrich) were heated at temperature between 55-60° C for 24 hours using a hot plate as heating source. Above mixture was cooled for 24 hours, then H_3PO_4 (4.88 ml, Aldrich) was added to the above mixture and refluxed for 24 hours. The yellow solids was recovered immediately by vacuum filtration, washed with cold water (100 ml) and acetone (100 ml) and dried in air at 110°C for 24 hours.

2.1.2 Preparation of $VOHPO_4 \cdot 0.5H_2O$

VPO (organic route)

V_2O_5 (2.00 g, Aldrich) and H_3PO_4 (1.66 ml, Aldrich) were refluxed with 1-butanol (50 ml, Aldrich) for 24 hours. The recovered blue solid was then heated under reflux in water for 2 hours (90ml H_2O/g solid) to remove the impurity $VO(H_2PO_4)_2$. The suspension was then filtered at hot, washed with acetone (50 ml) and dried in air at room temperature for 24 hours.

VPD (dihydrate route)

VPD is the reduction of vanadium phosphate $VOPO_4.2H_2O$ with alcohol as reducing agent and solvent.[2]

The $VOPO_4 \cdot 2H_2O$ (1.00 g) was refluxed in isobutanol (25 ml, Aldrich) for 24 hours. The pale blue solid was recovered by vacuum filtration and washed with alcohol (50 ml) and acetone (50ml). The recovered solid was then heated under reflux in water for 2 hours (90ml H_2O/g solid) to remove the impurity $VO(H_2PO_4)_2$. The suspension was then filtered hot, washed with warm water (100 ml) and dried in air at 110°C, 24 hours.

2.1.3 New VPD preparation routes

The influence of the alkane solvent was investigated in the VPD preparation method (Chapter 3). Different variables were used for this investigation (V:alcohol mole ratio, total volume, alcohol:alkane volume ratio (concentration of alcohol) and different alcohol structure).

2.1.3.1 Using different concentrations of 1-butanol and different total volumes

$VOPO_4 \cdot 2H_2O$ (1.00g) was refluxed in 1-butanol (25 ml) and different quantities (10, 25, 50, 75 100, 150 and 400 ml) of the alkane solvent (Heptane, octane, dodecane or hexadecane) for 24 hours. The resulting material recovered by vacuum filtration and washed with alcohol (50 ml) and acetone (50 ml) and dried in air at 110°C for 24 hours.

2.1.3.2 Using different concentrations of primary alcohol and same total volume (175 ml)

$VOPO_4 \cdot 2H_2O$ (1.00g) was refluxed in different quantities of the 1-butanol or 1-octanol and octane (0, 5, 15, 25, 50, 100, 125, 150, 160, 170 and 175 ml) total volume up to 175 ml for 24 hours. The resulting material was recovered by vacuum filtration and washed with alcohol (50 ml) and acetone (50 ml) and dried in air at 110°C for 24 hours.

2.1.3.3 Using same V: OH ratio (1:50) and same total volume (175 ml)

$VOPO_4 \cdot 2H_2O$ (V: alcohol = 1: 50) was refluxed in different quantities of the 1-butanol or 1-octanol and octane solvent (0, 5, 15, 25, 50, 100, 125, 150 and 160 ml) total volume up to 175 ml for 24 hours. The resulting material was recovered by vacuum filtration and washed with alcohol (50 ml) and acetone (50 ml) and dried in air at 110°C for 24 hours.

2.1.4 Preparation of $(VO)_2P_2O_7$ by using direct route

$VOPO_4 \cdot 2H_2O$ was reduced to the final catalyst in the gas phase. Catalyst transformation was carried out using the procedure outlined below. (Chapter 4)

Reaction conditions were

   (1) different time (6, 24, 72 hours)

   (2) temperature (450°C to 550°C)

   (3) different gas mixture (5% H_2/Ar, He and isobutanol)

$VOPO_4 \cdot 2H_2O$ (0.70 g) was loaded into the reactor and the desired gas flow established through the bypass using a bubble meter. The gas was passed over the $VOPO_4 \cdot 2H_2O$ and

the temperature ramped at 3°C / min to the desired reaction temperature and $VOPO_4 \cdot 2H_2O$

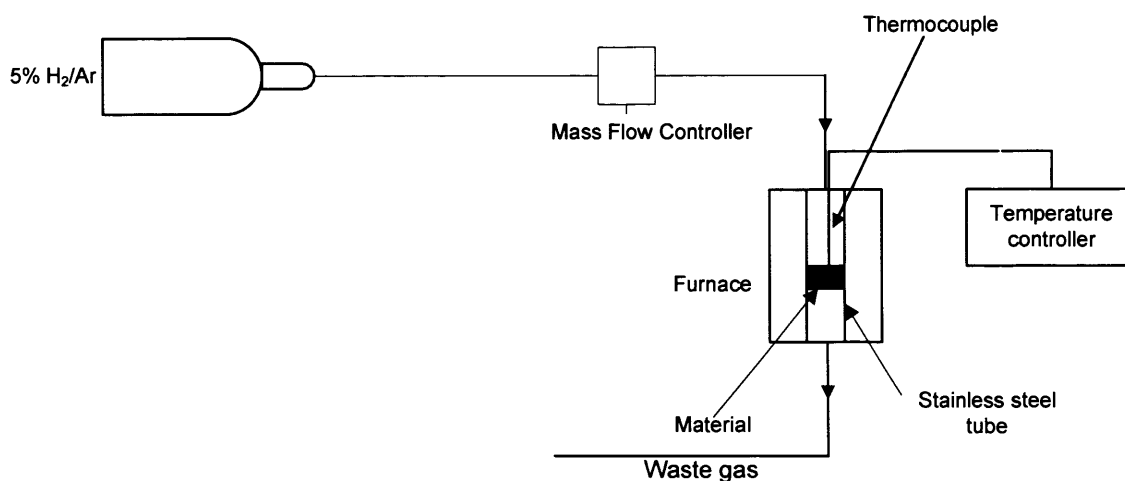for different times. Outline of the reactor has shown in Figure 2.1

Fig. 2.1 Schematic of the apparatus for the preparation of final catalyst using new route

2.2 Catalyst Testing

Butane oxidation was performed over a fixed catalyst bed in a stainless steel microreactor

(1/4" inner diameter). Butane and air were mixed from separate cylinders in a ratio of 1.5%

butane in air. The GHSV was maintained in the order of 3000 h^{-1}, and catalyst precursors

were activated for 72 hours at 400°C with 1.5% butane in air. The stationary values

(selectivity and conversion) were obtained after about 72 hours of the reaction. Thus,

conversion and selectivity were determined from the data collected between 80 to 100

hours (average value was calculated).

From the literature,[3] evolution of the conversion and selectivity to MA with time in the

oxidation of butane over various VPO catalysts are shown in Figure 2.2
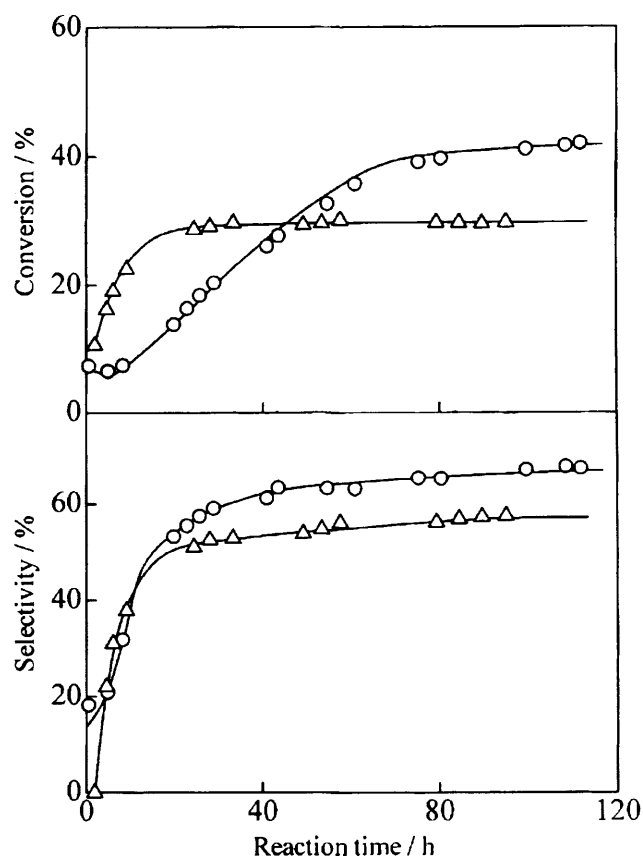
Fig. 2.2 Changes of conversion and selectivity to MA for butane oxidation over different

$VOHPO_4.0.5H_2O$ (A: O, B: Δ)

A: Material prepared using intercalation, exfoliation and reduction method.

B: Material prepared using standard VPD method.

The product stream was analysed with an online Varian 3400 Gas Chromatograph (GC)

fitted with a TCD detector and two columns, a 50 cm porapak Q and 2m 5X molecular

sieve. At injection, the porapak Q and molecular sieve column were in series, permitting

CO, N₂, and O₂ to move onto the molecular sieve. The molecular sieve was then switched

out of series to prevent CO_2, butane and oxygenate products from contaminating it. CO_2

then eluted from the porapak Q column. The molecular sieve column was switched back

into series to elute CO, N₂ and O₂, and switched out again to allow maleic anhydride,

butane to elute from the porapak Q. Outline of the reactor for butane oxidation has shown

in Figure 2.3
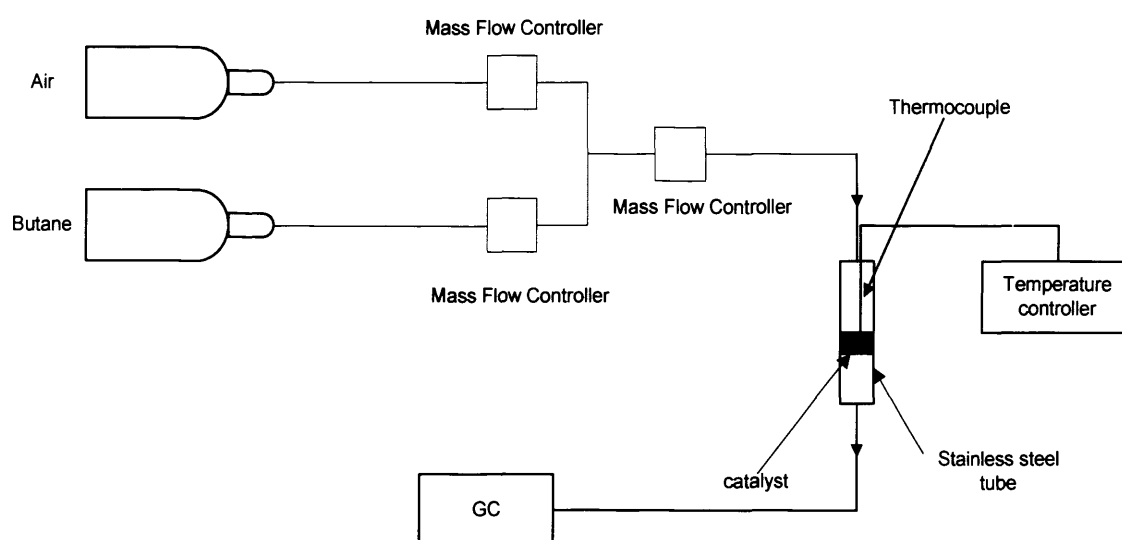
Fig. 2.3 Outline of the butane oxidation reactor

Only CO_2, CO and maleic anhydride (MA) were detected as products and the selectivity

and conversions were calculated based on the following equations

Selectivity to MA (%) = mMA / (mCO₂+mCO+mMA)x100   Eq. 2.1

m is mass of each product

Conversion (%) = mMA+mCO mCO$_2$ /m(MA+CO+CO$_2$+butane)x100   Eq. 2.2

Specific activity (mol MAh^{-1}m^{-2}) = butane flow (molh^{-1}) x MA conversion (%) x MA selectivity (%) / mass catalyst (g) / surface area (m^{2}g^{-1})   Eq. 2.3

2.3 Experimental Techniques

2.3.1 Powder X-ray Diffraction (XRD)

Powder X-ray diffraction is a versatile and non-destructive analytical technique for identification and quantitative determination of the various crystalline forms, known as phases of compounds present in powdered and solid samples. Identification is achieved by comparing the X-ray diffraction pattern or diffractogram obtained from an unknown sample with an internationally recognised database containing reference patterns for more than 70,000 phases and reported in the literature. Modern computer-controlled diffractometer systems use automatic routines to measure, record and interpret the unique diffractogram produced by individual constituents in even highly complex mixture.

A crystal lattice is a regular three dimensional distribution (cubic, rhombic, etc) of atoms in space. These are arranged so that they form a series of parallel planes separated from one another by a distance d, which varies according to the nature of the material. For any crystals or phases exist in a number of different orientations, each with its own specific d-spacing.

Investigations of the internal structure of the crystal depend on a penetrating radiation that will enter the material and will show interference effects as a result of scattering from the ordered array of scattering centers. X-rays have the necessary penetrating power and show interference effects since they have wavelengths of the same order of magnitude as the spacing of crystal planes.

In the Bragg method, the phenomenon is observed when nearly monochromatic x-rays are reflected from a crystal. A beam of X-rays is passed into a crystal, which is represented in Fig 2.4 by layers of particles.
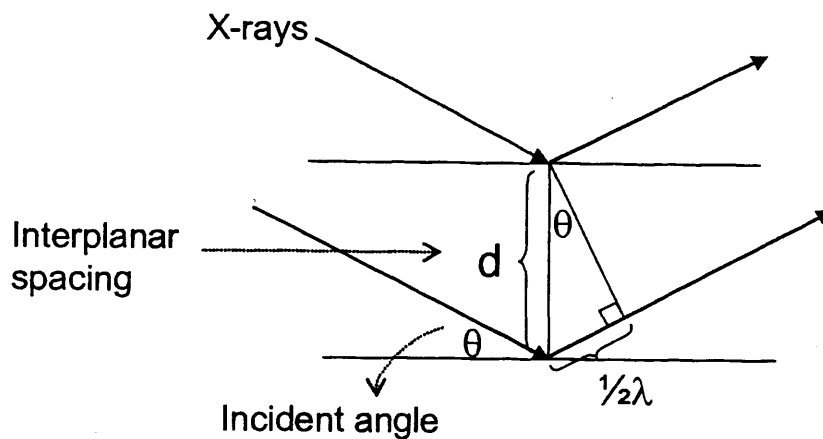
Fig. 2.4 Reflection of X-rays from the reflecting layers of crystal

The X-rays are scattered by interaction with the electrons of the atoms or ions of the crystal. Since X-rays are quite penetrating, each layer of atoms can be expected to scatter only a small part of the X-ray beam. If the crystal particles did not have a spacing of the same order of magnitude as the wavelength of the X-rays, simple reflections and scattering of the X-rays would occur.[4,5]

For some special angles, assuming a particular plane spacing d and a particular X-ray wavelength λ, as in figure 2.4, the waves we draw from successive planes will be in phase. The waves then will add to give a net resultant wave. Constructive interference occurs at these special angles. Constructive interference occurs when ever the phase of beams scattered from successive layers is shifted by an integral multiple of wavelengths. This happens when relation holds. This important equation is known as Bragg's diffraction law.

$$n\lambda = 2d\sin\theta \qquad n = 1, 2, 3\ldots\ldots \qquad \text{Eq. 2.4}$$

This basic equation shows that for a given value of the X-ray wave length λ, measurement of the angle θ or of the sin θ term gives the information on the spacing between planes through the scattering centres that make up the crystal.

The width of the peaks in a particular phase pattern provide an indication of the average crystallite size, large crystallites give rise to sharp peaks, while the peak width increases as crystallite size reduces. Peak broadening also occurs as a result of variations in d-spacing caused by micro-strain. However, the relationship between broadening at diffraction angle 2θ is different from that of crystallite size affects, making it possible to differentiate between the two phases

XRD patterns in this study were obtained by an Enraf Nonius FR590 X-ray generator with a Cu Kα Source fitted with an Inel 120 hemisperical detector.

2.3.2 Raman spectroscopy

When light is scattered from a molecule most photons are elastically scattered. The scattered photons have the same energy (frequency) and, therefore, wavelength, as the incident photons. However, a small fraction of light is scattered at optical frequencies different from, and usually lower than, the frequency of the incident photons. The process leading to this inelastic scatter is the termed the Raman effect. Raman scattering can occur with a change in vibrational, rotational or electronic energy of a molecule. Chemists are concerned primarily with the vibrational Raman effect. We will use the term Raman effect to refer to the vibrational Raman effect only.

The difference in energy between the incident photon and the Raman scattered photon is equal to the energy of a vibration of the scattering molecule. A plot of intensity of scattered light versus energy difference is a Raman spectrum.

The Raman effect arises when a photon interacts with the electric dipole of the molecule. It is a form of electronic spectroscopy, although the spectrum contains vibrational frequencies. In classical terms, the interaction can be viewed as a perturbation of the molecule's electric field. In quantum mechanics the scattering is described as an excitation to a virtual state lower in energy than a real electronic transition with nearly coincident de-excitation and a change in vibrational energy. The scattering event occurs in 10^{-4} seconds or less. The virtual state description of scattering is shown in figure 2.5
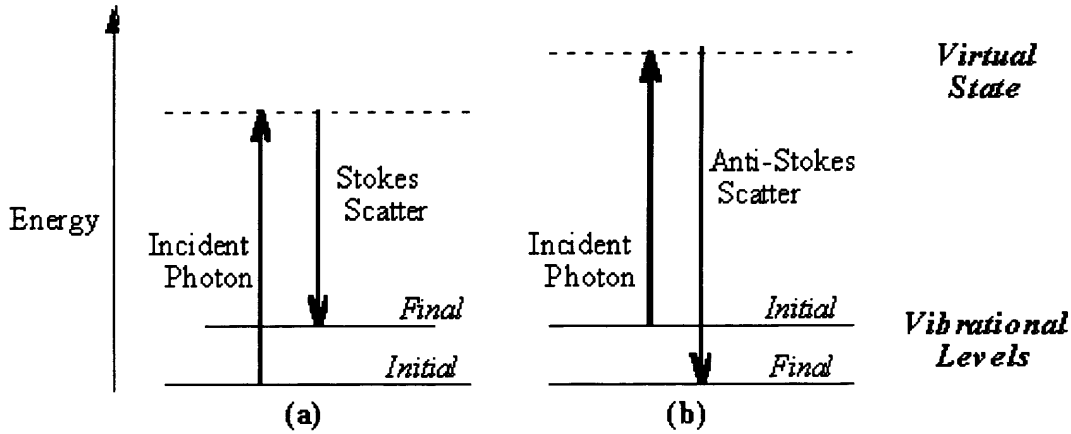
Fig. 2.5 Energy level diagram for Raman scattering; (a) Stokes Raman scattering (b) anti-Stokes Raman scattering.[4, 5]

The energy difference between the incident and scattered photons is represented by the arrows of different lengths in figure 2.2. Numerically, the energy difference between the initial and final vibrational levels, $\bar{\nu}$ or Raman shift in wave numbers (cm⁻¹), is calculated using following equation

$$\bar{V} = \frac{1}{\lambda_{incident}} - \frac{1}{\lambda_{scattered}}$$

Eq.2.5

in which $\lambda_{incident}$ and $\lambda_{scattered}$ are the wavelengths (in cm) of the incident and Raman scattered photons, respectively. The vibrational energy is ultimately dissipated as heat. Because of the low intensity of Raman scattering, the heat dissipation does not cause a measurable temperature rise in a material. It is known that material such as $VOPO_4.2H_2O$ can dehydrate. Therefore, a low power (10%) beam was used for characterizing VPO materials. Raman spectrums of $VOPO_4.2H_2O$ obtained using different power (10% and 80%) are shown in figure 2.6 and 2.7 respectively.
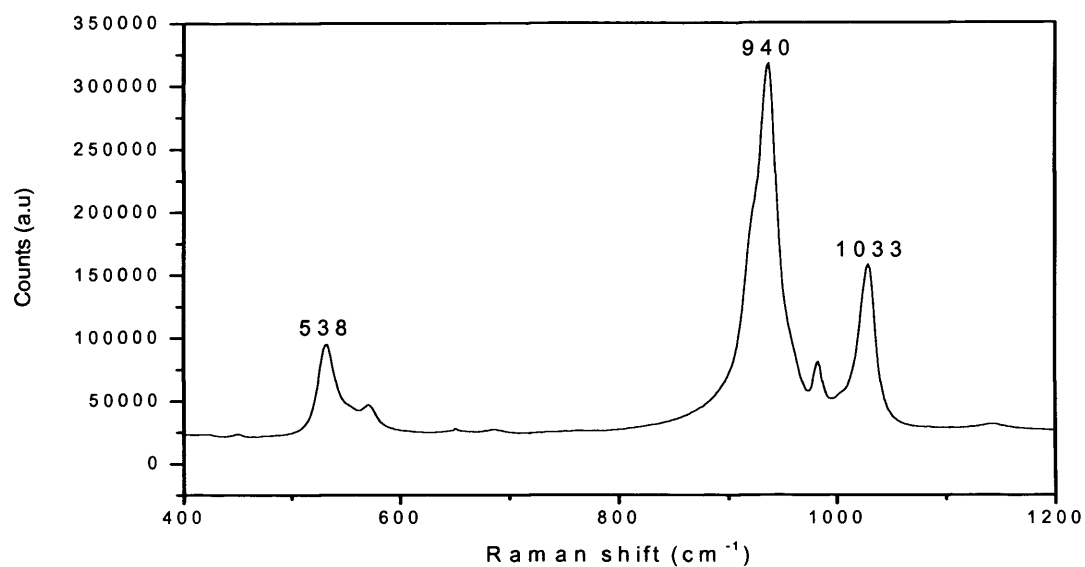
Fig. 2.6 Raman spectrum of $VOPO_4.2H_2O$ using low power beam (10%)
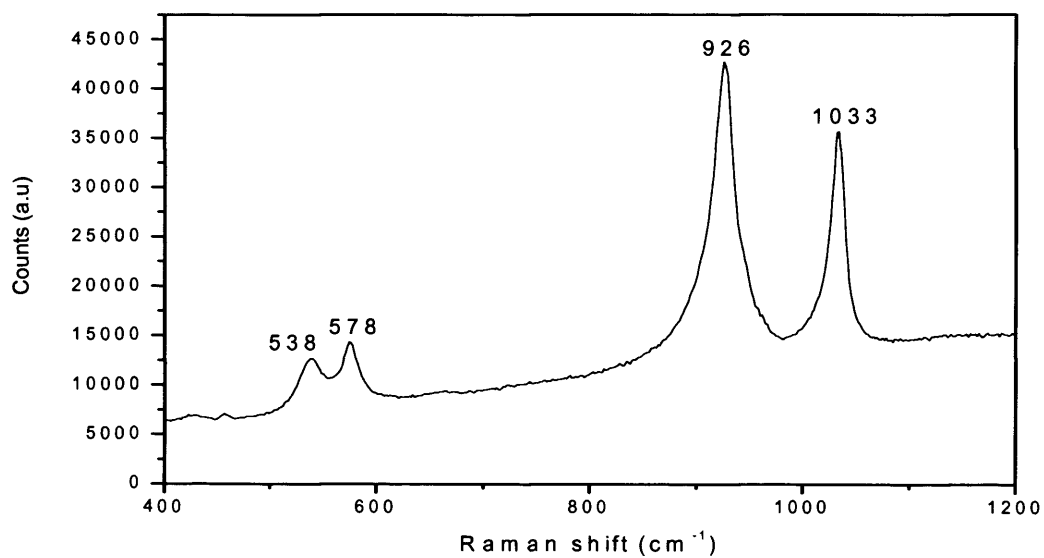
Fig. 2.7 Raman spectrum of $VOPO_4.2H_2O$ using high power beam (80%)

The Raman spectrum of $VOPO_4.2H_2O$ (Figure 2.6) is in agreement with published data[6] while spectrum (Figure 2.7) is $VOPO_4$.

At room temperature the thermal population of vibrational excited states is low, although not zero. Therefore, the initial state is the ground state, and the scattered photon will have lower energy (longer wavelength) than the exciting photon. This Stokes shifted scatter is what is usually observed in Raman spectroscopy. figure 2.5a depicts a Raman Stokes scattering.

A small fraction of the molecules are in vibrationally excited states. Raman scattering from vibrationally excited molecules leaves the molecule in the ground state. The scattered photon appears at higher energy, as shown in figure 2.5b. This anti-Stokes-shifted Raman spectrum is always weaker than the Stokes-shifted spectrum, but at room temperature it is strong enough to be useful for vibrational frequencies less than about 1500 cm^{-1}. The Stokes and anti-Stokes spectra contain the same frequency information. The ratio of anti-Stokes to Stokes intensity at any vibrational frequency is a measure of temperature. Anti-Stokes Raman scattering is used for contactless thermometry. The anti-Stokes spectrum is also used when the Stokes spectrum is not directly observable, for example because of poor detector response or spectrograph efficiency.

Raman spectra were determined using a Renishaw Ramascope spectrograph fitted with a green Ar^+ laser ($\lambda = 514.532$ cm^{-1})

2.3.3 Electron microscope (SEM and TEM)

The SEM is a type of electron microscope capable of producing high-resolution images of a sample surface. Due to the manner in which the image is created, SEM images have a characteristic three-dimensional appearance and useful for judging the surface structure of the sample.

In a typical SEM, electrons are emitted from a tungsten or lanthanum hexaboride (LaB_6) cathode and are accelerated towards an anode; alternatively, electrons can be emitted via field emission (FE). Tungsten is used because it has the highest melting point and lowest vapor pressure of all metals, thereby allowing it to be heated for electron emission. The electron beam, which typically has an energy ranging from a few hundred eV to 100 keV, is focused by one or two condenser lenses into a beam with a very fine focal spot sized 1 nm to 5 nm. When the primary electron beam interacts with the sample, the electrons lose energy by repeated scattering and absorption within a teardrop shaped volume of the specimen known as the interaction volume, which extends from less than 100 nm to around 5 µm into the surface. The size of the interaction volume depends on the beam accelerating voltage, the atomic number of the specimen and the specimen's density.

The energy exchange between the electron beam and the sample results in the emission of electrons and electromagnetic radiation which can be detected to produce an image, the most common imaging mode monitors low energy (<50 eV) secondary electrons. Due to their low energy, these electrons originate within a few nanometers from the surface. The electrons are detected by a scintillator-photomultiplier device and the resulting signal is rendered into a two-dimensional intensity distribution that can be viewed and saved as a digital image. The brightness of the signal depends on the number of secondary electrons

reaching the detector. If the beam enters the sample perpendicular to the surface, then the activated region is uniform about the axis of the beam and a certain number of electrons escape from within sample. As the angle of incidence increases, the escape distance of one side of the beam will decrease, and more secondary electrons will be emitted. Thus steep surfaces and edges tend to be brighter than flat surfaces, which results in images with a well-defined, three-dimensional appearance. Using this technique, resolutions of less than 1 nm are possible.

Images can be obtained due to the backscattered electrons (BSE) which consist of high-energy electrons originating in the electron beam, that are reflected or back-scattered out of the specimen interaction volume. Backscattered electrons may be used to detect contrast between areas with different chemical compositions, especially when the average atomic number of the various regions is different, since the brightness of the BSE image tends to increase with the atomic number.[7]

Backscattered electrons can also be used to form electron backscatter diffraction (EBSD) image. This image can be used to determine the crystallographic structure of the specimen.

SEM images were obtained using FEI XL 30 E.S.E.M instrument, at Earth Science Department, Cardiff University

TEM images were obtained by Prof. Chris Kiely and Dr. Andy Burrows in the materials science department at the Lehigh University, USA. Samples for transmission electron microscopy (TEM) examination were prepared by dispersing the catalyst powder in high purity ethanol, then allowing a drop of the suspension to evaporate on a holey carbon film supported on a 300 mesh copper TEM grid. TEM analyses were carried out in a 200kV JEOL 2000FX electron microscope equipped with a thermionic LaB_6 source.

2.3.4 Surface area measurement

Surface area is an attribute that is used by catalyst manufacturers and users to monitor the activity and stability of catalysts. There are different methods used to measure surface area and each method can yield different results. Most methods are based on the isothermal adsorption of nitrogen. Either a single point or multipoint method is used to calculate the surface area. The multipoint Brunauer, Emmett and Teller method is used to measure total surface area of catalyst, and is described in the following equation:

$$\frac{P}{V(P_0 - P)} = \frac{1}{V_m C} + \frac{(c-1)}{V_m C} * \frac{P}{P_0}$$

Eq. 2.6

Where V is the volume, reduced to standard conditions (STP) of gas adsorbed per unit mass of adsorbent at a given pressure P and constant temperature, V_m is the volume of gas adsorbed at STP per unit mass of adsorbent necessary to form a complete monolayer on the surface, P_0 is the saturation pressure at the measurement temperature, and C is a constant.

A linear relationship is obtained when $P/[V(P_0 - P)]$ is plotted against P/P_0, and the values of V_m and C can be obtained from the slope and intercept.

The surface area (SA) can be calculated based on the following equation

$$SA = (V_m * L * A_m) / V_{mol}$$

Eq. 2.7

Where L is the Avogadro constant, A_m is the average area occupied by the adsorbate in the filled monolayer (0.162 nm^2 for N_2) and V_{mol} is the molar volume of adsorbed gas at STP.[8]

Surface area measurements were carried out using a Micromeritics ASAP 2010 instrument, and N_2 was used as the adsorptive.

2.4 References

(1)   J. W. Johnson, D.C. Johnston, A. J. Jacobson and J. F. Brody, *J. Am. Chem. Soc.*, 1884, **106**, 8123

(2)   M. T. Sananes, I. J. Ellison, S. Sajip, A. Burrows, C. J. Kiely, J. C. Volta and G. J. Hutchings, *J. Chem. Soc., Faraday Trans.*, 1996, **92**(1), 137

(3)   Y. Kamiya, S. Ueki, N. Hiyoshi , N. Yamamoto and T. Okuhara, *Catalysis Today*, 2003, **78**, 281

(4)   Ira. N. Levine, *Physical Chemistry fourth edition,* 1995

(5)   Gordon. M. Barrow, *Physical Chemistry fifth edition, 1988*

(6)   E. Bordes, *Catal. Today*, 1994, **16**

(7)   L. E. Smart, E. A. Moore, *Solid State Chemistry, third edition,* 2005

(8)   P. W. Atkins, *Physical Chemistry, seventh edition,* 2001

Chapter 3

Control the Morphology of Vanadium Phosphate Catalyst Precursors by Adding Alkane Solvents

3.1 Introduction

The selective oxidation of of n-butane to maleic anhydride using vanadium phosphate catalysts has been well studied in recent years.[1-5] The reaction and catalysts continue to attract attention as it represents one of the few examples of the selective activation of an alkane at elevated temperatures. In particular, the structure and activity of vanadium phosphates has been extensively studied and continues to attract attention. The catalytic performance of vanadium phosphates depends on the method of preparation of the catalyst precursor, $VOHPO_4.0.5H_2O$[6-20], and the reaction conditions utilised for the *in situ* activation in n-butane/air to form the final catalyst.[6,7] The active catalyst comprises $(VO)_2P_2O_7$ in combination with some V^{5+} phosphates, typically α_I- and δ-$VOPO_4$, and the transformation of the precursor to the final catalyst is topotactic. Hence, the morphology of the precursor is of crucial importance in determining the eventual catalyst morphology and the performance following activation. In view of the importance of the morphology of the catalyst precursor, there have been numerous studies concerned with catalyst preparation. However, most studies use a standard preparation method in which V_2O_5 is used as a source of vanadium and H_3PO_4 is used as a source of phosphorus, and an alcohol is used as the reducing agent that is required to synthesise the V^{4+} precursor

phase. Notably, the addition of a solvent to this preparation procedure has not been considered in detail in any scientific publications and patents.

Recently, Okuhara and co-workers reported that intercalation and exfoliation of $VOPO_4.2H_2O$ crystallites proceeded with a stepwise heating below refluxing temperature in primary and secondary alcohols and the subsequent reduction of the exfoliated $VOPO_4.2H_2O$ brought about $VOHPO_4.0.5H_2O$ crystallites with different morphologies. Furthermore, $(VO)_2P_2O_7$ obtained from the precursor was highly active and selective for the selective oxidation of n-butane.[21-25]

Vanadium phosphate catalysts prepared by the reduction of $VOPO_4.2H_2O$ with 1-butanol are described and discussed in this chapter. In particular, the effect of the addition of an alkane during the reflux stage of the preparation has been investigated and these changes are demonstrated that the presence of a solvent can induce significant effects on both the structure and morphology of the vanadium phosphate.

3.2 Experimental

$VOPO_4.2H_2O$ (1.0 g) was refluxed with 1-butanol (25 ml) and different quantities of alkane solvents for 24 hours, and the resulting material was recovered by filtration. (more details in Chapter 2)

VOPO$_4$·2H$_2$O (V: alcohol = 1: 50) was refluxed in different quantities of the alcohols (1-butanol and 1-octanol) and octane solvent total volume up to 175 ml for 24 hours. The resulting material was recovered by vacuum filtration and washed with alcohol (50 ml) and acetone (50 ml) and dried in air at 110°C for 24 hours.

VOPO$_4$·2H$_2$O (1g) was refluxed of in different quantities of the alcohols (1-butanol and 1-octanol) and octane solvent total volume up to 175 ml for 24 h. The resulting material was recovered by vacuum filtration and washed with alcohol (50 ml) and acetone (50 ml) and dried in air at 110°C for 24 hours.

The new materials were activated *in situ* to give final catalysts and these materials were tested for the oxidation of *n*-butane to maleic anhydride. The precursors, catalysts were characterised using a combination of powder X-ray diffraction, laser Raman spectroscopy, BET surface area measurements, scanning electron microscopy and transmission electron microscopy.

3.3 Results

Characterisation of new materials prepared by reacting of VOPO$_4$·2H$_2$O with 1- butanol and differing amount of octane solvent

The XRD, laser Raman spectrum and SEM of new materials prepared using different amount of (10, 25, 50, 100, 400 ml) octane solvents are shown in Figure 3.1, 3.2 and 3.3 respectively.
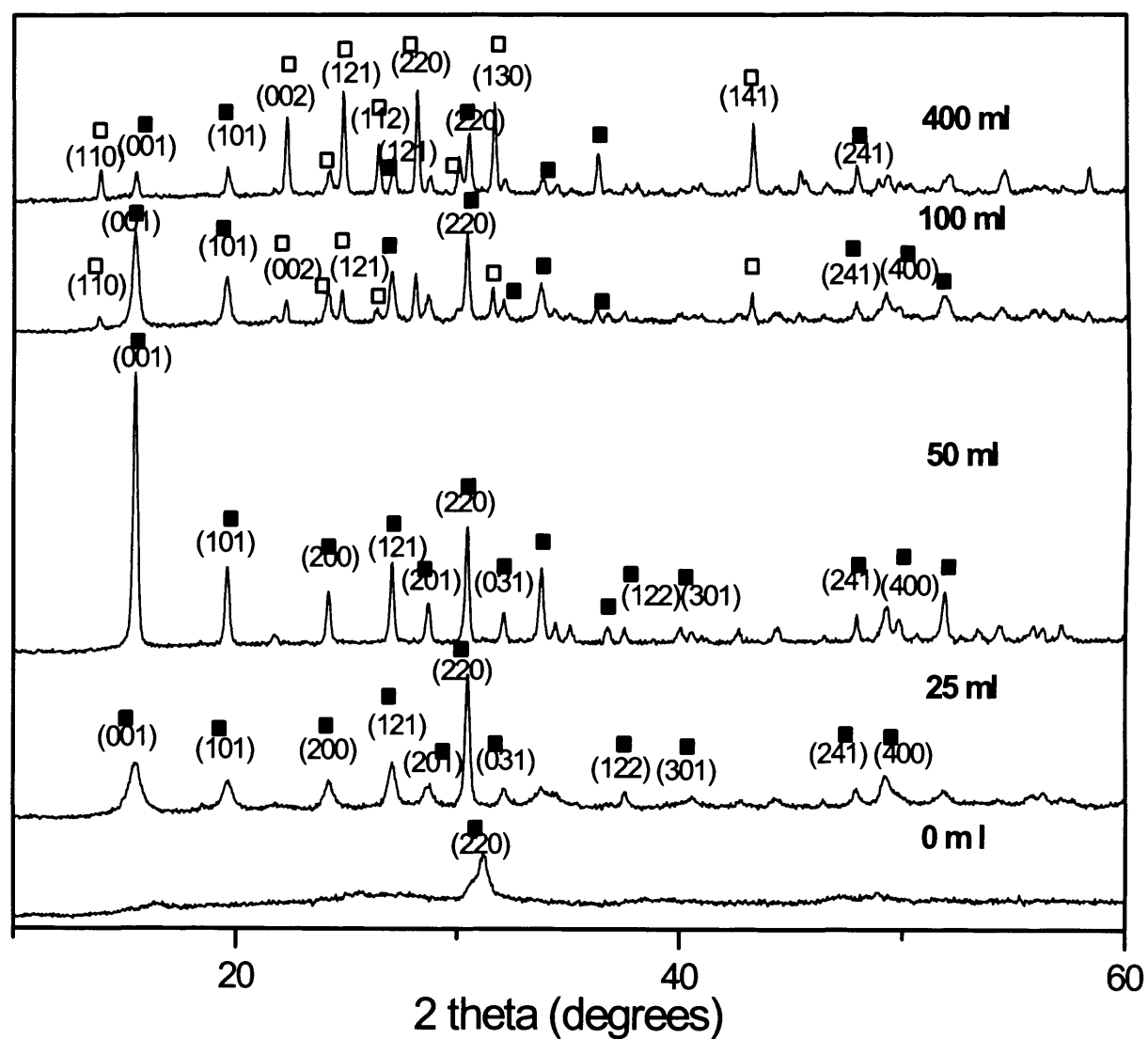
Fig. 3.1 Powder XRD patterns of the materials prepared by reacting of $VOPO_4 \cdot 2H_2O$ with 1-butanol and differing amounts of octane. Key ■ = $VOHPO_4 \cdot 0.5H_2O$; □ = $VO(H_2PO_4)_2$.

Table 3.1 Experimental details of material prepared using different amount of octane solvent

with $VOPO_4.2H_2O$ (1.00g) and 1-butanol (25 ml)

Material name	Amount of octane (ml)
B-0	0
B-25	25
B-50	50
B-100	100
B- 400	400

The XRD of B-0 material show only (Figure 3.1) $VOHPO_4.0.5H_2O$ as the main phase with the [220] reflection virtually the only feature present, with no evidence for any crystalline second phase. In addition, the high level of background noise and the broad peak widths of the reflections suggest that the material is not fully crystalline when compared with other materials (B-25, B-50, B-100 and B-400). The BET surface area of this material was 34 m^2/g.

The XRD patterns of B-25 materials have the (220) reflection (Figure 3.1) as the most dominant feature, with (001) the next most intense reflection with relative intensity of 30% when compared to (220). It indicated that the (001)/(220) intensities ratio increased when amount of octane is increased. Therefore, two types of morphology were present in this material which is $VOHPO_4.0.5H_2O$, rosette and $VOHPO_4.0.5H_2O$, platelet type. The BET surface area of this material was 26 m^2/g.

$VOHPO_4.0.5H_2O$ phase was observed in the XRD pattern of B-50 sample (Figure 3.1) with the [001] reflection as the major feature. Many other reflections are also present in the XRD

pattern, which can all be assigned to the $VOHPO_4.0.5H_2O$ phase. There are some differences in the relative intensities of the diffraction peaks in this material when compared with B-25 of same diffraction pattern (same planes) that indicated that the platelets become thicker as more octane is added (B-50), leading to an increase in intensity of the side planes in the XRD pattern. Further, X-ray line broadening decreases with increasing amount of octane solvent which indicates that large crystallites were obtained and also the crystallinity of these materials was better than B-0 and B-25 samples. Furthermore, $VOHPO_4.0.5H_2O$, platelet type morphology was present in this material. The BET surface area of this material was 6 m^2/g.

The XRD patterns of B-100 sample (Figure 3.1) have the (001) and (220) a reflection as the major features, therefore $VOHPO_4.0.5H_2O$ was the dominant phase in this material. There are number of other reflections also present, which is assigned to the $VO(H_2PO_4)_2$ phase that indicated, as more octane is added to the preparation (100 ml), $VOHPO_4.0.5H_2O$ phase partially switched to $VO(H_2PO_4)_2$. So, two types of materials are present in this material which are $VOHPO_4.0.5H_2O$ and $VO(H_2PO_4)_2$. The BET surface area of this material was 5 m^2/g.

The XRD patterns (Figure 3.1) of B- 400 material, most of the reflections can be indexed to $VO(H_2PO_4)_2$. However, trace amount of $VOHPO_4.0.5H_2O$ was present in these materials. The BET surface area of this material was 3 m^2/g.
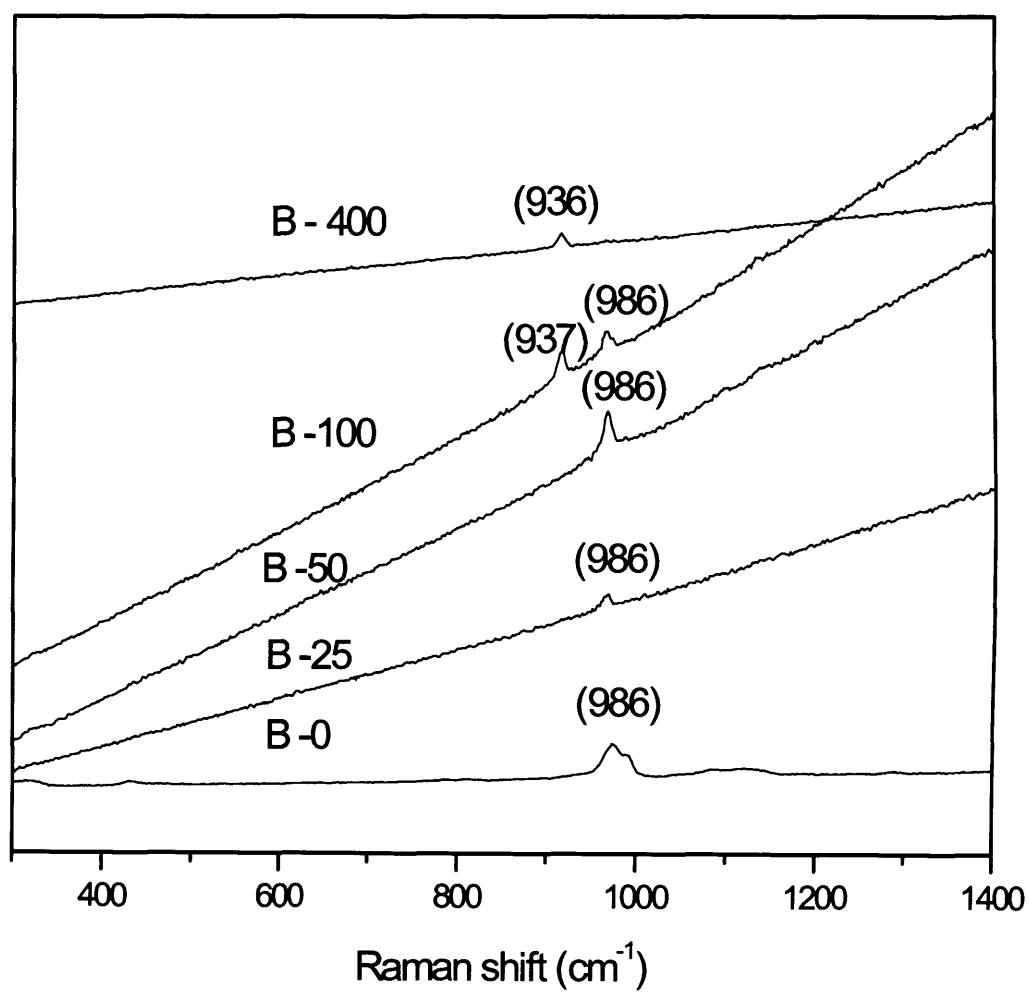
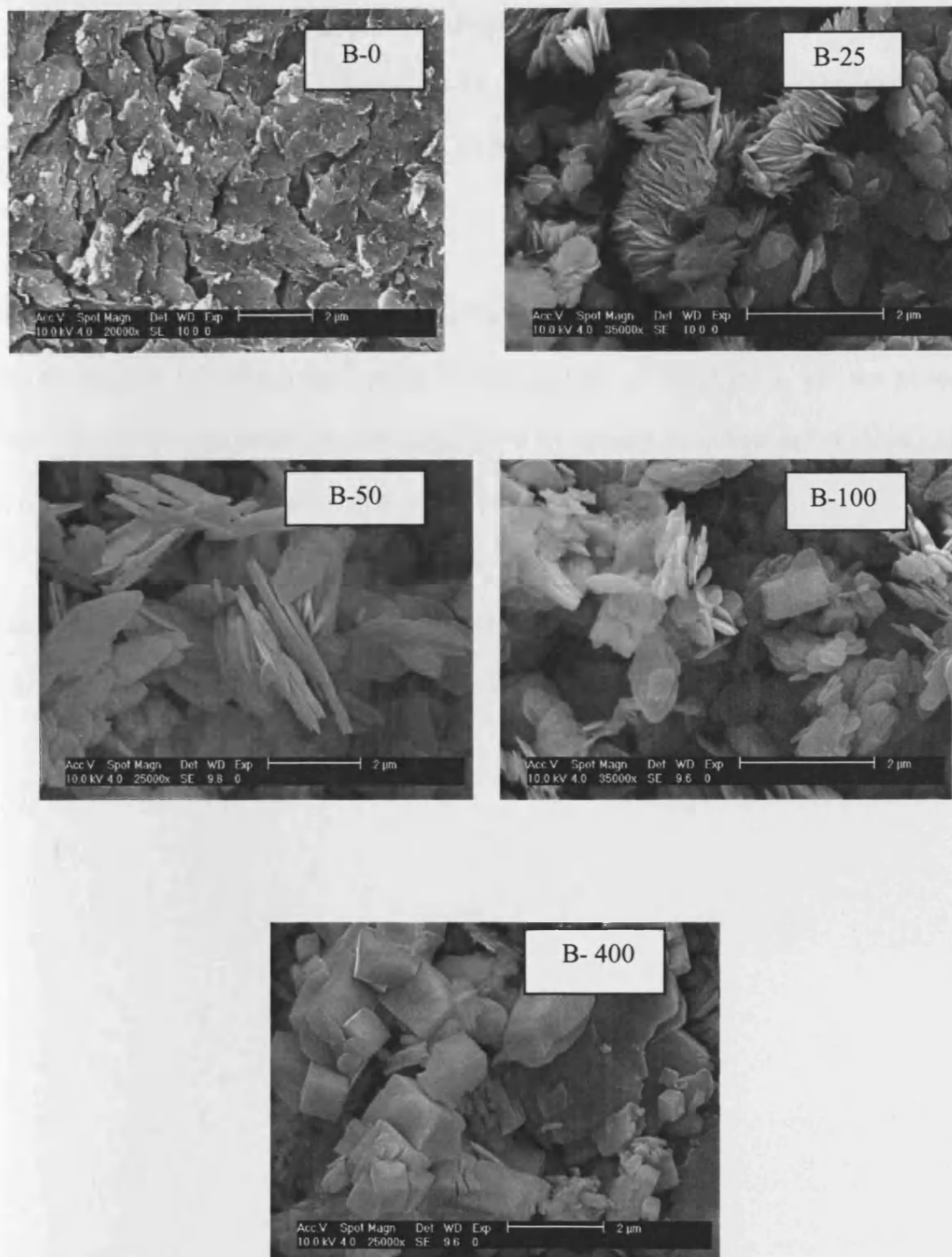Fig. 3.2 Raman spectrum of the materials formed by reacting of $VOPO_4 \cdot 2H_2O$ with 1-butanol and differing amounts of octane solvent.

The Raman spectra of B-0 sample (Figure 3.2), the P-O peak at 986 cm^{-1}, agreed with the well with published data[2] as being characteristic of $VOHPO_4.0.5H_2O$. Furthermore, Bordes *et al.* reported many spectra for VPD materials, these are bonding frequency of V=O at 1113 cm^{-1} and V-O-P bands at a high frequency, 1156 cm^{-1}. But, the rest of these peaks are not visible in $VOHPO_4 \cdot 0.5H_2O$ because the scattered photon appears at higher energy due to the background fluorescence, so the peak at V=O at 1113 cm^{-1} and V-O-P bands, 1156 cm^{-1} are weak Raman signal compared to that of 986, therefore this spectrum is not observed because of poor detector response or spectrograph efficiency.

Raman spectroscopy of B-25 and B-50 materials (Figure 3.2) shows the P-O peak at 986 cm^{-1} which is characteristic of $VOHPO_4.0.5H_2O$. The corresponding Raman spectrum of (Figure 3.2) B-100 sample showed a broad feature in 930 - 970 cm^{-1} region, consisting of two phases at 986 and 937 cm^{-1} , corresponding to $VOHPO_4.0.5H_2O$ and $VO(H_2PO_4)_2$ respectively.

The Raman spectra of B- 400 material agreed with the published spectra for $VO(H_2PO_4)_2$ with peak[2] (figure 3.2) at 937 cm^{-1} which is due to the P-O stretch of $VO(H_2PO_4)_2$. There were no Raman peaks for minor $VOHPO_4.0.5H_2O$ phase.

Fig. 3.3 The SEM of the materials formed by reacting of VOPO$_4$·2H$_2$O with 1-butanol and

differing amounts of octane solvent.

Figure 3.3 shows SEM micrographs of the materials. The B-0 sample material has largely amorphous irregular plates. Material, B-25 has platelet morphology. The platelets are considerably smaller than other materials (B-50). But, SEM did not give any evidence for rosette (VPD type) morphology.

The material (B-50) is made up of platelets. The material (B-100) consist of plate like crystal, which related to $VOHPO_4.0.5H_2O$ phase but morphology of $VO(H_2PO_4)_2$ can not be seen in SEM. The SEM examination of the material (B- 400) showed a combination of chunky blocks as major phase and isolated platelets as minor phase as shown in Figure 3.3.

The TEM of materials prepared using different amount of (0, 25, 50, 100 and 400 ml) octane solvents are shown in Figure 3.4 to 3.8 respectively.
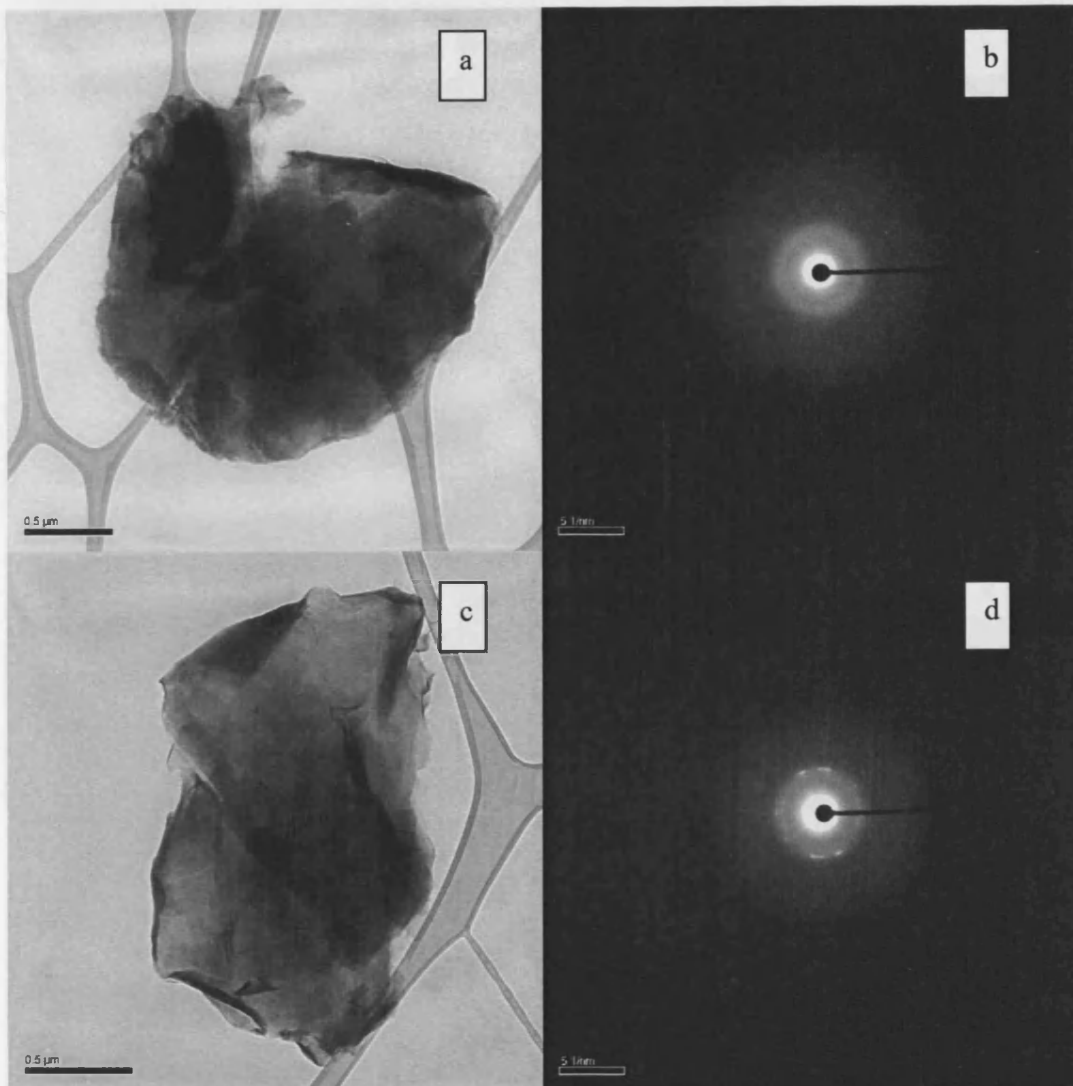
Fig. 3.4 The TEM of B-0 material

TEM examination of the B-0 sample revealed that irregular amorphous platelets as shown in Figure 3.4a. But, there were no [hkl] planes were observed from the diffuse amorphous diffraction pattern (figure 3.4b) of irregular amorphous platelet. Further, this material also has irregular disordered platelet as shown in figure 3.4c. Finally, diffraction pattern (figure 3.4 d) of the disordered platelet shows some evidence of limited crystallinity in this material.
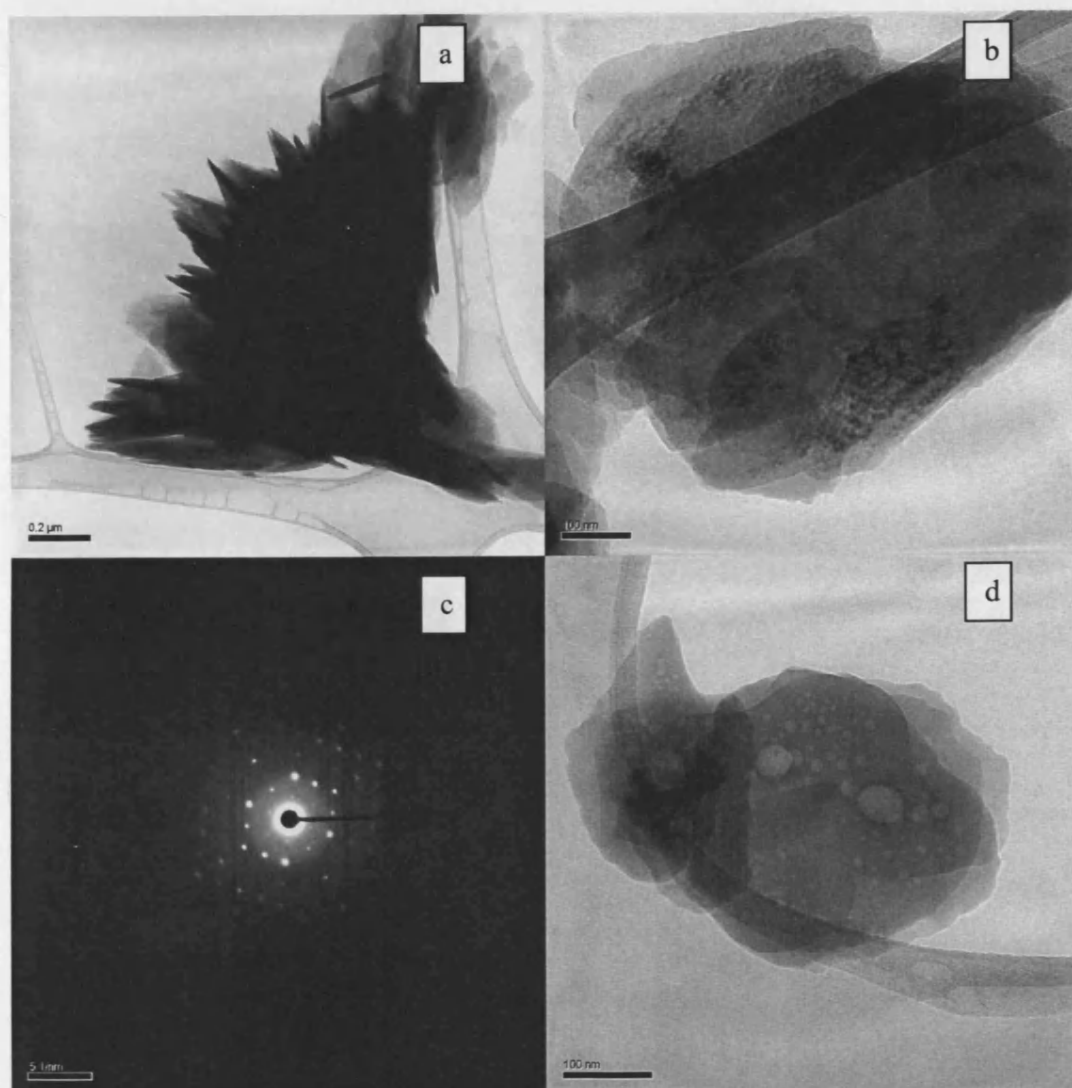
Fig. 3.5 The TEM of B-25 material

TEM examination of the B-25 material showed a combination of rosette shaped (VPD morphology) agglomerates and isolated platelets (VPO morphology) as shown in figure 3.5a and 3.5b respectively. Selected area diffraction patterns (figure 3.5c) obtained at normal incidence to the isolated platelets always gave a characteristic geometry pattern which could be indexed to the [001] $VOHPO_4.0.5H_2O$ direction. An isolated platelet of residual disordered material shows some evidence of surface pitting or internal porosity as shown in figure 3.5d.
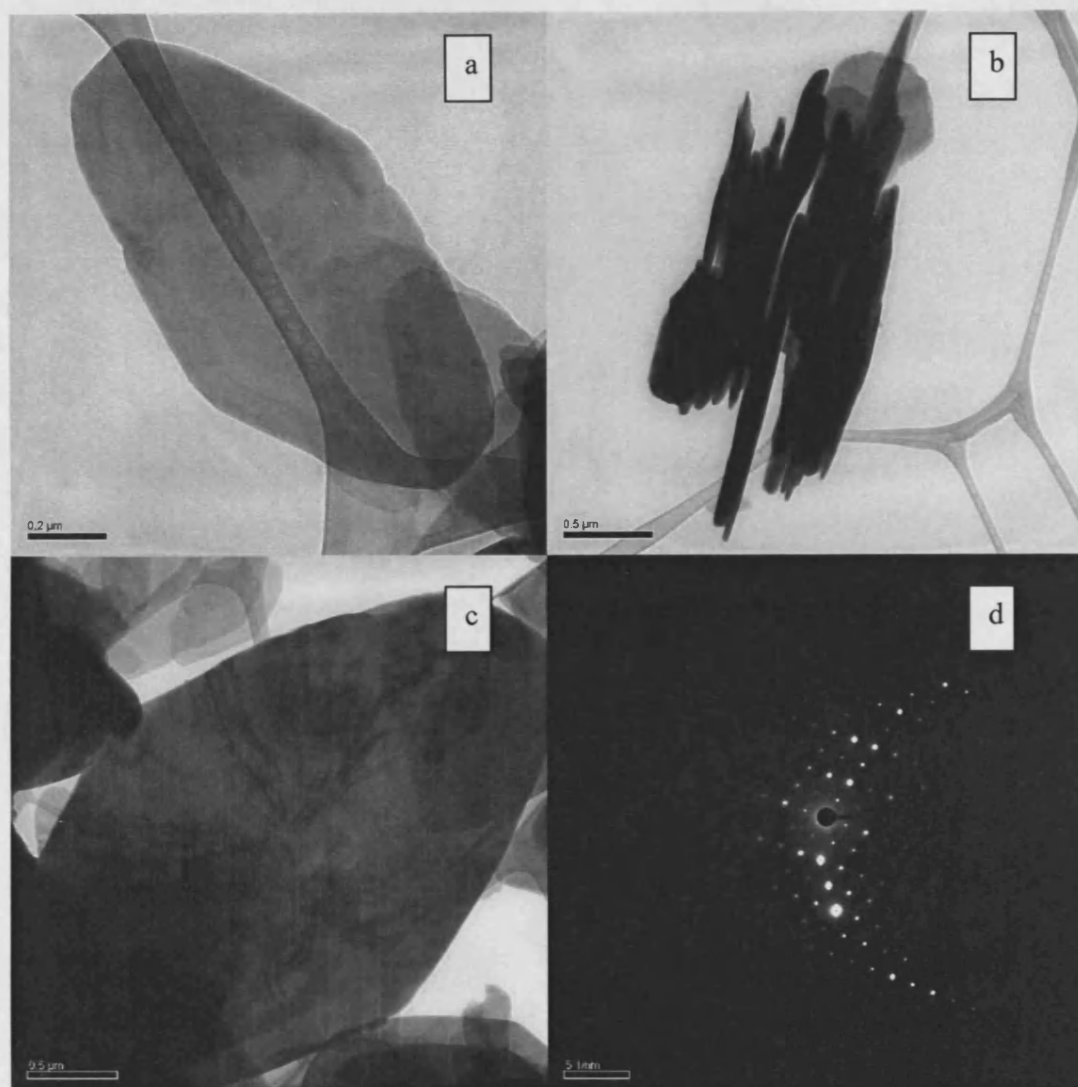
Fig. 3.6 The TEM of B-50 material

TEM micrographs obtained from the B-50 material is shown in figure 3.6a. It displays that isolated platelet of $VOHPO_4.0.5H_2O$ shows the characteristic tombstone morphology. Lattice image, such as shown in figure 3.6b, was obtained from the individual edge-on platelets. Image of a single crystal platelet of $VOHPO_4.0.5H_2O$ is shown in figure 3.6c. Selected area diffraction patterns (figure 3.6d) obtained at normal incidence to the platelets always gave a

characteristic geometry pattern which could be indexed to the [001] $VOHPO_4.0.5H_2O$ direction.
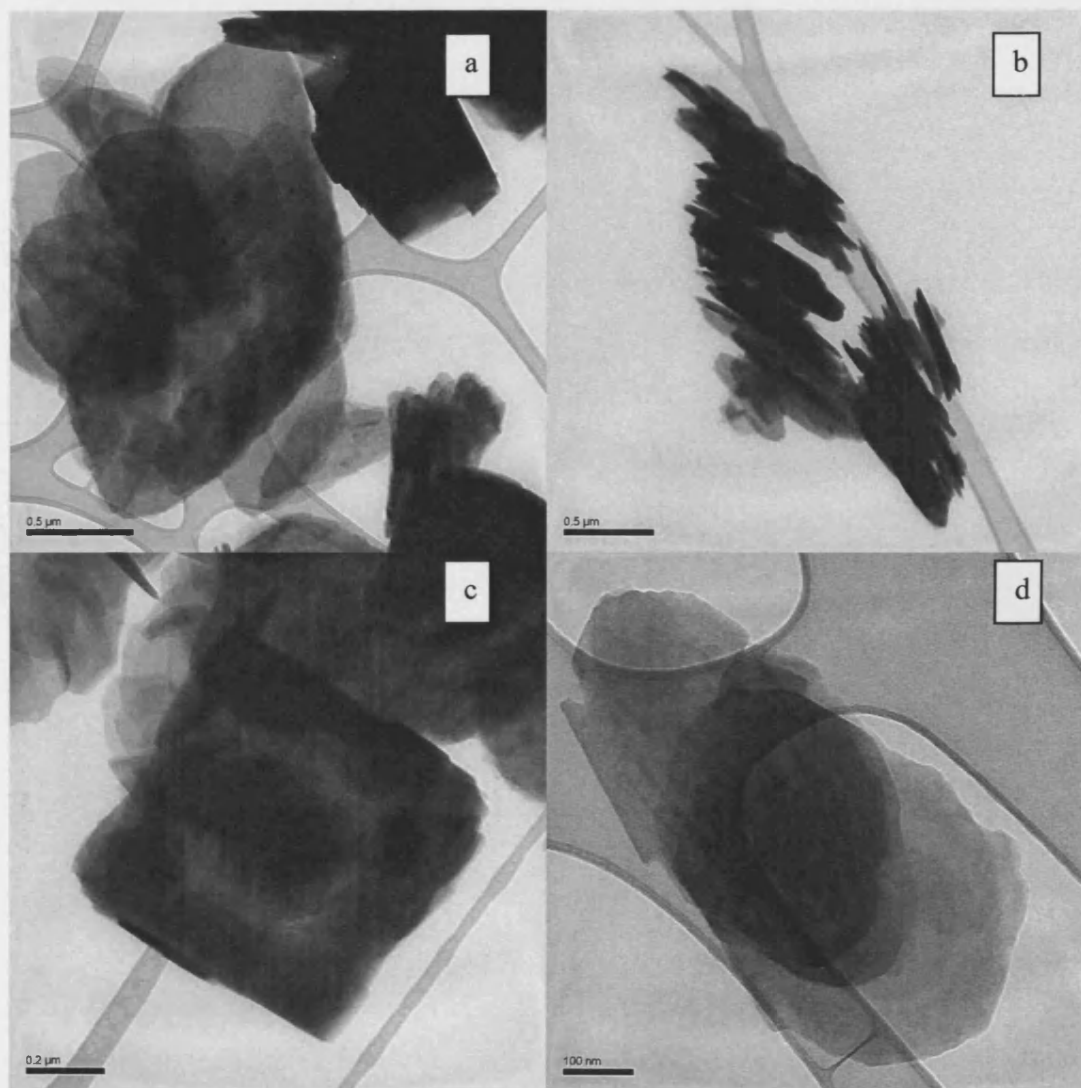
Fig. 3.7 The TEM of B-100 material

Two distinct morphologies are clearly observed in this micrograph (figure 3.7a) which are tombstone-like $VOHPO_4.0.5H_2O$ platelets and blocky $VO(H_2PO_4)_2$ phase crystallites. Lattice image, such as shown in figure 3.7b, was obtained from the individual edge-on platelets. A second trace amount of blocky crystal of $VO(H_2PO_4)_2$ seen in the material is shown in figure

3.7c. Further, some rare platelets of residual disordered material were also observed as shown in figure 3.7d.
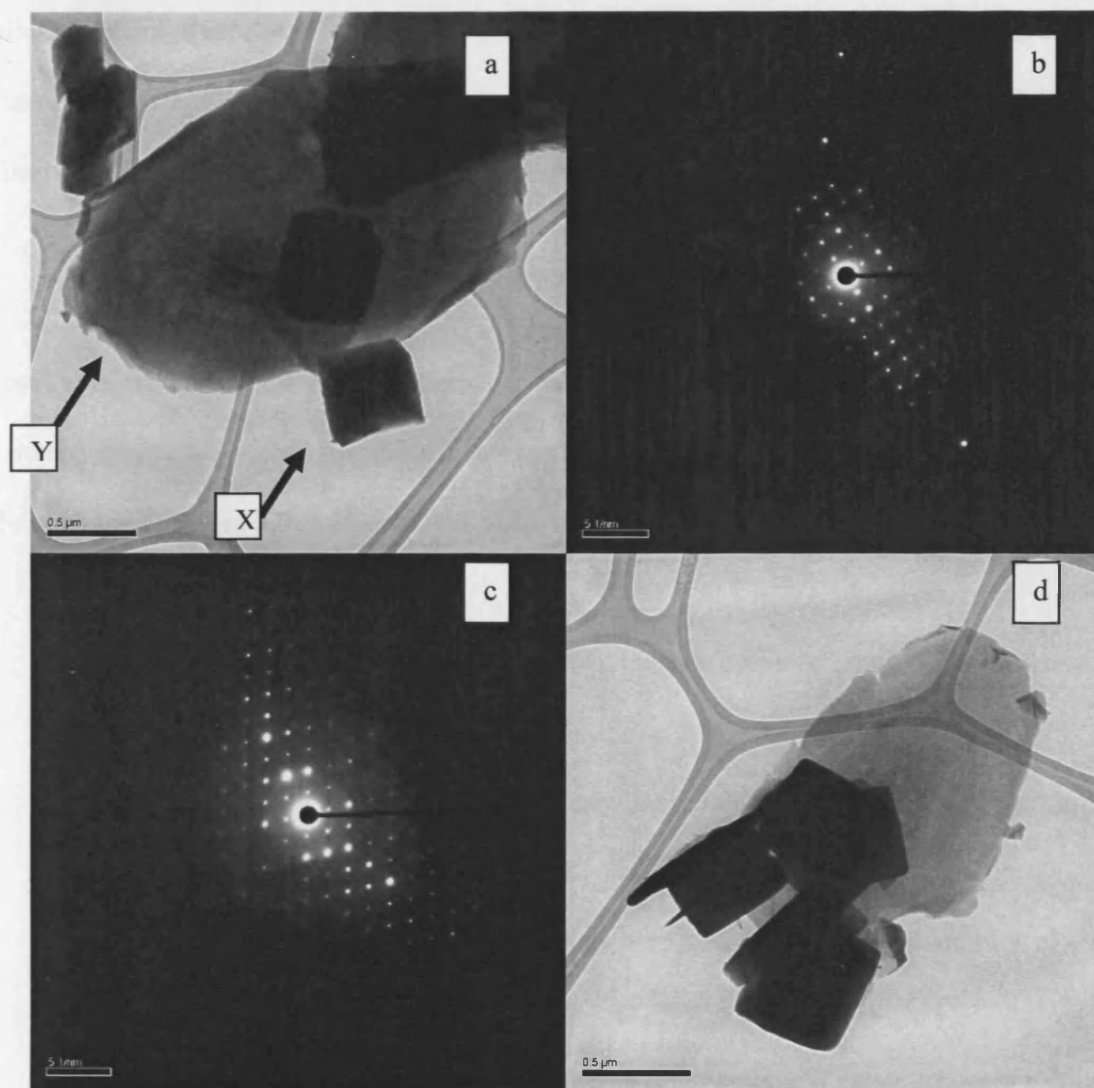
Fig. 3.8 The TEM of B- 400material

TEM examination of the B- 400 material showed a combination of blocky $VO(H_2PO_4)_2$, (X) crystals and some crystalline $VOHPO_4.0.5H_2O$ platelets (Y) as shown figure 3.8a. Selected area diffraction patterns (figure 3.8b) obtained at normal incidence to the cube face of crystal X always gave a characteristic geometry pattern which could be indexed to the [110] direction of

$VO(H_2PO_4)_2$. Based on the selected area diffraction pattern in the platelet at normal direction of crystal Y (in figure 3.8a) which corresponds to the [001] direction of $VOHPO_4.0.5H_2O$. Micrograph of figure 3.8d shows that B- 400 material has a mixture of residual platelet of disordered material and blocky crystallites. Therefore, three distinct morphologies are clearly observed in this material which is platelet, disordered platelet and blocky crystal.

Finally, heptane, dodecane and hexadecane were used for this investigation. The relationship between morphology changes and the amount of alkane used are shown in Table 3.2. These changes are shown in XRD, Raman and SEM, corresponding to the following Appendix.

(1) Appendix 3.1 - The XRD patterns of new materials prepared using different amount of (0, 25, 50 and 100 ml) heptane solvent

(2) Appendix 3.2 - The Raman spectrum of new materials prepared using different amount of (0, 25, 50 and 100 ml) heptane solvent

(3) Appendix 3.3 - The SEM of new materials prepared using different amount of (0, 25, 50 and 100 ml) heptane solvent

(4) Appendix 3.4 – The XRD patterns of new materials prepared using different amount of (10, 25, 50 and 100 ml) dodecane solvent

Table 3.2 The relationship between morphology changes and amount of alkane used

Solvent type	Amount of solvent (ml)	XRD (phases)	Raman (main frequency)	SEM (morphologies)
Heptane	25	$VOHPO_4.0.5H_2O$ (platelet, rosette)	$VOHPO_4.0.5H_2O$	platelet, rosette
Heptane	50	$VOHPO_4.0.5H_2O$ (platelet, rosette)	$VOHPO_4.0.5H_2O$	platelet, rosette
Heptane	75	$VOHPO_4.0.5H_2O$	$VOHPO_4.0.5H_2O$	platelet
Heptane	100	$VOHPO_4.0.5H_2O$	$VOHPO_4.0.5H_2O$	platelet
Dodecane	10	$VOHPO_4.0.5H_2O$ (platelet, rosette)	$VOHPO_4.0.5H_2O$	platelet
Dodecane	25	$VOHPO_4.0.5H_2O$ (platelet, rosette)	$VOHPO_4.0.5H_2O$	platelet
Dodecane	50	$VO(H_2PO_4)_2$	$VOHPO_4.0.5H_2O$	platelet
Dodecane	100	$VOHPO_4.0.5H_2O$, $VO(H_2PO_4)_2$	$VO(H_2PO_4)_2$	blocky
Hexadecane	10	$VOHPO_4.0.5H_2O$ (platelet, rosette)	$VOHPO_4.0.5H_2O$	platelet
Hexadecane	25	$VOHPO_4.0.5H_2O$ (platelet, rosette)	$VOHPO_4.0.5H_2O$	platelet
Hexadecane	50	$VOHPO_4.0.5H_2O$, $VO(H_2PO_4)_2$	$VOHPO_4.0.5H_2O$	blocky
Hexadecane	75	$VO(H_2PO_4)_2$	$VO(H_2PO_4)_2$	blocky
Hexadecane	100	$VO(H_2PO_4)_2$	$VO(H_2PO_4)_2$	blocky

When alonger chain alkane (dodecane, hexadecane) were used, the same changes were observed but these changes were observed using smaller amounts of higher boiling temperature alkane. A mixture of VPD and VPO type materials were obtained when 10 ml of hexadecane or dodecane solvent was used. These changes have shown in XRD patterns with (220) and (001) as the main peaks of the materials (Appendix 3.7 and Appendix 3.4), the peaks are assigned to mixture of rosette and platelet morphology of the materials, but SEM (Appendix 3.9 and Appendix 3.6) only indicated that materials have platelet morphology. Further, mixture of rosette and platelet morphology of the material were obtained by using 25 ml of octane solvent that indicating, longer chain alkanes (dodecane, hexadecane) switch the morphology of these materials with smaller amounts of alkane solvent as compared with short chain alkane solvent (octane, heptane). Additionally, in the case of heptane solvent, these changes were observed with using high amount of heptane solvent and SEM (Appendix 3.3) of the material clearly indicated that mixture of rosette and platelet morphology was observed when 25 and 50 ml of heptane was introduced. Surface area of these materials gave same results that platelet morphology materials were between 8-16 m^2/g and blocky or chunky morphology materials were between1-3 m^2/g. However, the surface area of the mixture of platelet and rosette morphology materials was higher than of other materials; 18-32 m^2/g.

In the absence of an alkane $VOPO_4.2H_2O$ is reduced to $VOHPO_4.0.5H_2O$ in VPD preparation method. Furthermore, different morphology materials can be obtained when adding of different amount of alkane solvent. Addition of larger amounts of alkane switches to $VO(H_2PO_4)_2$ whereas, low amounts of alkane leads to $VOHPO_4.0.5H_2O$.

Morphology changes were obtained when changing the amount of alkane solvents while keeping the same amount of $VOPO_4.2H_2O$ (1 g) and 1-butanol (25 ml), therefore four variables were involved in these preparations. These are reaction temperature, V: alcohol mole ratio, total volume and alcohol: alkane volume ratios.

To try and determine the key influences on the changes, two sets of experiments were carried out to investigate the effect of adding alkane into the reaction. Firstly, the V: alcohol mole ratio and alcohol: alkane volume ratios were changed with keeping the same total volume. Second one is keeping the same V: alcohol (1:50 mole) mole ratio and total volume while changing the alcohol: alkane volume ratio.

First set of experiments details are shown in table 3.3. The XRD and SEM of new materials prepared using different amount of 1-butanol (175, 170, 160. 150, 125, 75, 50, 25, 5 and 0 ml) and octane solvent are shown in figure 3.9 and 3.10 respectively.

Table 3.3 - Experimental details of material prepared using different amount of 1-butanol and octane solvent with $VOPO_4.2H_2O$ (1 g)

| Material name	Mass of $VOPO_4.2H_2O$ (g)	V:OH mole ratio	1-Butanol (ml)	Octane (ml)
B1-175	1	1:350	175	0
B1-170	1	1:340	170	5
B1-160	1	1:320	160	15
B1-150	1	1:300	150	25
B1-125	1	1:250	125	50
B1-75	1	1:150	75	100
B1-50	1	1:100	50	125
B1-25	1	1:50	25	150
B1-5	1	1:20	5	170
B1-0	1		0	175
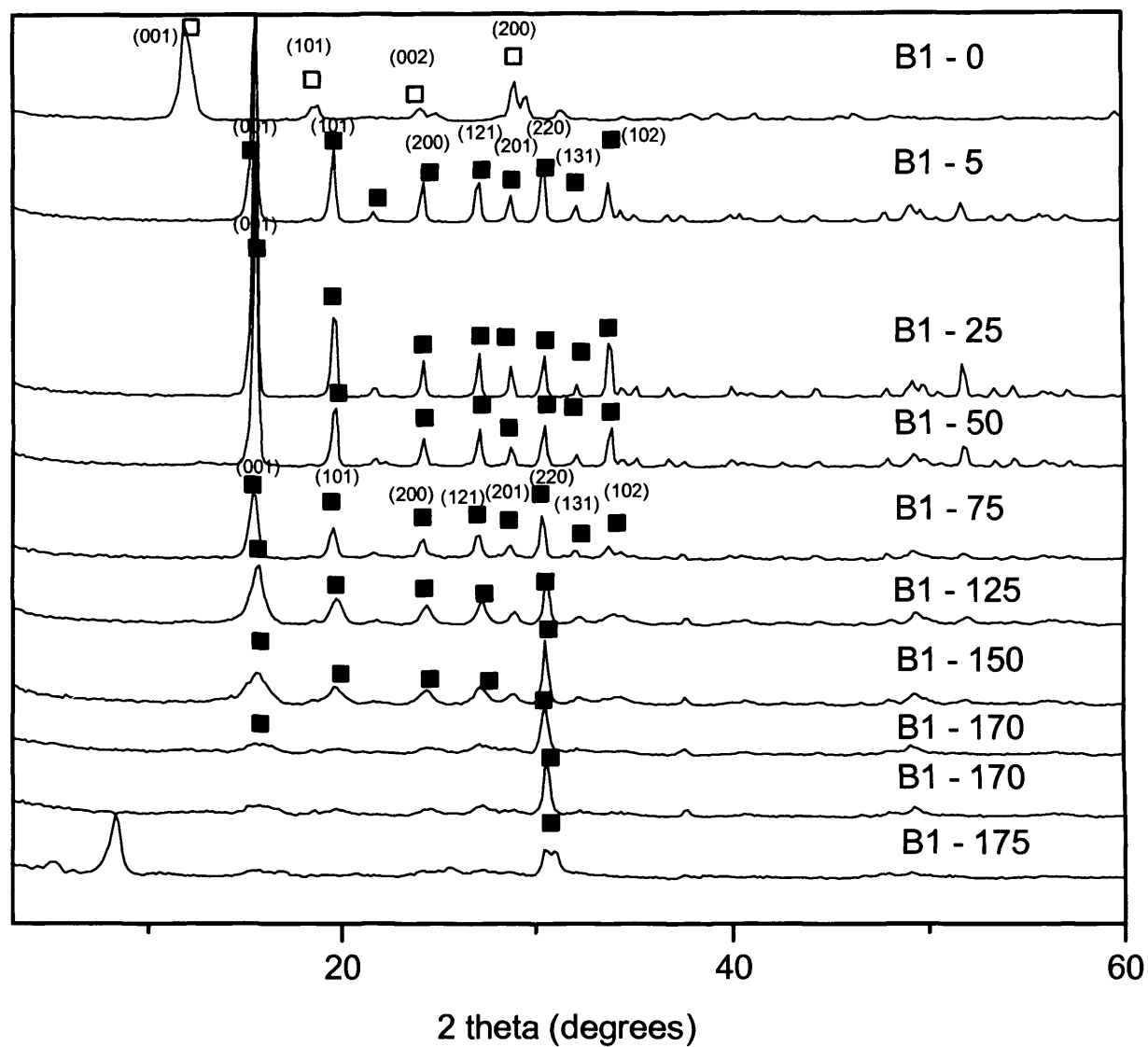
Fig. 3.9 The XRD of new materials prepared using different amount of 1-butanol and octane

solvent. Key ■ = $VOHPO_4.0.5H_2O$; □ = $VOPO_4.2H_2O$

The XRD patterns of materials (figure 3.9) prepared using different amount of V: alcohol mole ratio and octane solvent and the same total volume (175 ml), illustrate that the material obtained without the addition of alkane (B1-175) shows the XRD pattern $VOHPO_4.0.5H_2O$ with (220) as the main reflection. But, SEM shows that material did not give rosette morphology (figure 3.10). When small amounts of octane are added into the preparation there is a decrease in the intensity of the (220) reflection and an increase in the intensity of the (001) reflection (5, 25, 50, 100, 125 and 150 ml), indicating that there is a switch from mixture of $VOHPO_4.0.5H_2O$ (rosette) and $VOHPO_4.0.5H_2O$ (platelet) type to VPO (platelet) type morphology.
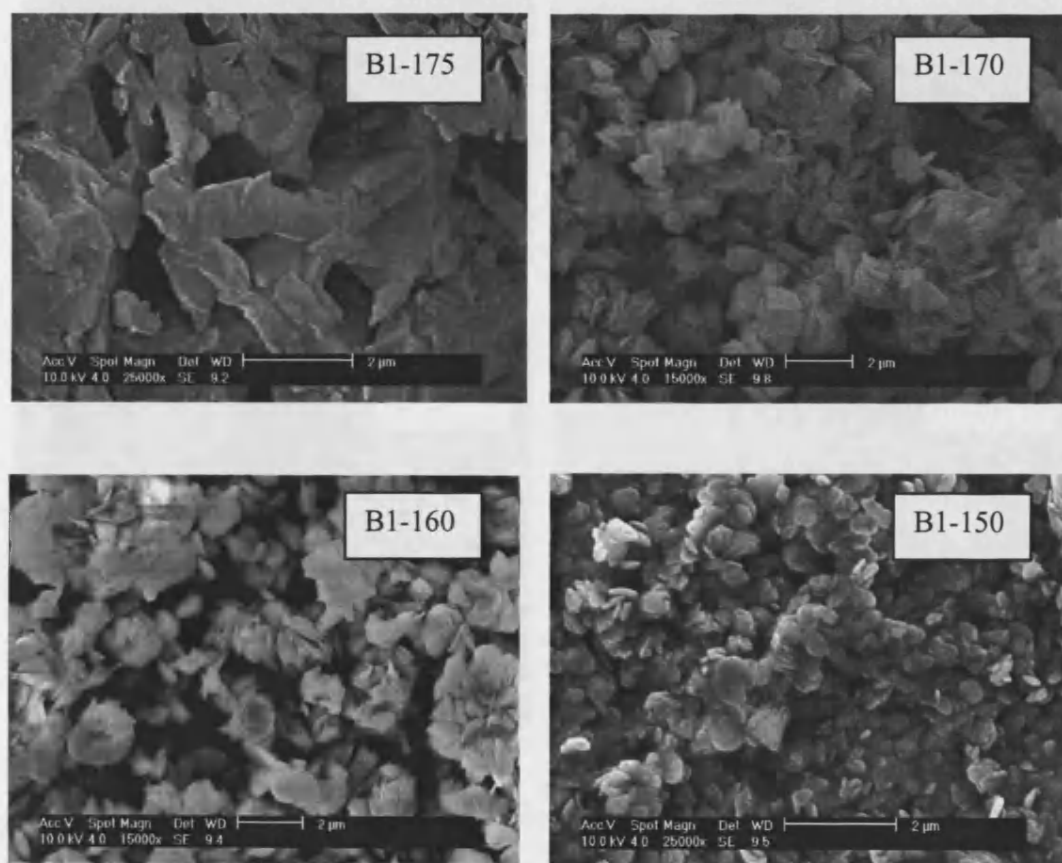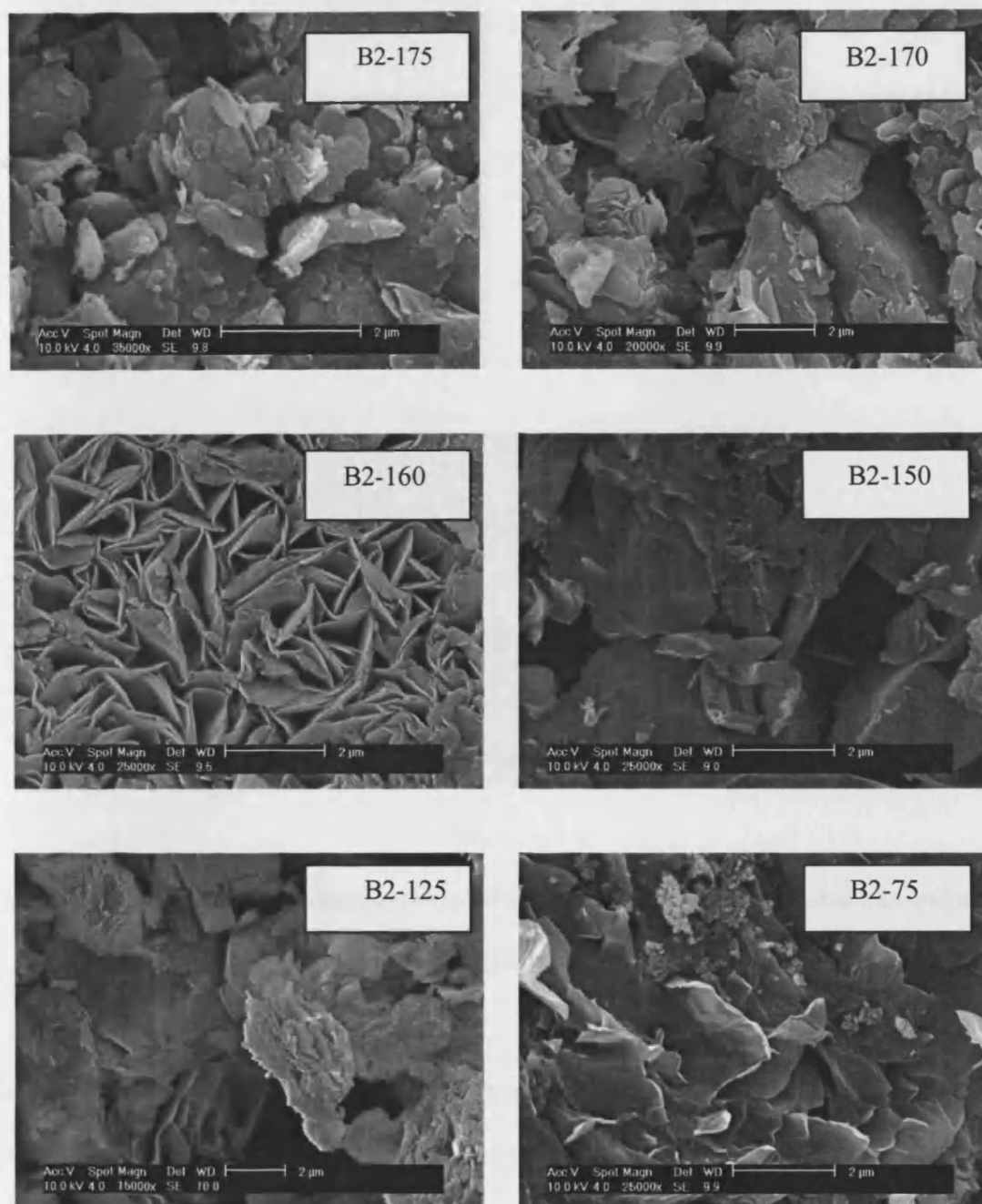

Fig. 3.10 The XRD of new materials prepared using different amount of 1-butanol and octane solvent
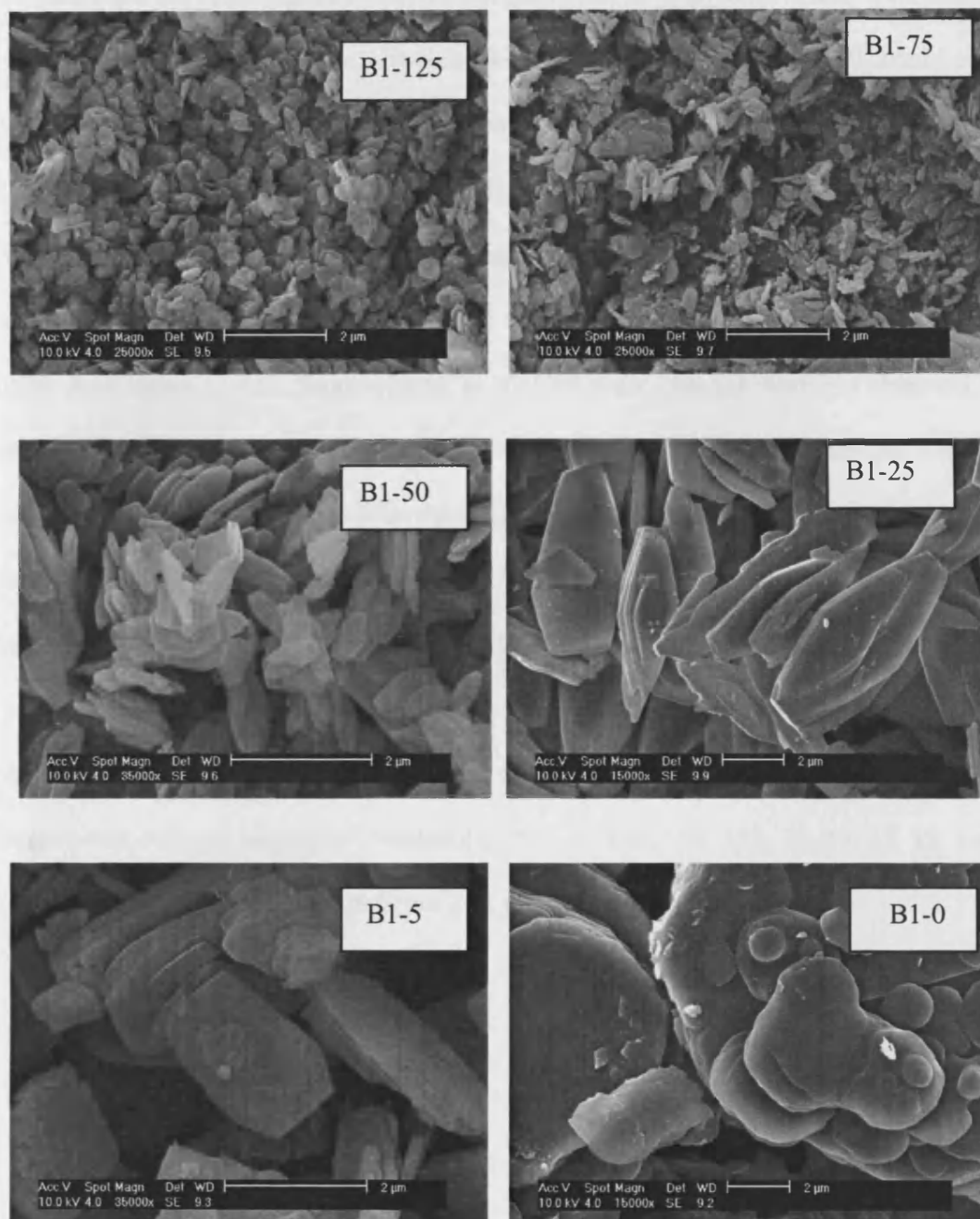
Fig. 3.10 The XRD of new materials prepared using different amount of 1-butanol and octane

solvent

This is shown in the SEM (figure 3.10) of these materials, with the B1-170 and B1-160 sample

showing both rosettes and platelets, whereas B1-150, B1-125, B1-75 and B1-50 consist only of

thin platelets. The SEM shows that the platelets become thicker as more octane is added (B1-

25). Therefore, morphology changes were obtained by changing the amount of octane and

alcohol. The reaction temperature was measured for all these experiments and it was $\approx 118°C$.

Furthermore, when higher boiling temperature alcohols were used or when $VOHPO_4.0.5H_2O$

samples were heated in the alkane without an alcohol these changes were not observed. This

implies that the reaction temperature does not influence the reaction mechanism. Therefore,

V:alcohol mole ratio or alcohol: octane volume ratio may be an influence in these morphology

changes. So, the the next experiment was carried out with constant V:alcohol mole ratio (1:50)

and a constant total volume with changing the alcohol:octane volume ratio.

Second set of experiments details are shown in table 3.4. The XRD and SEM of new materials

prepared using different amount of 1-butanol (175, 170, 160. 150, 125, 75, 50, 25, 15, 5 and 0

ml) and octane solvent are shown in figure 3.11 and 3.12 respectively.

Table 3.4 Experimental details of material prepared using different amounts of 1-butanol and

octane solvent with $VOPO_4.2H_2O$ (V: alcohol = 1:50)

| Material name	Mass of $VOPO_4.2H_2O$ (g)	V:OH mole ratio	1-Butanol (ml)	Octane (ml)
B1-175	7	1:50	175	0
B2-170	6.75	1:50	170	5
B2-160	6.5	1:50	160	15
B2-150	6	1:50	150	25
B2-125	5	1:50	125	50
B2-75	3	1:50	75	100
B2-50	2	1:50	50	125
B2-25	1	1:50	25	150
B2-15	0.6	1:50	15	160
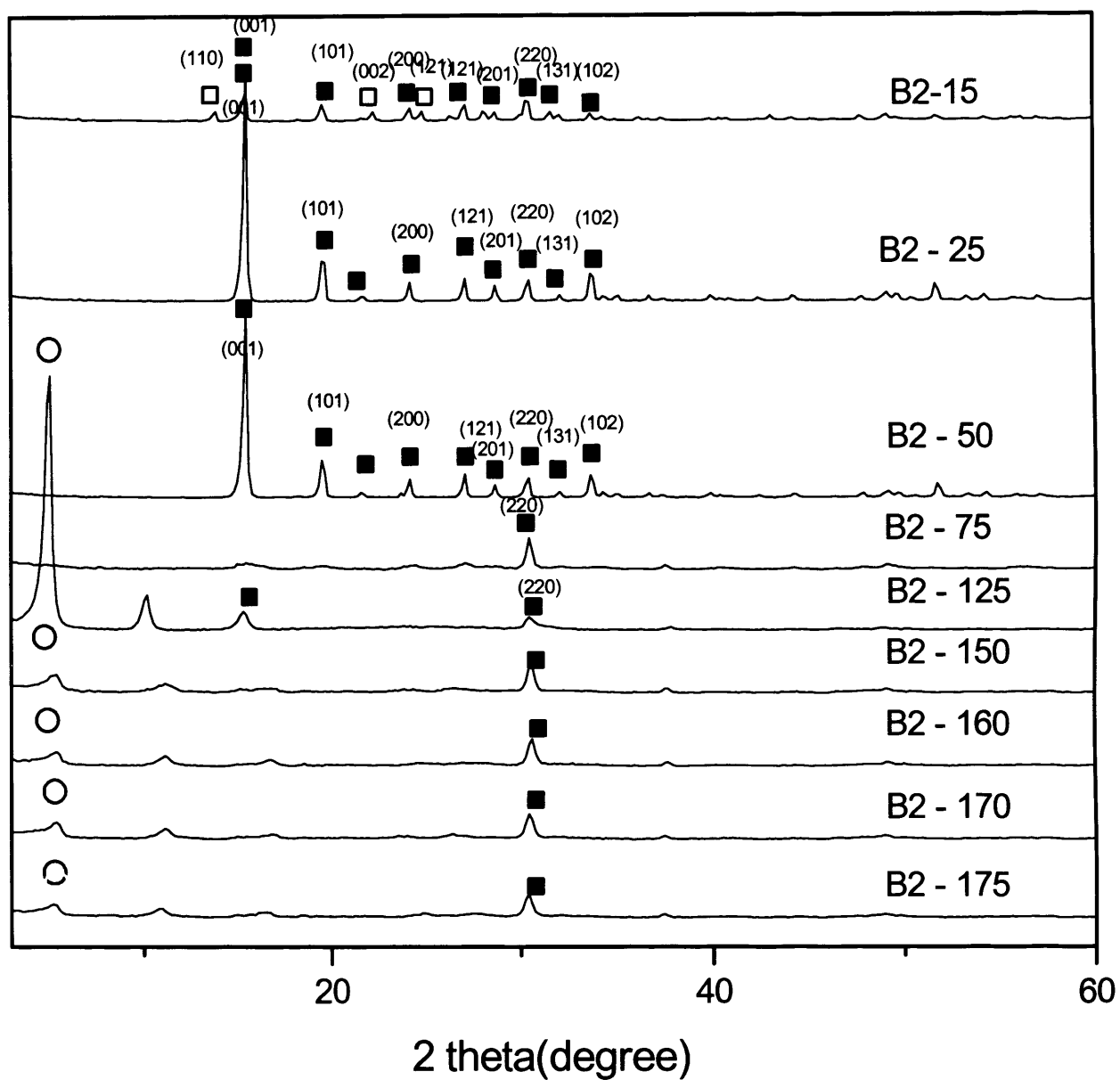
Fig. 3.11 The XRD of new materials prepared using different amount of 1-butanol and octane

solvent. Key ■ = VOHPO$_4$.0.5H$_2$O; □ = VO(H$_2$PO$_4$)$_2$; VOPO$_4$ intercalates = O

Fig. 3.12 The XRD of new materials prepared using different amount of 1-butanol and octane
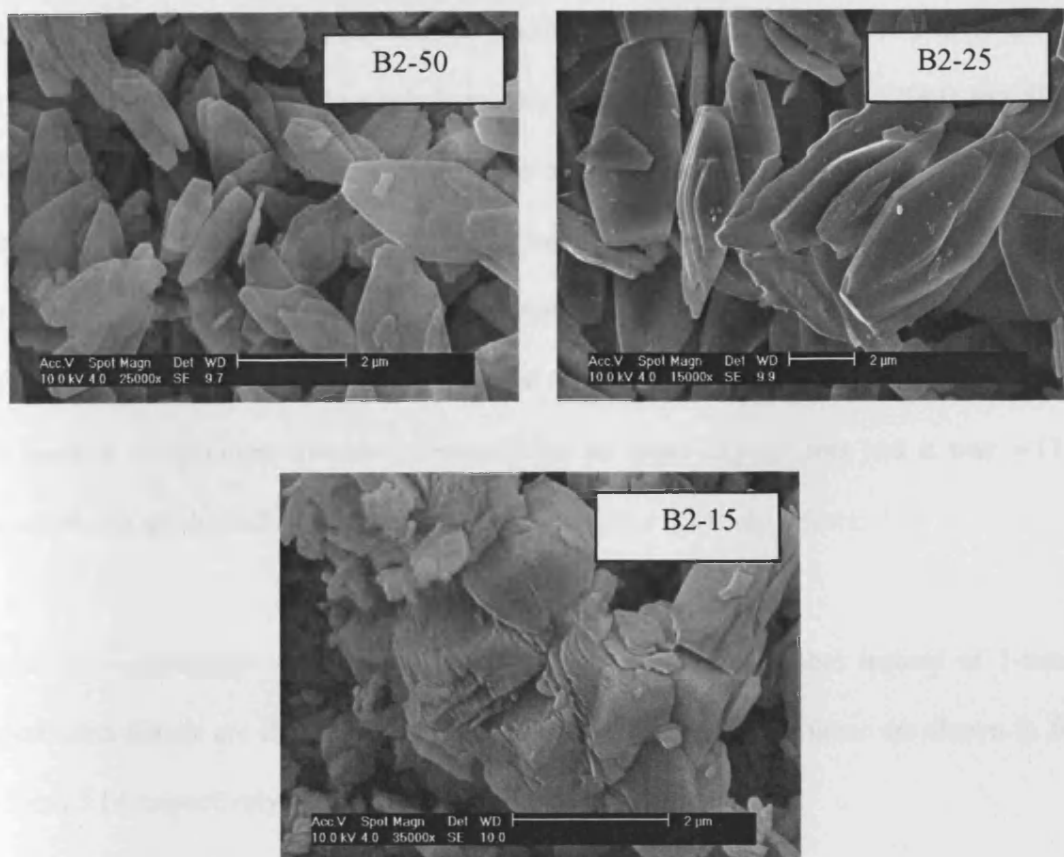
solvent

Fig. 3.12 The XRD of new materials prepared using different amount of 1-butanol and octane

solvent

The XRD patterns of materials (figure 3.11) prepared using different amount of 1-butanol and

octane solvent with the same V:alcohol mole ratio (1:50) and the same total volume, show

those materials (B2-175 to B2-75) have [220] reflection is the most dominant feature in the

sample and additionally higher d-space (16.612 Å) peak also was present in these materials at

two theta five , this indicates that $VOPO_4 \cdot 2H_2O$ may be intercalated by 1-butanol. The

observed result differs when compared with previous results.[14] Where the standard

$VOHPO_4 \cdot 0.5H_2O$ has only one main peak in the XRD pattern. It may be mixture of

VOHPO$_4$·0.5H$_2$O and VOPO$_4$ intercalates. Furthermore, SEM (figure 3.12) of these materials did not show any well defined morphology which is platelet or rosette. The XRD and SEM of B2-50 and B2-25 indicate that materials have platelet morphology but the size of these platelets is different; where platelets of B2-25 are bigger than B2-50 plates. The XRD of B2-15 shows that material has VO(H$_2$PO$_4$)$_2$ as the major phase. Therefore, VOHPO$_4$·0.5H$_2$O phase switching to VO(H$_2$PO$_4$)$_2$ phase were obtained by changing the alcohol:octane volume ratio. The reaction temperature was also measured for all these experiments and it was ≈118°C. Therefore, the alcohol:alkane volume ratio is a key factor for these effects.

The above experiments were repeated using 1-octanol as the alcohol instead of 1-butanol. Experiments details are shown in Table 3.5. The XRD and SEM of these are shown in figure 3.13 and 3.14 respectively.

Table 3.5 Experimental details of material prepared using different amount of 1-octanol and

octane solvent with $VOPO_4.2H_2O$ (1 g)

| Material name	Mass of $VOPO_4.2H_2O$ (g)	V:OH mole ratio	1-Octanol (ml)	Octane (ml)
O1-175	1	1:175	175	0
O1-160	1	1:160	160	15
O1-150	1	1:150	150	25
O1-135	1	1:135	135	40
O1-125	1	1:125	125	50
O1-100	1	1:100	100	75
O1-75	1	1:75	75	100
O1-50	1	1:50	50	125
O1-40	1	1:40	40	135
O1-15	1	1:15	15	160
O1-0	1	-	0	175
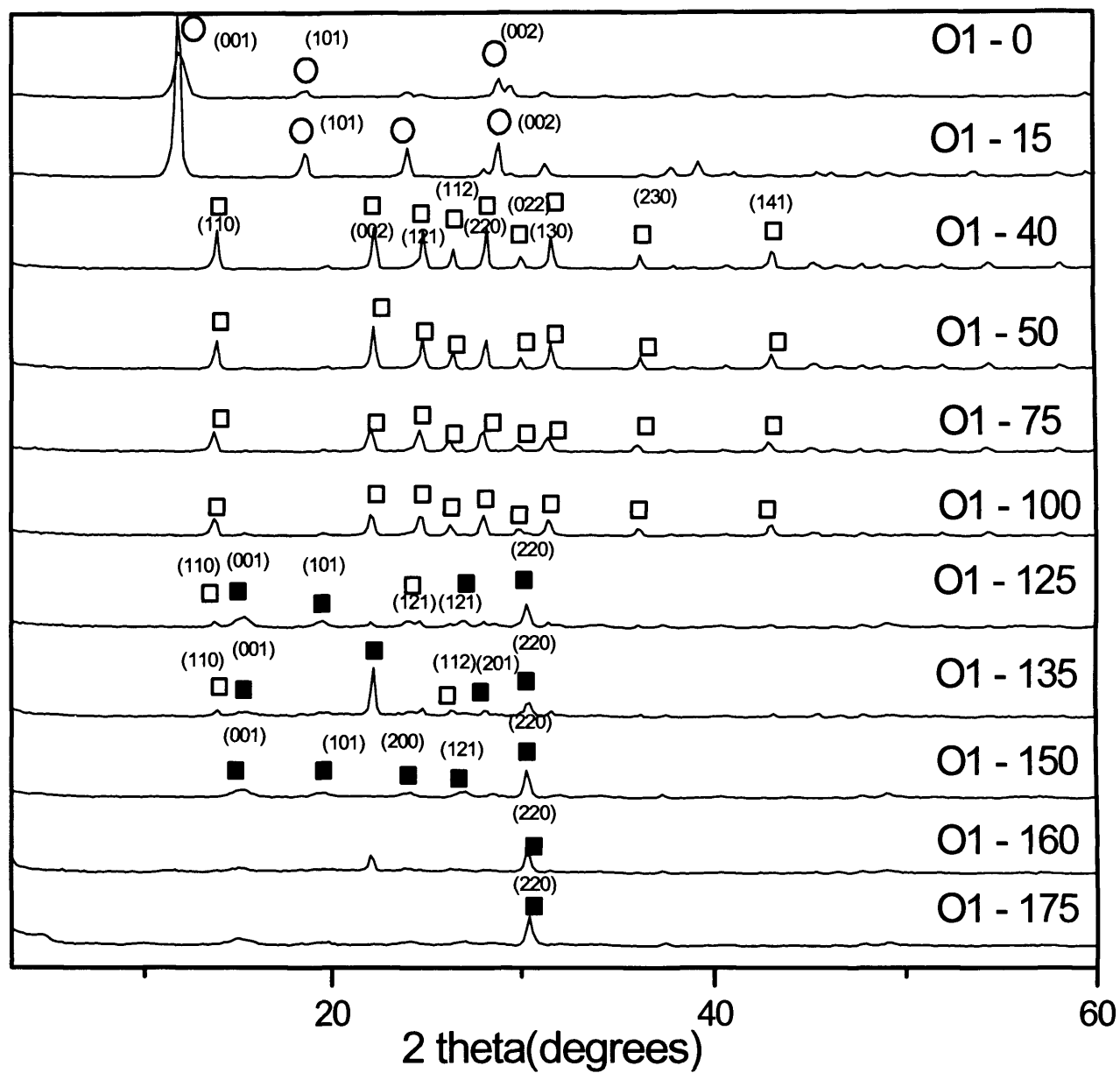
Fig. 3.13 The XRD of new materials prepared using different amount of 1-octanol and octane

solvent. Key ■ = VOHPO₄.0.5H₂O; □ = VO(H₂PO₄)₂ ; VOPO₄ .2H₂O = O
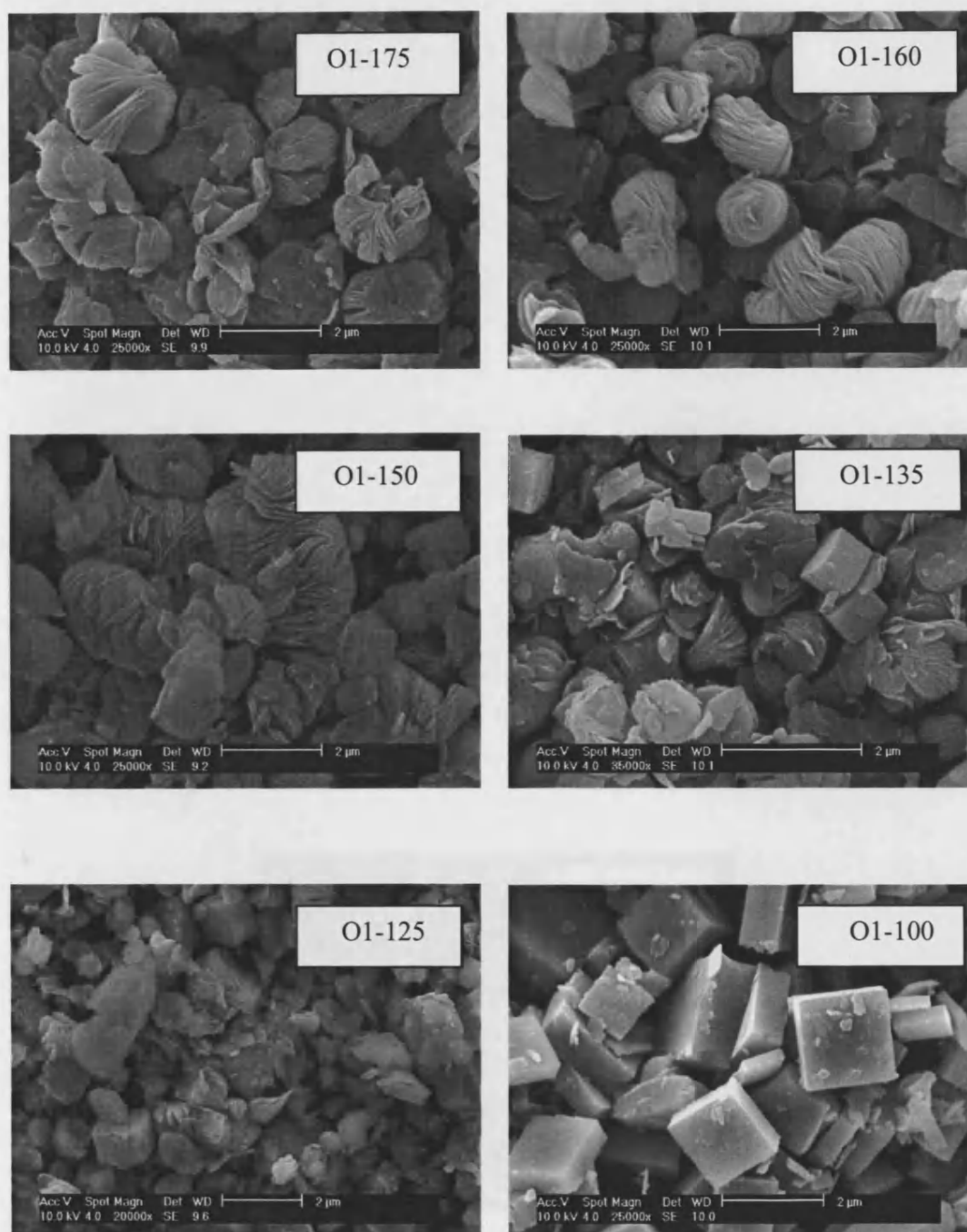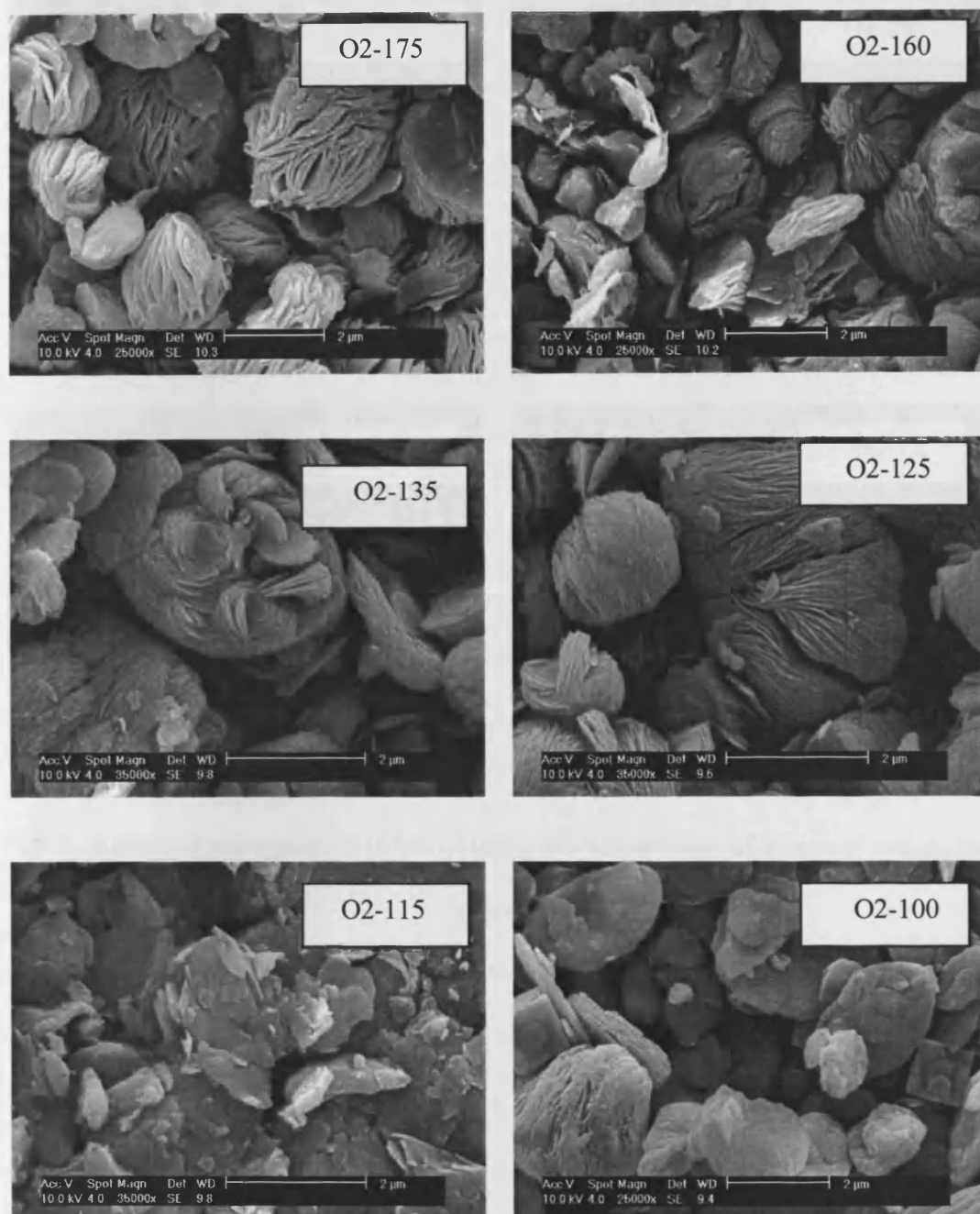
Fig. 3.14 SEM of new materials prepared using different amount of 1-octanol and octane
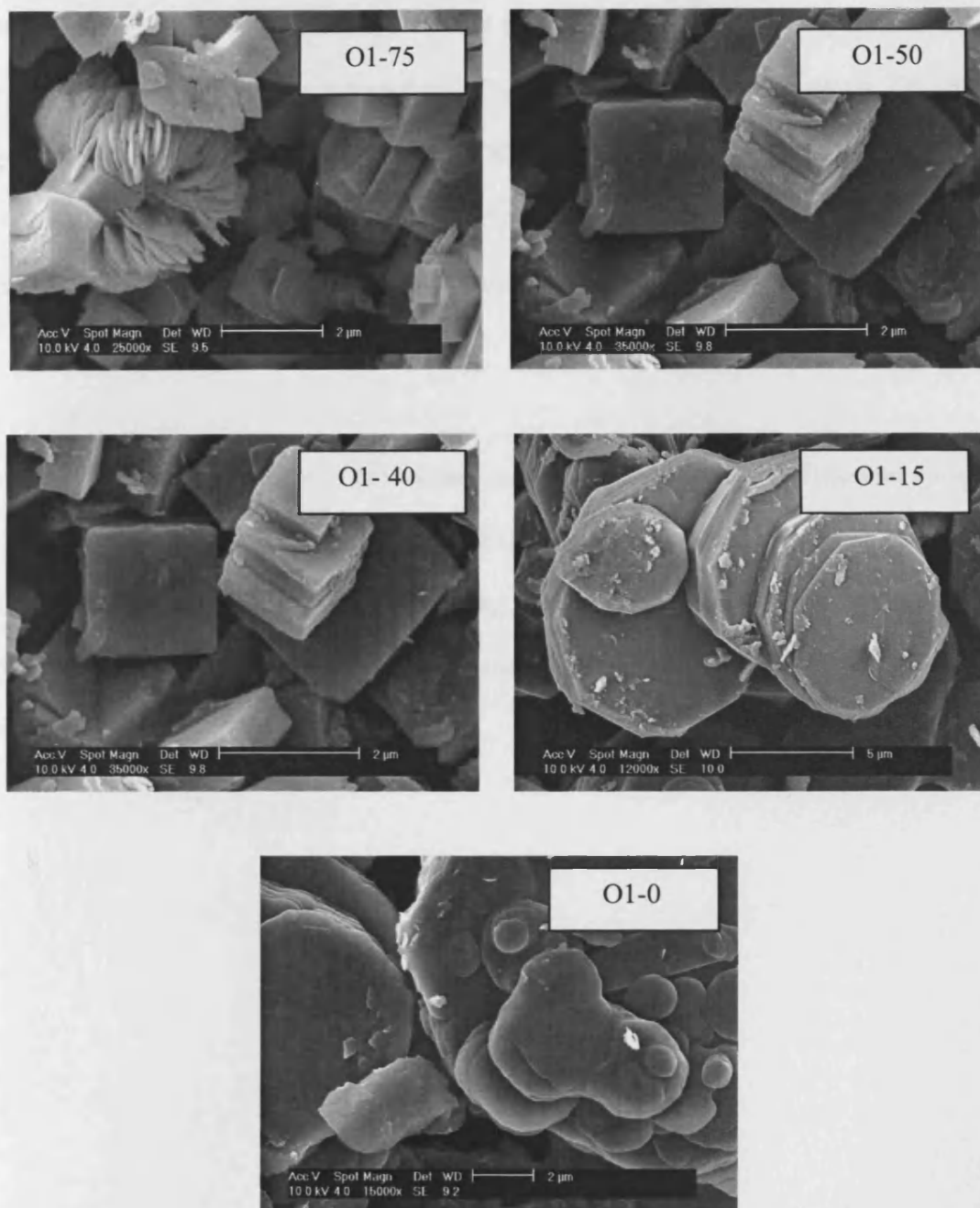
solvent

Fig.3.14 SEMof new materials prepared using different amount of 1-octanol and octane solvent

When 1-octanol was replaced with 1-butanol morphology changes were observed. The XRD patterns obtained for O1-175, O1-160 and O1-150 showed that $VOHPO_4.0.5H_2O$ was the only

phase (figure 3.13). SEM of these materials in figure 3.14 show that all preparations led to a mixture of platelet and rosette morphology. The XRD patterns of the materials, O1-135 and O1-125 in figure 3.13, show a mixture of $VOHPO_4.0.5H_2O$ and $VO(H_2PO_4)_2$. Materials O1-100 to O1-40 have characteristic of $VO(H_2PO_4)_2$, by XRD. For all these experiments, the V:alcohol mole ratio and alcohol: alkane volume ratios were different.

Therefore, the next experiments were carried out with keeping the same V:alcohol mole ratio while changing alcohol: alkane volume ratio. Experiments details are shown in Table 3.6. The XRD and SEM of new materials prepared using different amount of 1-octanol (175, 160. 150, 135, 125, 115, 100, 75, 50, 40, 15 and 0 ml) and octane solvent are shown in figure 3.15 and 3.16 respectively.

Table 3.6 Experimental details of material prepared using different amount of 1-octanol and

octane solvent with $VOPO_4.2H_2O$ (V:alcohol = 1:50)

Material name	Mass of $VOPO_4.2H_2O$ (g)	V:OH mole ratio	1-Octanol (ml)	Octane (ml)
O2-175	3.5	1:50	175	0
O2-160	3.2	1:50	160	15
O2-135	2.75	1:50	135	40
O2-125	2.5	1:50	125	50
O2-115	2.3	1:50	115	60
O2-100	2	1:50	100	75
O2-75	1.5	1:50	75	100
O2-50	1.0	1:50	50	125
O2-40	0.8	1:50	40	135
O2-15	0.3	1:50	15	160
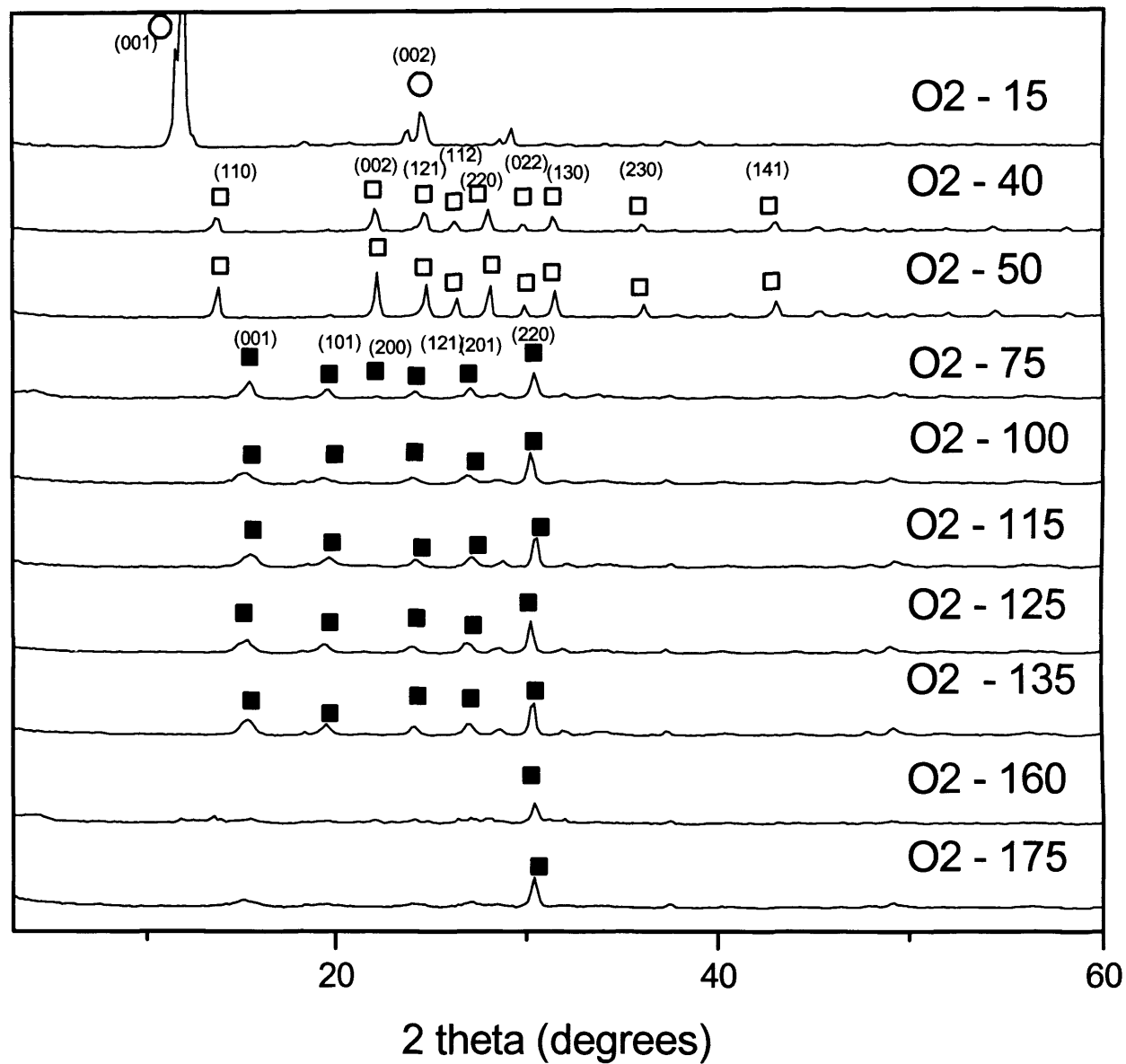
Fig. 3.15 The XRD of new materials prepared using different amount of 1-octanol and octane

solvent. Key ■ = $VOHPO_4.0.5H_2O$; □ = $VO(H_2PO_4)_2$; $VOPO_4 .2H_2O$ = O

Fig. 3.12 SEM of new materials prepared using different amount of 1-octanol and octane
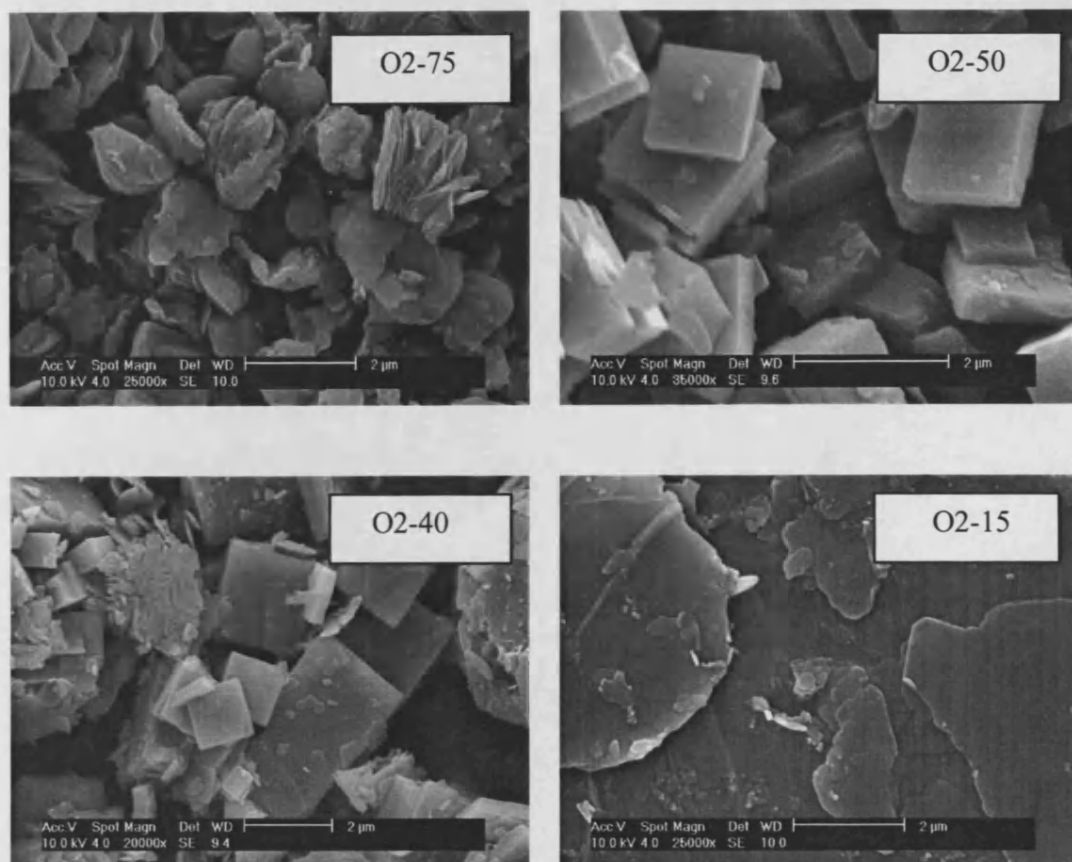
solvent

Fig. 3.16 SEM of new materials prepared using different amount of 1-octanol and octane

solvent

The XRD pattern of (O2-175) in (figure 3.15) shows the (220) as the main reflection and SEM shows that materials have rosette morphology. Materials, O2-160 to O2-75 have characteristic of VOHPO$_4$.0.5H$_2$O as major phase. Therefore, different morphology changes were obtained by changing the alcohol:alkane volume ratio.

Different types of materials can be synthesized when changing the amount of alkane solvent in VPD preparation method. Low amount of alkane solvent gave rosette morphology meanwhile platelet or blocky morphology obtained when increasing the amount of alkane solvent.

3.4 Catalyst testing and characterization

3.4.1 Characterization of catalyst

Characterisation of catalysts after catalyst testing were carried out, precursor was prepared by

reacting of VOPO$_4$.2H$_2$O with 1-butanol and differing amount of octane solvent
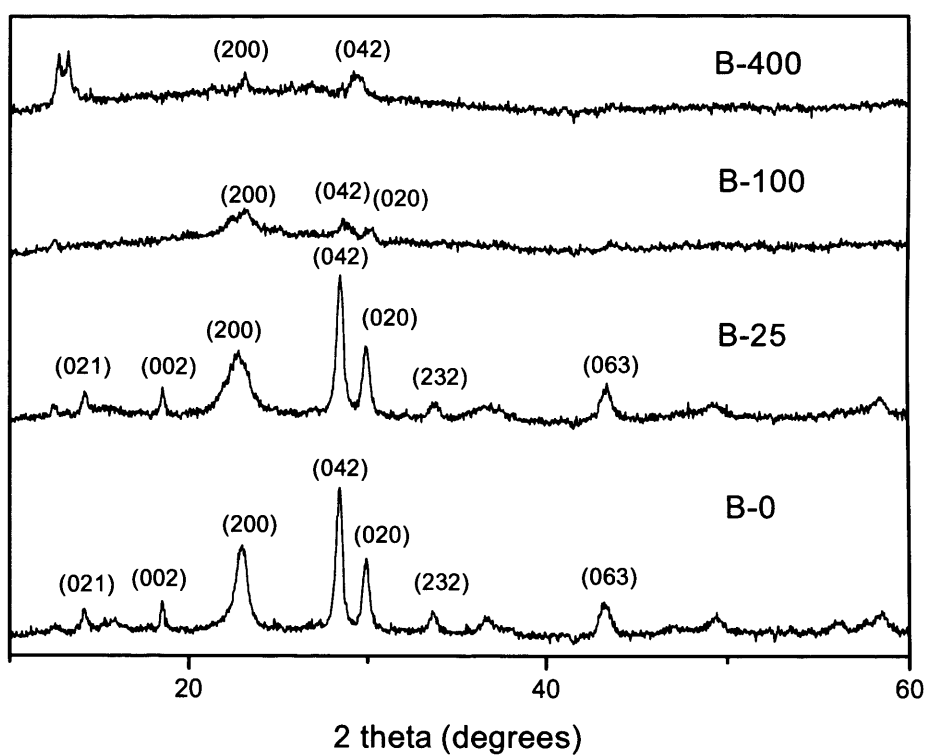
Fig. 3.17 The XRD patterns of final catalysts

The XRD patterns of the catalysts derived from the new preparation route using octane as a co-solvent are shown in figure 3.17. Catalysts obtained from the B-0 and B-25 material gave similar patterns, with all the peaks indexed to $(VO)_2P_2O_7$. But, crystallinity of these final catalysts and intensities of these peaks are different. According to the literature, (200) plane is more active for n-butane oxidation in the final catalyst[2] and (200) reflection is considerably broadened due to a combination of several overlapping peaks (200, 102, 040) with very similar plane spacing (0.386, 0.406 and 0.414 nm respectively). The fact that no characteristic lines from any $VOPO_4$ phases are present in figure 3.17 suggests that such phases are either completely absent or are present at levels below the detection level of the XRD technique. XRD patterns of the final catalyst prepared from the B-100 material suggest that it is poorly crystallized and small number of peaks can be assigned to $(VO)_2P_2O_7$. Catalyst obtained from the B- 400 sample gave different patterns than B-0 and B-25 material, but intensity of (200) plane is very small in the B-400 catalyst.
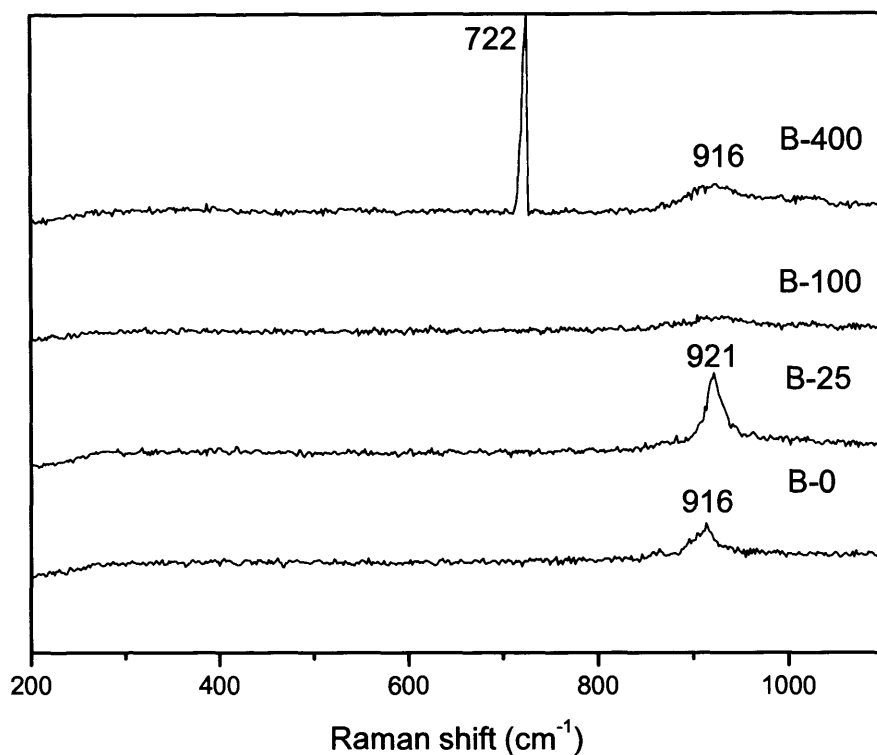
Fig. 3.18 The Raman spectrum of final catalysts

The Raman spectra of catalyst obtained from the B-0 and B-25 sample have a very strong peak at 916 and 921 cm^{-1} respectively as their main feature. This has been assigned to the P-O stretch of $(VO)_2P_2O_7$. Raman band of catalyst obtained from the B- 400 material was observed at 722 cm^{-1} due to the $VO(PO_3)_2$ phase which could result from the transformation of $VO(H_2PO_4)_2$.
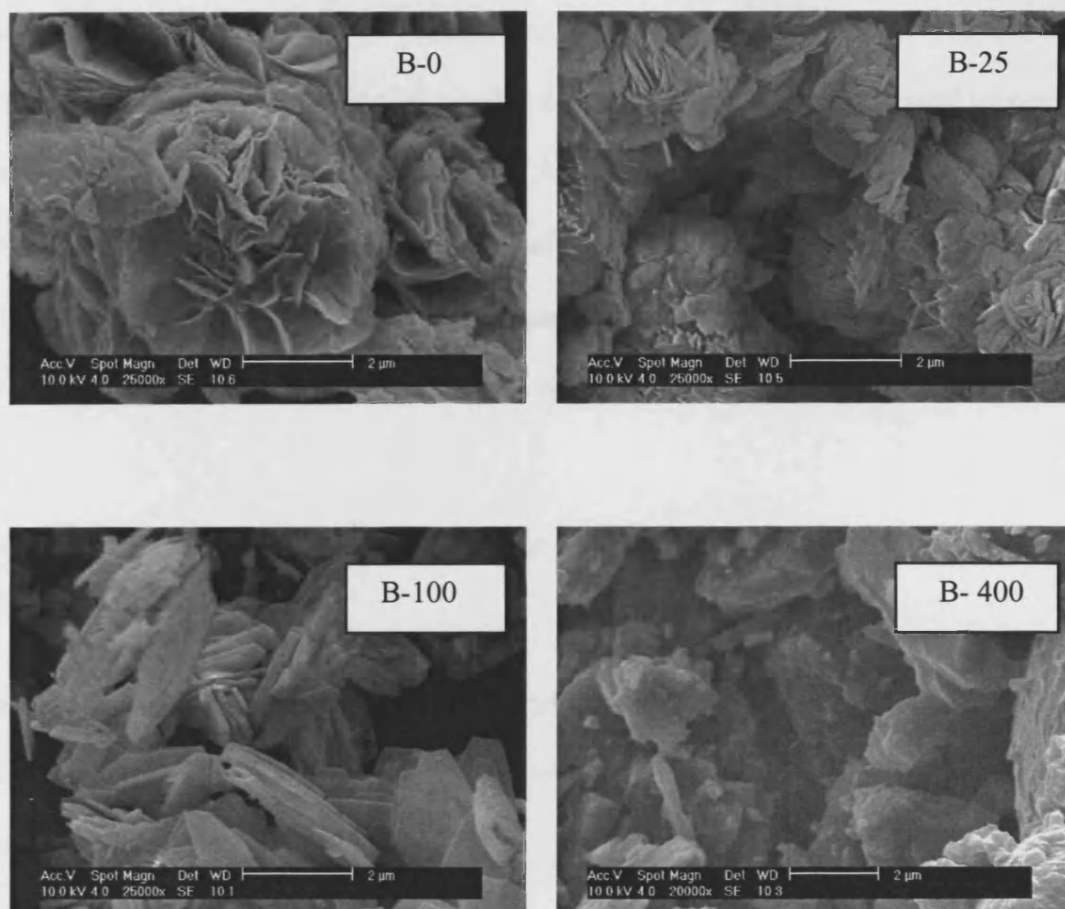
Fig.3.19 The SEM of final catalysts

Figure 3.19 shows an SEM micrograph of the final catalyst. A topotactic transformation has obviously occurred, since the activated material has retained the characteristic platelet morphology (B-100 and B-25) of the precursor material.

3.4.2 Catalyst testing

The oxidation of *n*-butane was carried out in a microreactor with a standard mass of catalyst (0.5 g). *n*-Butane and air were fed to the reactor *via* calibrated mass flow controllers to give a

feedstock composition of 1.5% *n*-butane in air. The products were then fed *via* heated lines to an on-line gas chromatograph for analysis. The reactor comprised a stainless steel tube with the catalyst held in place by plugs of quartz wool. A thermocouple was located in the centre of the catalyst bed and temperature control was typically ±1°C. Carbon mass balances of ≥ 97% were typically observed. Catalyst samples were heated *in situ* (1.5% *n*-butane in air) at 400°C by heating the sample from room temperature at a rate of 3°C/min.

3.4.2.1 Evaluation of VPO materials as catalysts for butane oxidation

The importance of vanadium phosphates as catalysts for alkane activation, four materials (B-0, B-25, B-100 and B-400) were tested for the selective oxidation of butane and the results are summarized in Table 3.7.

The catalyst, B-0 and B-25 prepared by *in situ* activation exhibit the best performance among the tested catalysts that the butane oxidation of the B-0 and B-25 materials produced a maleic anhydride selectivity of 50% at a butane conversion of 60 and 70% respectively, whereas the B-100 material showed the same selectivity (50%) of B-0 and B-25 material but low conversion. Therefore, $VOHPO_4.0.5H_2O$ is the best preferred catalyst precursor for butane oxidation. Furthermore, $VOHPO_4.0.5H_2O$ is the preferred catalyst precursor for commercial catalyst.[1,5,26] The catalyst, B-400 exhibits low selectivity to maleic anhydride.

Table 3.7 Catalyst performance of vanadium phosphorous catalysts for the oxidation of butane

to maleic anhydride.[a]

Material name	Surface area (m^2/g)		Conversion (%)	Selectivity (%)			Specific activity (10^{-5} mol m^{-2} h^{-1})
	Precursor	Catalyst		MA	CO	CO$_2$	
B-0	34	32	61	51	22	27	1.25
B-25	26	25	70	52	23	25	1.95
B-100	5	7	27	53	19	28	2.62
B- 400	3	2	6	-	27	73	0

[a] Reaction conditions: 1.5% butane in air, 400° C, 3000 h^{-1}

The catalyst materials were cooled to room temperature following the reaction and were characterized by XRD and laser Raman spectroscopy (figure 3.17 and 3.18). Catalyst (B-0, B-25 and B-100) contains mainly $(VO)_2P_2O_7$ (figure 3.17).This is known to be a very active phase for butane oxidation.[26]

The catalytic data for butane oxidation at 385°C of VPO and VPD catalysts prepared using isobutanol and a VPA catalyst has been reported by Hutchings et al.[27] (Table 3.8).

Table 3.8 Catalyst performance of VPA, VPO and VPD for the oxidation of butane to maleic

anhydride.[27]

Catalyst	Surface area (m^2/g)		Conversion (%)	Selectivity (%)			Specific activity (10^{-5} mol m^{-2} h^{-1})
	Precursor	Catalyst		MA	CO	CO_2	
VPA	3	4	11	52	41	7	1.24
VPO	11	14	27	52	34	14	1.35
VPD	32	43	62	64	21	14	1.19

Previously, Sananes et al.[28] reported the difference in catalytic behavior at 367°C of VPD and

VPO catalyst prepared with 1-octanol and 2-octanol (Table 3.9).

Table 3.9 Catalyst performance of VPD and VPO for the oxidation of butane to maleic

anhydride.[28]

Catalyst	Surface area (m^2/g)	Conversion (%)	Selectivity (%)			Specific activity (10^{-5} mol m^{-2} h^{-1})
	Catalyst		MA	CO	CO_2	
VPD	31.2	31	51	31	16	0.50
VPO	7.4	5	59	40	0	0.27

The selectivity of the B-0, B-25 and B-100 materials for butane to maleic anhydride oxidation

is close to that reported by Hutchings et al.[27] and Sananes et al[28]. However, the specific

activity of B-25 and B-100 materials is higher than previous studies[27]. Therefore, these

catalysts exhibit a marked increase in specific activity compared to the previous studies.

3.5 Discussion

The alcohol:alkane volume ratio is a key factor for these morphology changes. Firstly, two scenarios were investigated. The first one is that $VOPO_4.2H_2O$ may react with alkane, and then reduced with the alcohol to platelet, rosette or blocky morphology (figure 3.20). The second possibility is $VOPO_4.2H_2O$ may be initially reduced by the alcohol (1-butanol or 1-octanol) to form $VOHPO_4.0.5H_2O$ with a rosette structure then the alkane may switch the morphology of $VOHPO_4.0.5H_2O$ to platelet or blocky (figure 3.21).
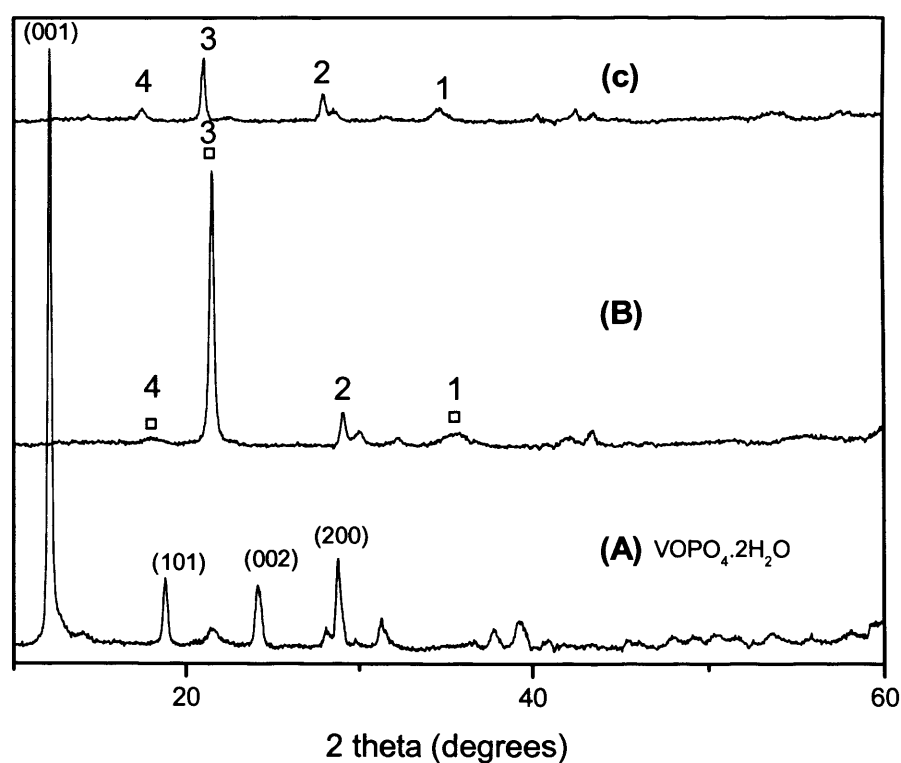
Fig. 3.20 $VOPO_4.2H_2O$ was reacted with octane and alcohol. Key $\square$ = α_I-$VOPO_4$

To investigate the first scenario, $VOPO_4.2H_2O$ (1g, A) was reacted with octane (50 ml) to form material (B) (figure 3.20). This was then reacted with 1-butanol (25 ml) to form material (C). B was assigned to α_I-$VOPO_4$ (marked - □). But the XRD of (C) was different from (B) that peak positions of (C) shifted from corresponding peak positions of (B) [marked in numbers] because the alcohol may be intercalated between the $VOPO_4$ layers. This indicates that refluxing in alkane dehydrates $VOPO_4.2H_2O$ to α_1-$VOPO_4$ which can not react further.

For the investigation of the second possibility, $VOHPO_4.0.5H_2O$ (1g) was reacted with octane (50 ml) as shown in figure 3.21 because $VOHPO_4.0.5H_2O$ with a rosette morphology forms if $VOPO_4.2H_2O$ reacts with 1-butanol.
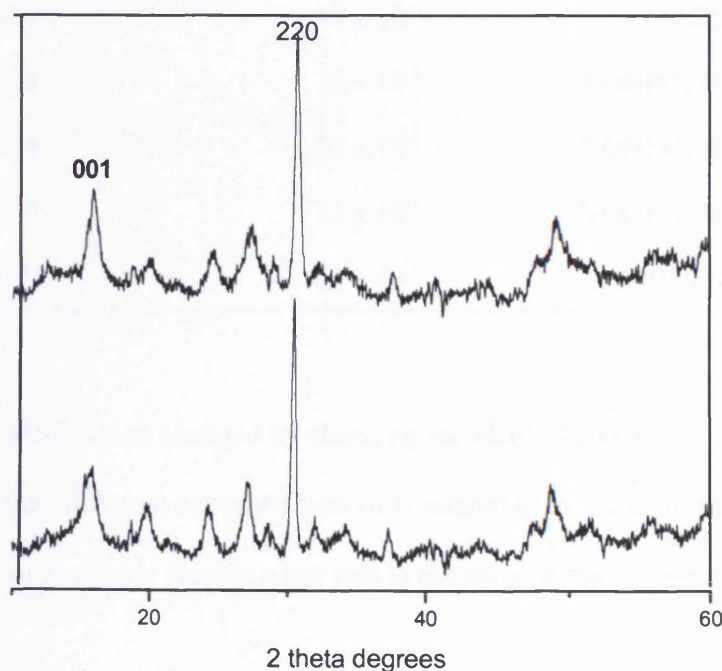
Fig. 3.21 VPD (1g) was reacted with octane (50 ml)

According to XRD (figure 3.21), the morphology of $VOHPO_4.0.5H_2O$ did not change by reacting with octane. Therefore, the second possibility was not true. Therefore, another idea was introduced that different concentration of alcohols obtained by changing the alcohol: alkane volume ratios were the key factor. Based on the XRD results (figure 3.11 and 3.15), the concentration of alcohol in each material was calculated and correlated to the different morphology materials obtained by changing the concentration of alcohol (Table 3.10).

Table 3.10 –Concentration of alcohol and morphology

Material name	Concentration of alcohol (mol / l)	Morphology
B2-15	9.88×10^{-1}	$VO(H_2PO_4)_2$
O2-50	18×10^{-1}	$VO(H_2PO_4)_2$
B2-25	15×10^{-1}	$VOHPO_4.0.5H_2O$ - platelet
O2-75	27×10^{-1}	$VOHPO_4.0.5H_2O$ - platelet
B2-50	31×10^{-1}	$VOHPO_4.0.5H_2O$ - platelet
O2-175	63×10^{-1}	$VOHPO_4.0.5H_2O$ - rosette

Concentration of alcohol was changed by changing the alcohol:alkane volume ratio. Based on the above calculation, different concentrations of 1-butanol gave different materials. Therefore, the concentration of alcohol is playing a key role in the reaction mechanism.

According to reaction kinetics, different concentrations of 1-butanol have a different oxidizing rate and the concentration of alcohol has a linear relationship with oxidizing rate of alcohol.

Furthermore, the reaction rate between 1-butanol and $VOPO_4.2H_2O$ will be changed with respect to the different oxidizing rate of 1-butanol.

It was reported in the literature[14,29] that $VO(H_2PO_4)_2$ can be formed from $VOPO_4.2H_2O$ whilst the ratio of V to P is changing from 1:1 to 1:>2. This suggests that $VOPO_4.2H_2O$ dissociates in the alcohol to give "V^{5+}" and "P" species in the solution as it dissolves. To form $VOHPO_4.0.5H_2O$ and $VO(H_2PO_4)$ from $VOPO_4.2H_2O$ the V^{5+} must be reduced to to V^{4+} by the alcohol. In the literature it has been shown that in order for $VOHPO_4.0.5H_2O$ to be formed the $V_2O_5 + H_3PO_4$ the initial step is reduction of V^{5+} to V^{4+} shows it goes via V_4O_9 and a V^{4+} alkoxide.[27,30,31]

The literature suggests that $VOHPO_4.0.5H_2O$ and $VO(H_2PO_4)_2$ can be obtained whilst the V: P ratios kept at 1:1 and 1:>>1 respectively.[8,29] It was found during this study that $VOHPO_4.0.5H_2O$ was obtained (B2-50 and B2-25) by using a high concentration of alcohol. The high concentration of the alcohol results in a fast reaction rate (between 1-butanol and $VOPO_4.2H_2O$) and a faster reduction rate (V^{5+} to V^{4+}). Therefore it can be suggested that $VOHPO_4.0.5H_2O$ is obtained whilst V^{4+}: P ratio kept at approximately 1:1 due to the fast reduction of V^{5+}

It was also found that material $VO(H_2PO_4)_2$ was obtained (B2-15 and O2-50) by using a low concentration of alcohol. The low concentration of alcohol results in a decreased reaction rate (between 1-butanol and $VOPO_4.2H_2O$) and a slower reduction rate (V^{5+} to V^{4+}). The slower

reduction rate means that the V^{4+}:P ratio is 1:>>1 and the excess phosphorous favours the formation of $VO(H_2PO_4)_2$ which has a V:P ratio of 1:2.

It can be concluded that rate of reduction governs whether "V^{4+}":P is close to 1:1 or 1:>>1 which is the key factor in determining which phase is formed. A scheme of the proposed mechanism of material formation is shown in figure 3.22.
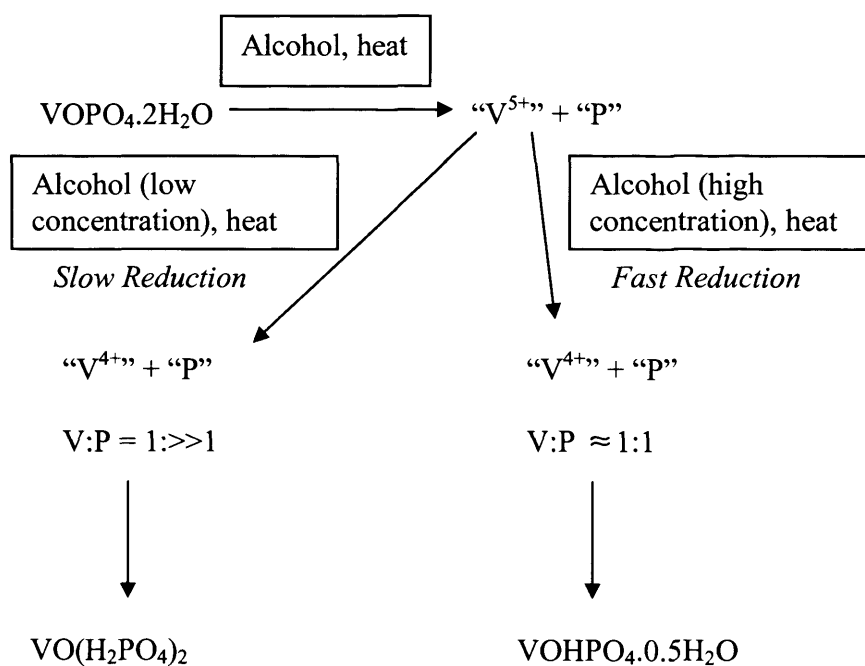

Fig. 3.22 Scheme of material formation

When $VOPO_4.2H_2O$ is reduced using an alcohol as the solvent and reducing agent $VOHPO_4.0.5H_2O$ is formed. However, previous studies have shown that when an aldehyde is used $VO(H_2PO_4)_2$ is formed. Further, in organic chemistry, alcohol will be oxidised to

aldehyde when it participates in reduction reaction while aldehyde will be oxidised to carboxylic acid when aldehyde participates in the reduction reaction. Furthermore, in organic chemistry, the rate of the reduction will be faster when alcohol is used when compared to aldehyde at same reaction conditions because in the case of alcohol, reactive group of –O-H attached directly to the C atom but in the case of aldehyde, =O attached with C atom and the reactivity of –O-H is higher than the reactivity of =O. Therefore, the aldehyde is not as good a reducing agent as the corresponding alcohol and so there will be a V^{4+}: P ratio of 1:>>1 favouring the formation of $VO(H_2PO_4)_2$.

Further, a mixture of $VO(H_2PO_4)_2$ and $VOHPO_4.0.5H_2O$ was formed when 15 ml of 1-butanol and 160 ml of octane were reacted but there was no reaction when 15 ml of 1-octanol and 160 ml of octane were reacted. With octanol, the concentration was not enough to reduce the $VOPO_4.2H_2O$ but, in the case of 1-butanol, 15 ml of 1-butanol and 160 ml of octane switched the morphology from $VOPO_4.2H_2O$ to $VO(H_2PO_4)_2$ and $VOHPO_4.0.5H_2O$, so, this concentration was enough to reduce the $VOPO_4.2H_2O$. In organic chemistry, 1-butanol can be easily oxidized to aldehyde when compared with 1-octanol at same reaction conditions because of less (+) inductive effect that alkyl group of $CH_3 - (CH_2)_6$- has higher electron releasing power than $CH_3 - (CH_2)_2$-, therefore more negative charge will be formed on C atom which is directly connected with O-H group, so (+) inductive effect of 1-octanol is higher than 1-butanol therefore less (+) inductive effect is more favour for oxidation of alcohol. Therefore, reducing power of 1-butanol is higher than the 1-octanol and the rate will be higher than the 1-octanol.

Therefore, concentration of alcohol can be changed by adding the alkane solvent which is changing the oxidizing rate of alcohol and the reaction rate between alcohol and $VOPO_4.2H_2O$. Furthermore, high concentration of alcohol gave $VOHPO_4.0.5H_2O$ while low concentration of alcohol gave $VO(H_2PO_4)_2$ because of different rate of the material formation. Therefore, different concentration of alcohols gave different materials.

Although the results show that $VOHPO_4.0.5H_2O$ is formed at high concentrations of alcohol it was observed that different morphologies of $VOHPO_4.0.5H_2O$ were obtained at different alcohol:alkane ratios (Table 3.10). At higher concentrations of alcohol an XRD pattern with the (220) crystal plane as the dominant feature; this is characteristic of $VOHPO_4.0.5H_2O$, with a rosette morphology. Whilst at lower concentrations the (001) is the dominant feature in the XRD pattern indicating $VOHPO_4.0.5H_2O$ is formed with a platelet morphology. Therefore, the concentration of the alcohol can also affect the morphology of the precipitated crystals.

Solution-phase synthesis is one of the most important methods to control the morphology of the materials. Further, the precipitation process is a key method to synthesis materials of different morphology materials in solution phase. It can be said that the concentration of ions in solution is a deciding factor for obtaining material of different morphology in the precipitation method.

$VOPO_4. 2H_2O$ is soluble in alcohol but not in alkane, and, V^{5+} reduction to V^{4+} takes place in the alcohol medium only. Because of these two above mentioned factors the amount of alcohol in the medium plays a very important role in deciding the concentration of V^{4+} ions in the

solution and hence it affects the supersaturation ratio. Due to the varying degree of supersaturation ratio from the varied alcohol content in the mixture, we get different morphologies of $VOPO_4.0.5H_2O$.

Li et al.[32] observed a similar result, but for $BaSO_4$ crystals from Ba^{2+} ions and SO_4^{2-} ions They also reported that initial Ba^{2+} ion and SO_4^{2-} concentration affects the morphology of the resultant $BaSO_4$ crystals. For example, a rod-like morphology was obtained for $BaSO_4$ when the initial concentration of the constituent ions were low (0.001 mol/l). When the concentration was increased (0.005 mol/l) a snow like morphology was obtained whereas at higher concentration of the constituent ions a leaf-like morphology (0.02 mol/l) or spherical morphology were obtained (0.1 mol/l).

In this study the initial amount of $VOPO_4.2H_2O$ (1 g) used in the reaction if fully dissolved in the solvent gives rise to a solution of 0.028 mol/l. From our previous reaction scheme for the mechanism (figure 3.22) we postulate that the $VOPO_4.2H_2O$ dissolves to give a V^{5+} species and a phosphorous species and the V^{5+} is then reduced to V^{4+} quickly. We can therefore expect to have a solution with 0.028 mol/l and a V^{4+} concentration $\leq$ 0.028 mol/l, depending on the rate which is governed by the concentration of alcohol. The values are very similar to the concentrations investigated by Li et al.[32] which show that this is a plausible explanation for the different morphologies observed. This could also explain the differences observed for primary and secondary alcohols. Both will have a similar reduction rate so both give $VOHPO_4.0.5H_2O$, but the secondary alcohol will react slightly slower due to the inductive effect explaining the

differences observed with a rosette for the fastest rate and a platelet morphology for the slightly slower rate.

In another study, Cano et al.[33] obtained different morphologies of 2-(4-isobutylphenyl) propionic acid when it was crystallized from different solvents. he proposed a chemical interaction between the solvent and the carboxyl group stops crystal growth in a particular plane. This is not the case for this study as the solvent mixtures both contain the same components, however this could explain the differences observed with different solvents such as primary and secondary alcohols.

From the above discussion, it is clearly evident that the alcohol concentration in the reaction medium affects the V^{4+} concentration, and in turn affects the degree of supersaturation. From literature it is known that varying degree of supersaturation affects the morphology of the resultant crystal and hence the alcohol concentration affects the degree of supersaturation and in turn affects the morphology of the resultant $VOHPO_4.0.5 H_2O$.

3.6 Conclusions

We have shown that adding an alkane co-solvent to the reaction can change the product formed. We suggest that this is due to the change in reaction rate of the V^{5+} to V^{4+} reduction which is the key step in our proposed mechanism to determine the product formed.

A fast reduction led to a V^{4+}:P ratio of approximately 1:1 with $VOHPO_4.0.5 H_2O$ as the major product. A slow rate led to a V^{4+}:P ratio of 1:>>1 with $VO(H_2PO_4)_2$ as the major product.

Small changes in the rate were shown to have an effect on the $VOHPO_4.0.5\ H_2O$ morphology. This is thought to be due to a slight change in the supersaturation of the reactants in solution which has been show previously to have a large influence on the morphology of the crystals formed.

Evaluation of the materials as catalysts for the oxidation of *n*-butane to maleic anhydride shows that the materials exhibit higher specific activities for *n*-butane oxidation than previous studies.

3.7 References

(1)   G. Centi, *Catal. Today*, 1994, **16**.

(2)   E. Bordes, *Catal. Today*, 1987, **1**, 499.

(3)   J.T. Gleaves, J.R. Ebner and T.C. Knechler, *Catal. Rev. Sci. Eng.*, 1988, **30**, 49.

(4)   G. Centi, F. Trifiro, G. Busca, J. Ebner and J. Gleaves, *Faraday Discuss.*, 1989, **87**, 215.

(5)   G.J. Hutchings, *Appl. Catal.*, 1991, **72**, 1.

(6)   G.J. Hutchings, A. Desmartin Chomel, R. Olier and J.C. Volta, *Nature*, 1994, **368**, 41.

(7)   C.J. Kiely, A. Burrows, G.J. Hutchings, K.E. Bere, J.C. Volta, A. Tuel and M. Abon, *J. Chem. Soc., Faraday Disc.*, 1996, **105**, 103.

(8)   J.W. Johnson, D.C. Johnston, A.J. Jacobson and J.F. Brody, *J. Am. Chem. Soc.*, 1984, **106**, 8123.

(9)   H.S. Horowitz, C.M. Blackstone, A.W. Sleight and G.Teufer, *Appl. Catal.*, 1988, **38**, 211.

(10)   E.W. Arnold and S. Sundaresan, *Appl. Catal.*, 1988, **41**, 457.

(11)   K. Ait-Lachgar, M. Abon and J.C. Volta, *J. Catal.*, 1991, **171**, 383.

(12)   E. A. Lombardo, C.A Sanchez and L.M. Conaglia, *Catal Today*, 1992, **15**, 407.

(13)   F. Benabdelouahab, J.C. Volta and R. Olier, *J. Catal.*, 1994, **148**, 334.

(14)   I.J. Ellison, G.J. Hutchings, M.T. Sananes and J.C. Volta, *J. Chem. Soc., Chem. Commun.*, 1994, 1093.

(15)   V.V. Guliants, J.B. Benziger and S. Sundaresan, *Chem. Mater.*, 1995, **7**, 1485.

(16)   V.V. Guliants, J.B. Benziger, S. Sundaresan, I.E. Wachs and J.-M. Jehng, *Chem. Mater.*, 1995, **7**, 1485.

(17)   V.V. Guliants, J.B. Benziger, S. Sundaresan, N. Yao and I.E. Wachs, *Catal Lett.*, 1995, **32**, 379.

(18)   V.A. Zazhigalov, J. Haber, J. Storch. L.V. Bogutskaya and I.V. Bacherikova, *Appl. Catal.*, 1996, **135**, 155.

(19)   C.J. Kiely, A. Burrows, S. Sajip, G.J. Hutchings, M.T. Sananes, A. Tuel and J.C. Volta, *J. Catal.*, 1996, **162**, 31.

(20)   V.V. Guliants, J.B. Benziger, S. Sundaresan. I.E.Wachs , J.-M. Jehng and J.E. Roberts, *Catal. Today*, 1996, **28**, 275

(21)   N. Yamamoto, T. Okuhara and T. Nakato, *J. Mater. Chem*, 2001, **11**, 1858

(22)   Y. Kamiya, S. Ueki, N. Hiyoshi, N. Yamamoto and T. Okuhara, *Catal. Today*, 2003, **78**,281

(23)   Y. Kamiya, N. Hiyoshi, N. Ryumon and T. Okuhara, *Journal of Molecular Catalysis A:Chemical*, 2004, **220**, 103

(24) Y. Kamiya, N. Yamamoto, H. Imai, S. Komai and T. Okuhara, *Microporous and Mesoporous Materials* 2005, **81**, 49

(25) N. Yamamoto, N. Hiyoshi and T. Okuhara , *Chem. Mater*, 2002, **14**, 3882

(26) G. J. Hutchings, *J. Mater. Chem.,* 2004, **14**, 3385

(27) G. J. Hutchings, C. J. Kiely, M. T. Sananes-Schulz, A. Burrows and J. C. Volta. *Catal. Today,* 1998, **40**, 273

(28) M. T. Sananes, I. J. Ellision, S. Sajip, A. Burrows, C. J. Kiely, J. C. Volta and G. J. Hutchings, *J. Chem. Soc., Faraday Trans.,* 1996, **92** (1). 137

(29) Jonathan. K. Bartley, *Ph.D thesis*, 1999

(30) T. Doi and T. Miyake, *Appl. Catal. A*, 1997, **164**, 141

(31) T. Miyake and T. Doi, *Appl. Catal.,* 1995, **131**, 43

(32) S. Li, J. Xu and G. Luo, *J. Crystal Growth* 2007, **304**, 219

(33) H. Cano, N. Gabas and J. P. Canselier , *J. Crystal Growth* 2001, **224**, 335

Chapter 4

Catalyst Preparation Using New Preparation Route

4.1 Introduction

It is generally accepted that the (200) surface in $(VO)_2P_2O_7$ is a key factor for butane oxidation.[1-3] Many researchers are agreed that $(VO)_2P_2O_7$ plays an important role in the oxidation of butane to maleic anhydride.[4] These arguments are mainly based on the observation that only crystalline $(VO)_2P_2O_7$ is obtained after long catalytic reactions. Bordes et al.[5] also has demonstrated that the (200) plane is selective for the formation of MA, while side planes (001), (021) etc. are active for non selective oxidation such as to CO_2 and CO etc.

Previous studies reported that the active catalyst, $(VO)_2P_2O_7$ can be obtained from $VOHPO_4.0.5H_2O$ precursors, therefore, many researchers have developed new preparation routes for making catalyst precursors and these precursors when reacted with 1.5% butane/air at 400°C to obtain selective catalyst.[6-9]

In this chapter, a new preparation route was developed to synthesize the final catalyst directly from $VOPO_4 \cdot 2H_2O$ (figure 4.1) and these catalysts were tested for n-butane oxidation. This route involves reducing $VOPO_4.2H_2O$ at high temperature to obtain the final catalyst. Different reducing agents and conditions were analyzed (isobutanol and He or H_2/Ar with different flow rates), among these conditions 50 ml/min, H_2/Ar was found to

be a better agent and condition for this transformation. The advantage of this transformation

is that the final catalyst can be prepared without making catalyst precursors.

$$VOPO_4.2H_2O \xrightarrow{\text{VPD or VPO route}} VOHPO_4.0.5H_2O$$

50 ml/min, 5% H2/Ar, 550°C, 72 h

1.5% Bu/Air, 400°C, >72hr

$(VO)_2P_2O_7$
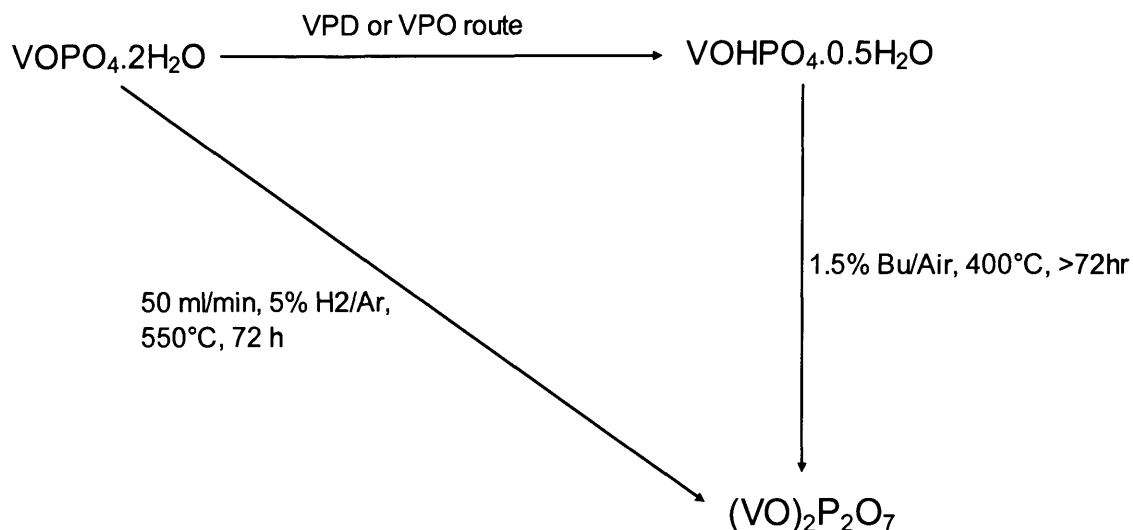
Fig. 4.1 Phase transformations in the VPO system

Furthermore, $VOPO_4 \cdot 2H_2O$ was also prepared using *pyro* phosphoric acid and the organic

solvent based on the standard preparation method and the results can be directly compared

with those published in the literature.[10] Finally, the prepared $VOPO_4 \cdot 2H_2O$ were

transformed into the final catalyst via new route for *n*-butane oxidation.

4.2 Experimental

Pyro-phosphoric acid was used to make $VOPO_4 \cdot 2H_2O$ via the standard preparation

method.[10] $VOPO_4 \cdot 2H_2O$ was also prepared using organic preparation route (more details in

Chapter 2).

$VOHPO_4 \cdot 0.5H_2O$ was prepared via the standard VPO route. Firstly V_2O_5, H_3PO_4 and 1-

butanol were refluxed for 24 hours. The pale blue product was filtered by using vacuum

pump, washed with alcohol and acetone. The recovered product was refluxed with water for

5 hours to remove the impurity $VO(H_2PO_4)_2$. The final product was filtered at hot stage then washed with warm water, and dried in air at 110°C for 24 hours. The different $VOPO_4\cdot2H_2O$ were then reduced under different conditions to give the final catalyst. The sample was placed in a quartz reactor tube (internal diameter 11 mm) and heated in a furnace at temperature, 550°C for 72 hours. A stream of 5 % H_2/Ar mixture was passed over the sample at flow rate, 50 ml/min. These catalysts were tested for n-butane oxidation to maleic anhydride. The catalyst data for butane oxidation were compared with catalyst data obtained from standard VPD and VPO materials. The $VOPO_4\cdot2H_2O$ and the final catalyst were characterized using a combination of powder X-ray diffraction, laser Raman spectroscopy, BET surface area measurements and scanning electron microscopy.

Table 4.1 Details of material preparations and their labels

Entry	V_2O_5 Source	Phosphoric Acid	Solvent	Label	Reduction Conditions	Label
1	Aldrich	*ortho*	H_2O	DHOA (standard)	50 ml, 5% H_2/Ar, 550° C, 72 h	POA
2	Aldrich	*pyro*	H_2O	DHPA	50 ml, 5% H_2/Ar, 550° C, 72 h	PPA
3	Aldrich	*ortho*	isobutanol	DN	50 ml, 5% H_2/Ar, 550° C, 72 h	PN
4	Aldrich	*ortho*	1-butanol	VPO standard	1.5% butane in air, 400° C, 72 h	$(VO)_2P_2O_7$ Standard (VPO-*py*)
5	DHOA		isobutanol	VPD standard	1.5% butane in air, 400° C, 72 h	$(VO)_2P_2O_7$ Standard (VPD-*py*)

4.3 Results

4.3.1 Standard VOPO₄·2H₂O (DHOA) preparation

The XRD pattern, the laser Raman spectrum and SEM of $VOPO_4 \cdot 2H_2O$ prepared using the standard route have shown in figure 4.1, 4.2 and 4.3 respectively.
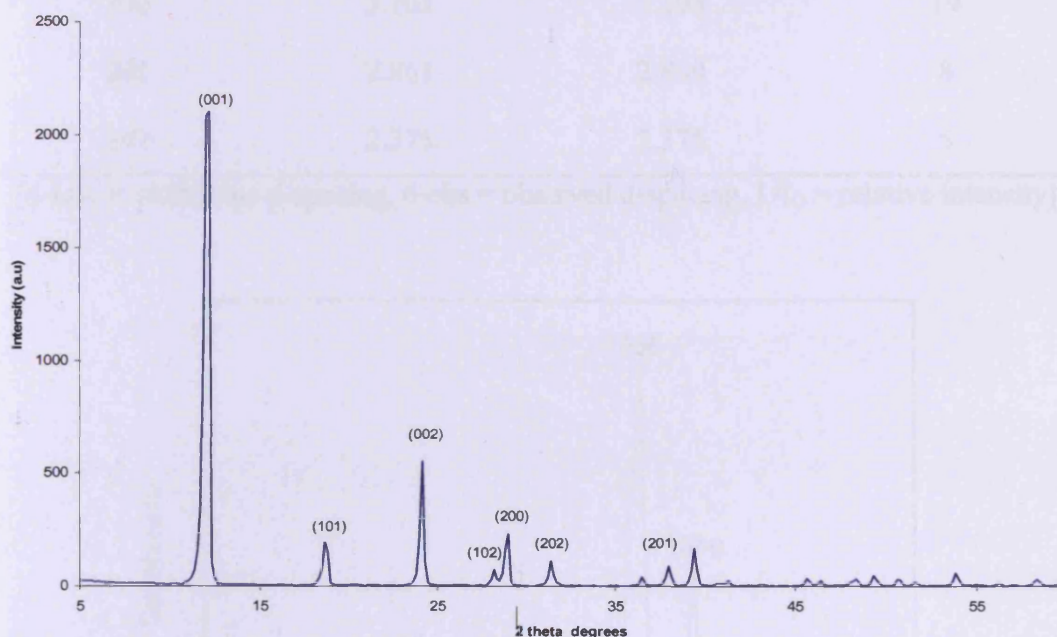
Fig. 4.1 The XRD pattern of $VOPO_4 \cdot 2H_2O$ (DHOA) prepared using the standard route

The powder X-ray diffraction pattern (figure 4.1) corresponds to $VOPO_4 \cdot 2H_2O$, with the dominant reflection at 11.9° (d-spacing = 7.3 Å) indexed to the (001) plane (Table 4.2).

Table 4.2 The XRD reflections of $VOPO_4 \cdot 2H_2O$ prepared using standard route

VOPO$_4 \cdot$2H$_2$O[5,11]		VOPO$_4 \cdot$2H$_2$O (observed)	
hkl	d- calc	d- obs	I /I$_O$
001	7.410	7.369	100
101	4.756	4.754	14
002	3.705	3.690	24
102	3.181	3.173	5
200	3.101	3.103	19
201	2.861	2.860	8
202	2.378	2.375	5

[d-calc = calculated d-spacing, d-obs = observed d-spacing, I /I$_O$ = relative intensity]
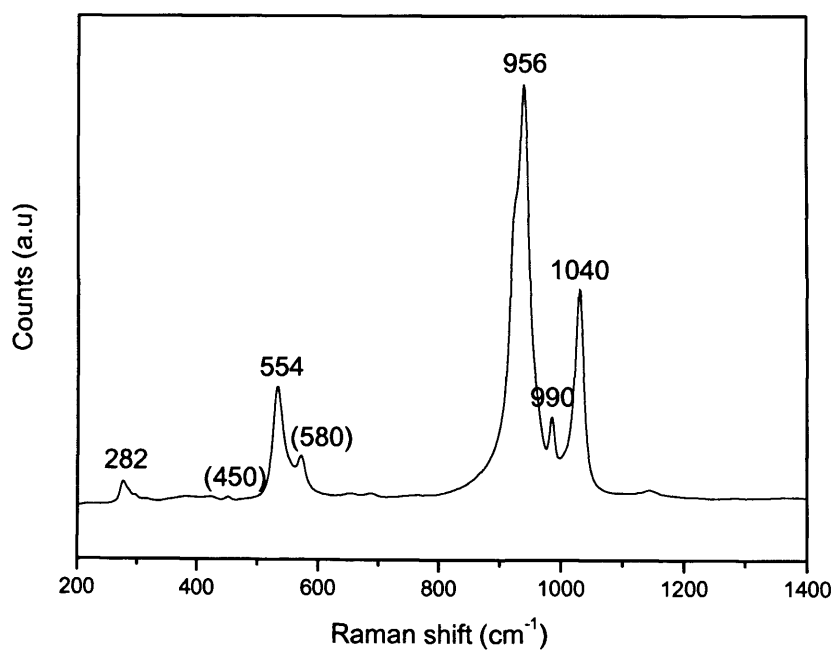
Fig. 4.2 The laser Raman spectrum of $VOPO_4 \cdot 2H_2O$ (DHOA) prepared using the standard route

Table 4.3 The Raman peaks of $VOPO_4 \cdot 2H_2O$ prepared via standard route

$VOPO_4 \cdot 2H_2O^{5,11}$		$VOPO_4 \cdot 2H_2O$ (observed)	
Peaks (cm^{-1})	I/Io	Peaks (cm^{-1})	I/Io
1039	strong	1040	strong
988	medium	990	medium
952	very strong	948	very strong
658	weak	660	Very weak
542	strong	540	medium
451	weak	450	very weak
281	medium	281	weak
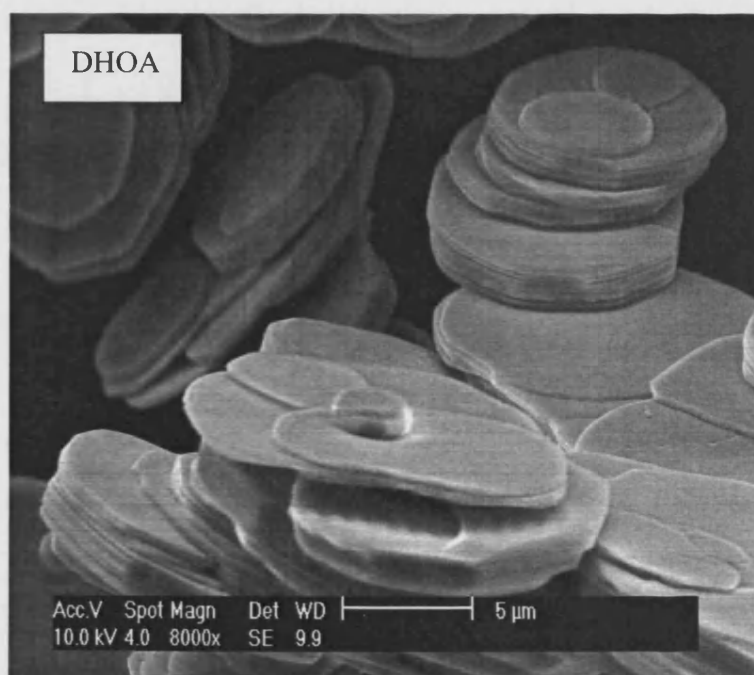
Fig. 4.3 The SEM of $VOPO_4 \cdot 2H_2O$ prepared using the standard route

The Raman spectrum (figure 4.2) agrees with published spectra of $VOPO_4 \cdot 2H_2O$ (Table 4.3). The main band at 956 cm^{-1} is due to the symmetric stretch of P-O in the PO_4^{3-} tetrahedra and the bands at 990 cm^{-1} and 1040 cm^{-1} are due to the V-O and V-O-P stretching modes, respectively. The SEM (figure 4.3) micrograph of the $VOPO_4 \cdot 2H_2O$ prepared using standard route illustrates that the sample has a plate morphology. The surface area of DHOA was between 1-3 m^2/g.

4.3.2 Characterization of $VOPO_4 \cdot 2H_2O$ (DHPA) using *pyro*-phosphoric acid

The XRD, Raman and SEM of $VOPO_4 \cdot 2H_2O$ prepared using *pyro*-phosphoric are shown in figure 4.4, 4.5 and 4.6 respectively.
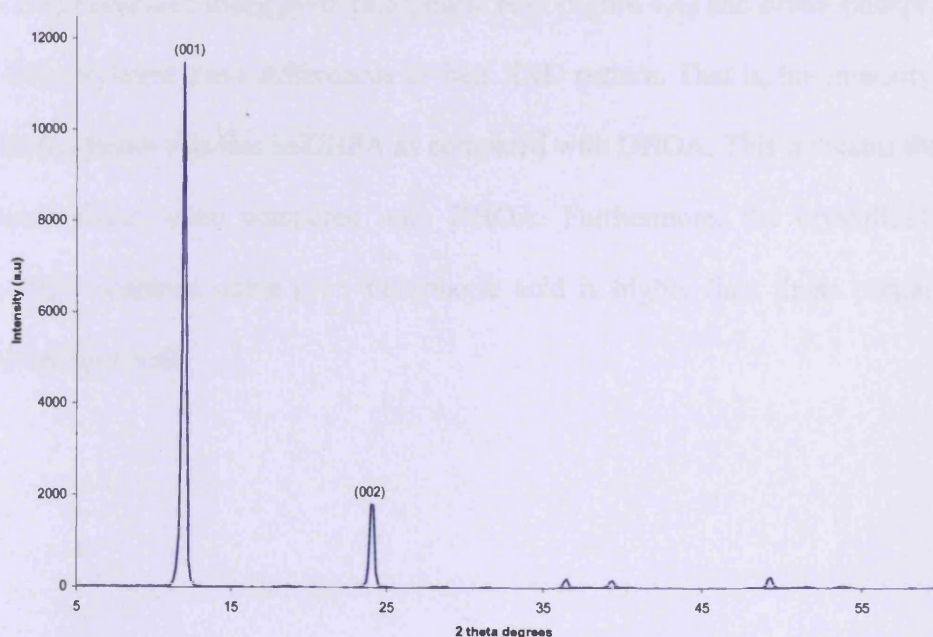
Fig. 4.4 The XRD pattern of $VOPO_4 \cdot 2H_2O$ (DHPA) prepared using *pyro* – phosphoric acid

Table 4.4 The XRD reflections of $VOPO_4 \cdot 2H_2O$ prepared using *pyro*-phosphoric acid

VOPO₄·2H₂O[5, 11]		VOPO₄·2H₂O using *pyro*-phosphoric acid	
hkl	d-calc	d-obs	I/I$_O$
001	7.410	7.369	100
101	4.756	4.754	1
002	3.705	3.690	17
102	3.181	3.173	1
200	3.101	3.103	1
201	2.861	-	-
202	2.378	2.460	1

[d-calc = calculated d- spacing, d-obs = observed d- spacing, I/I$_O$ = relative intensity]

$VOPO_4 \cdot 2H_2O$ prepared using *pyro*–phosphoric acid (figure 4.4) and *ortho*–phosphoric acid (figure 4.1) displayed some differences in their XRD pattern. That is, the intensity of some of the smaller peaks was less in DHPA as compared with DHOA. This indicates that DHPA has thinner plates when compared with DHOA. Furthermore, the crystallinity of the $VOPO_4.2H_2O$ prepared using *pyro*–phosphoric acid is higher than those prepared using *ortho*–phosphoric acid.
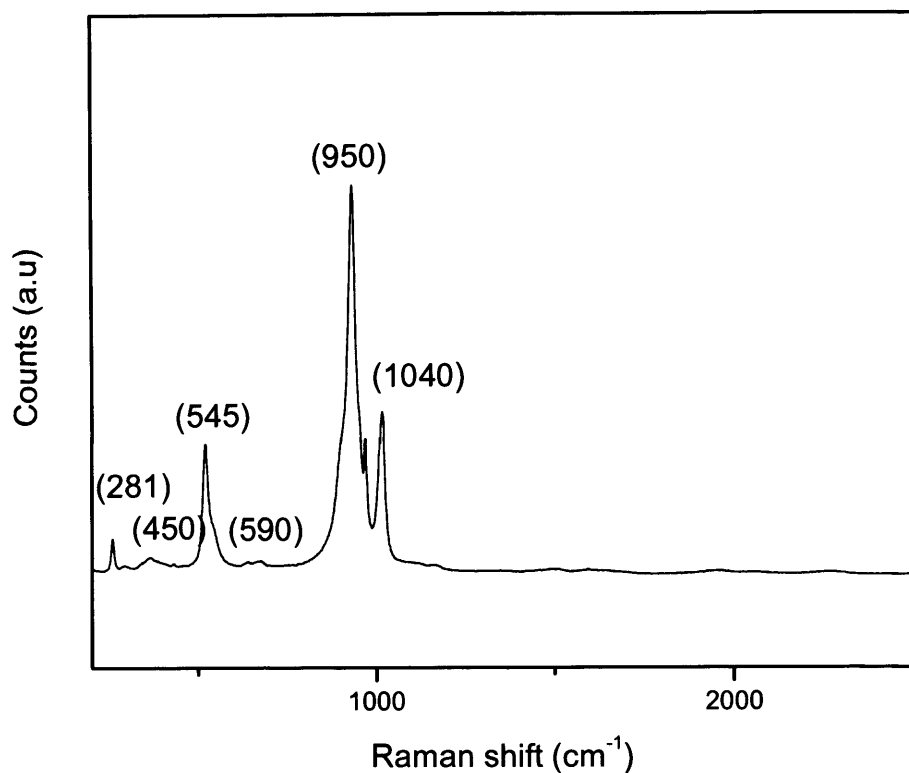
Fig. 4.5 The laser Raman spectrums of different $VOPO_4 \cdot 2H_2O$ (DHPA)

The Raman spectrum of DHPA (figure 4.5) were very close and in agreement with the published spectra of $VOPO_4 \cdot 2H_2O$[11] (Table 4.3) and are similar when compared to the spectrum of DHOA. This is expected as Raman spectroscopy reveals stretching frequencies and bending modes between the atoms and as such is a fingerprint technique. Therefore, any differences observed in the morphology or crystallinity of the samples would not be seen using Raman spectroscopy.

Fig. 4.6 The SEM of VOPO$_4 \cdot$2H$_2$O

The SEM micrograph (figure 4.6) of the VOPO$_4 \cdot$2H$_2$O prepared using the *pyro*-phosphoric acid has a platelet morphology. The surface area of DHPA was between 1-3 m^2/g.

4.3.3 Characterization of VOPO$_4 \cdot$2H$_2$O prepared in organic solvent

The XRD pattern and SEM of VOPO$_4 \cdot$2H$_2$O prepared using organic solvent designated as DN are shown in Figure 4.7 and 4.8.

VOPO$_4 \cdot$2H$_2$O prepared using organic solvent route has a very different XRD pattern compared to the standard materials (Table 4.1). It is interesting to note that the [001] and [200] reflections in figure 4.7 are considerably broadened as compared with standard VOPO$_4 \cdot$2H$_2$O.

The XRD (Figure 4.7) indicated that the morphology of this material is different from the normal material ... they do not form regular plates ... the surface area of the VOPO₄·2H₂O ...

4.14 Example of VO(H₂O)₀.₅H₂O preparation using VPO method

The XRD result ... VOPO₄·2H₂O ... VPO ... are shown in figures 4.7, 4.8/4.9 respectively
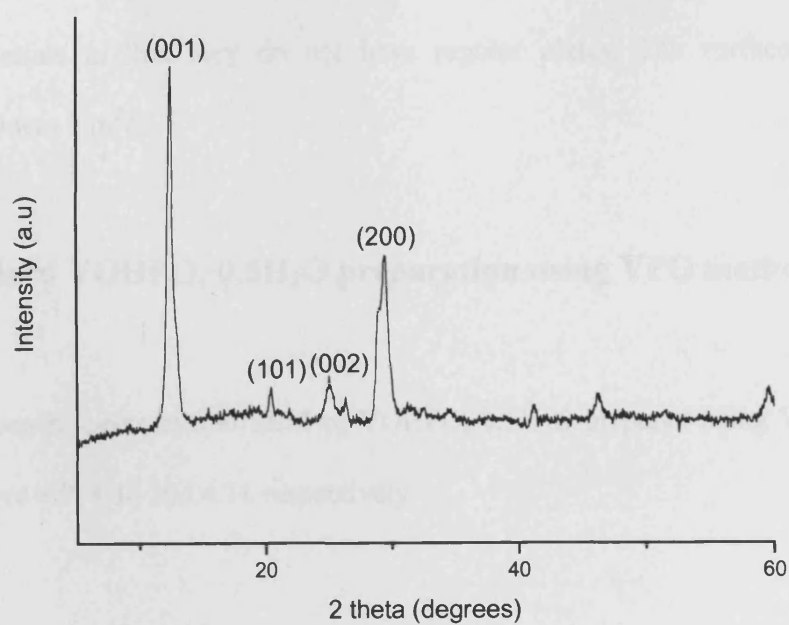
Fig. 4.7 The XRD pattern of VOPO₄·2H₂O prepared using new method (DN).
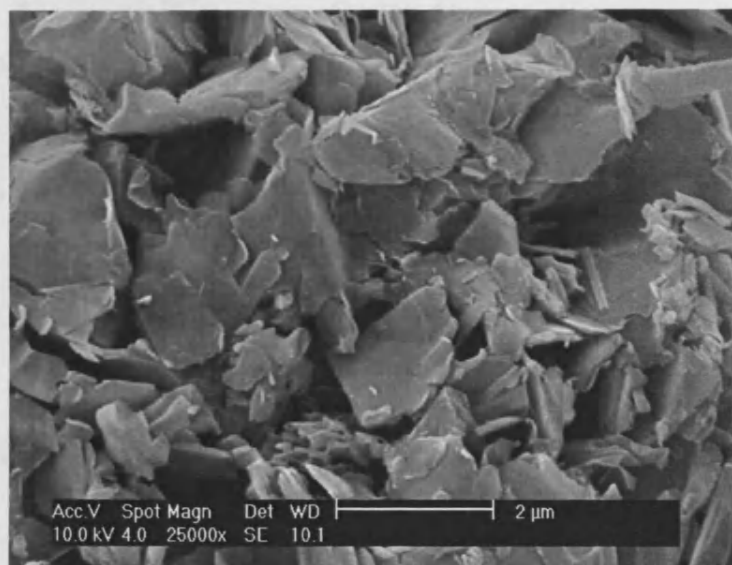
Fig. 4.8 The SEM of DN.

The SEM (figure 4.8) indicated that the morphology of this material is different from the standard materials in that they do not have regular plates. The surface area of this $VOPO_4 \cdot 2H_2O$ was 3 m^2/g.

4.3.4 Standard $VOHPO_4 \cdot 0.5H_2O$ preparation using VPO method

The XRD, Raman spectrum and SEM of $VOHPO_4 \cdot 0.5H_2O$ prepared using VPO route are shown in figure 4.9, 4.10 and 4.11 respectively.
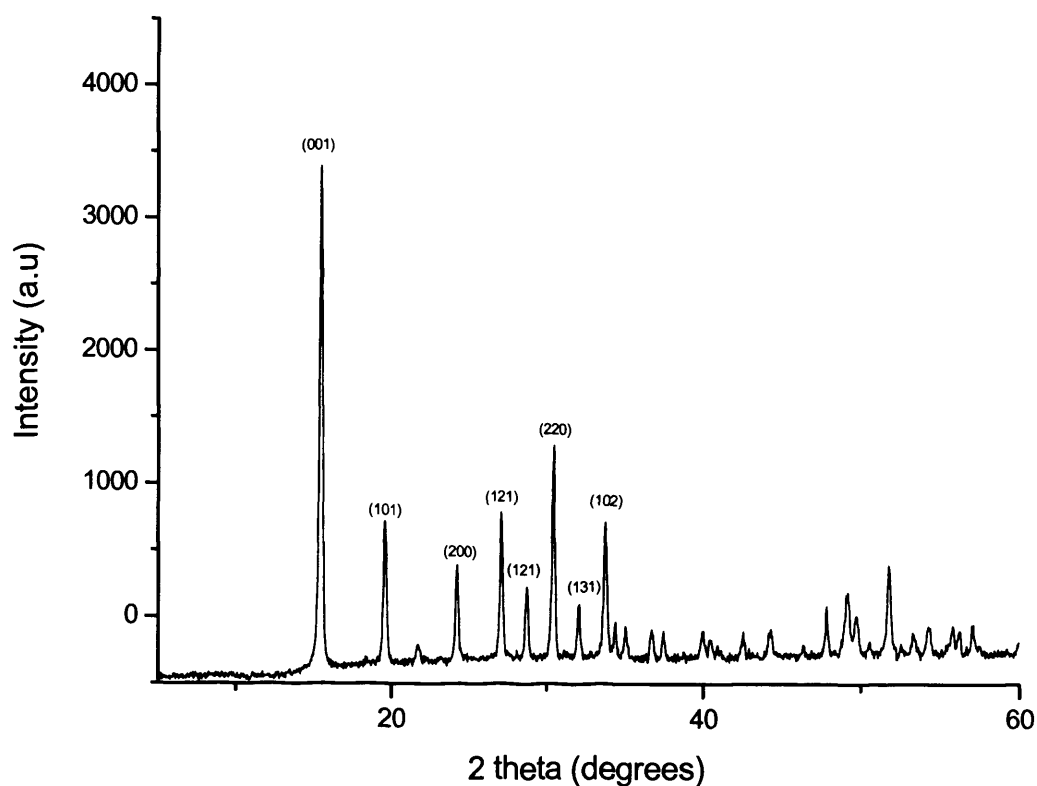
Fig. 4.9 The XRD pattern of $VOHPO_4 \cdot 0.5H_2O$ prepared via VPO route
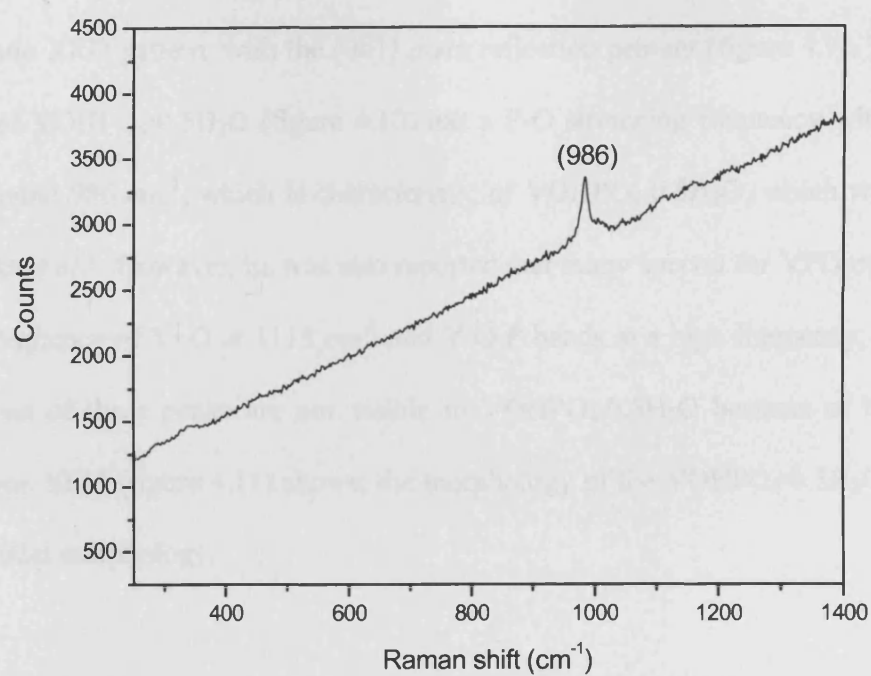
Fig. 4.10 The Raman spectrum of VOHPO₄·0.5H₂O prepared via VPO route
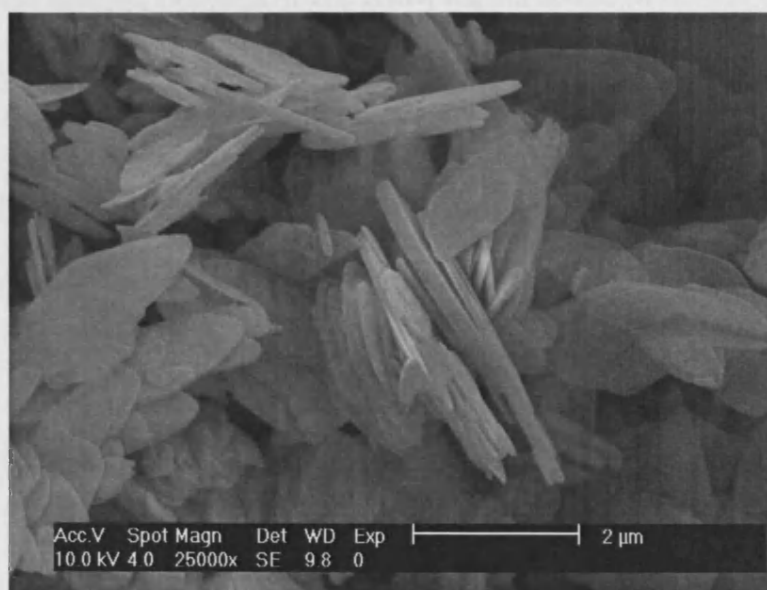
Fig. 4.11 The SEM of VOHPO₄·0.5H₂O prepared via VPO route

VOHPO$_4$·0.5H$_2$O materials prepared via VPO route using 1-butanol as an alcohol have a characteristic XRD pattern, with the [001] main reflection present (figure 4.9). The Raman spectrum of VOHPO$_4$·0.5H$_2$O (figure 4.10) has a P-O stretching frequency with a Raman shift of around 986 cm^{-1}, which is characteristic of VOHPO$_4$·0.5H$_2$O, which was reported by Guliants et al.[11] However, he was also reported that many spectra for VPO materials the bonding frequency of V=O at 1113 cm^{-1} and V-O-P bands at a high frequency, 1156 cm^{-1}. But, the rest of these peaks are not visible in VOHPO$_4$·0.5H$_2$O because of background fluorescence. SEM (figure 4.11) shows, the morphology of the VOHPO$_4$·0.5H$_2$O precursor have a platelet morphology.

4.3.5 Characterisation of (VO)$_2$P$_2$O$_7$

Standard VOHPO$_4$·0.5H$_2$O (VPO) were activated in situ under a flow of 1.5% butane in air, to give the active catalyst, (VO)$_2$P$_2$O$_7$. The XRD, Raman and SEM of final catalyst ((VPO-py) are shown in Figure 4.12, 4.13 and 4.14 respectively.

All XRD peaks indexed to (VO)$_2$P$_2$O$_7$.[5,11] The (200) plane of the final catalyst has been reported to be a key factor for selective n-butane oxidation.
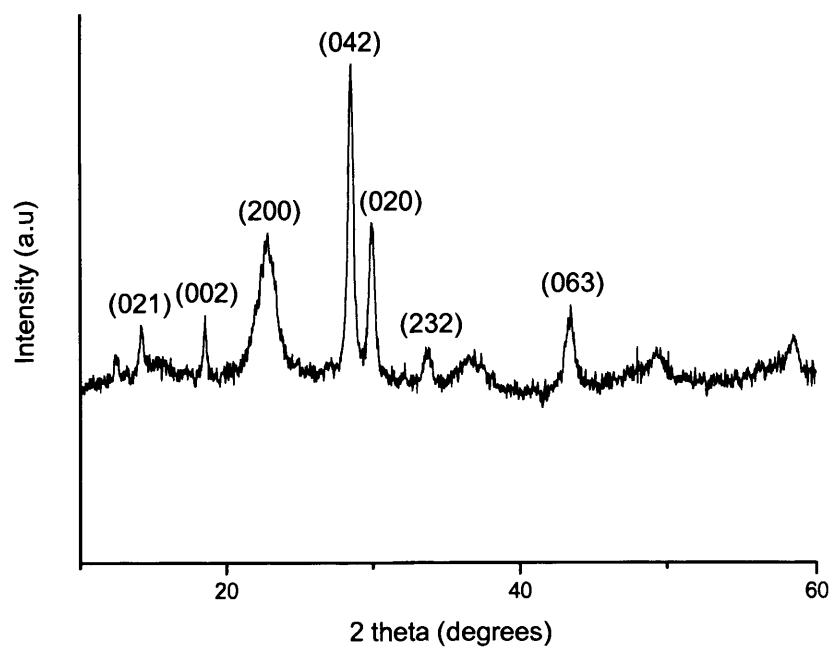
Fig. 4.12 The XRD patterns of the of the $(VO)_2P_2O_7$ (VPO-*py*).
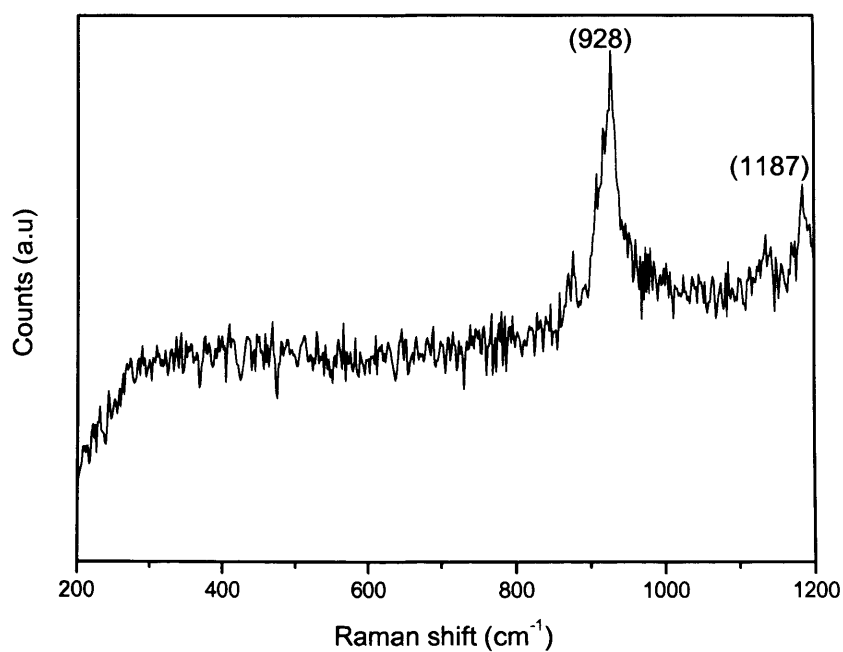
Fig. 4.13 Raman spectrum of the of the final catalyst (VPO-*py*)
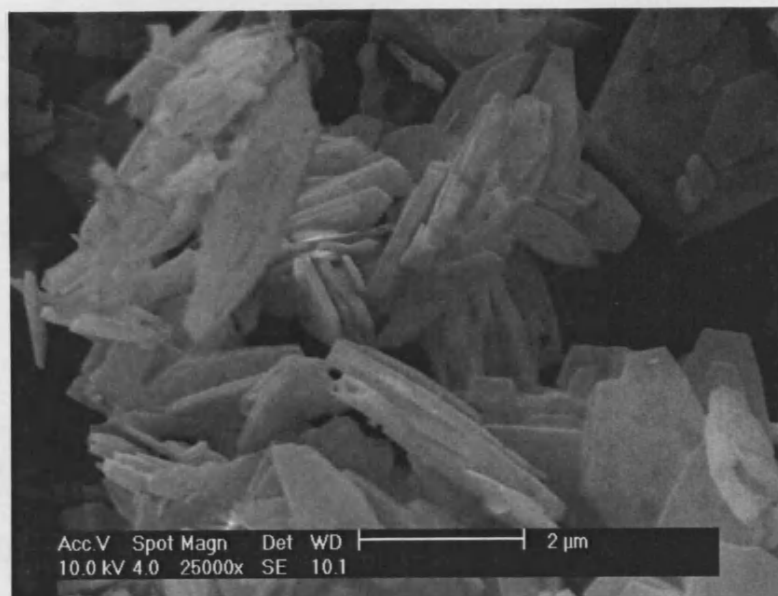
Fig. 4.14 SEM of the final catalyst (VPO-*py*)

Table 4.6 The Raman spectrum of $(VO)_2P_2O_7$ reported by Guliants *et al.*[5, 11]

Peaks (cm^{-1})	I/Io
1191	weak
1135	weak
1006	very weak
930	strong
920	very strong
797	very weak
457	very weak
391	very weak
274	weak
258	weak
193	very weak
112	very weak

Raman spectrum of the final catalyst (Figure 4.13) have a very strong peak at 928 cm^{-1} as their main feature. This has been assigned to P-O-P asymmetric stretch.[11] The only other $(VO)_2P_2O_7$ peak detected is the high frequency band at 1187 cm^{-1}, due to the strong bonding of the pyrophosphate ion. The morphology of the final catalyst remains unchanged.

4.3.6 Characterization of materials prepared using direct route [(VO)$_2$P$_2$O$_7$]

$VOPO_4 \cdot 2H_2O$ of DHOA was reduced with 5% H_2/Ar at a flow rate 50 ml/min and temperature of 550°C for 72 hours. It is designated as POA. The XRD patterns are shown in Figure 4.15. These materials were compared with the standard materials.[11]
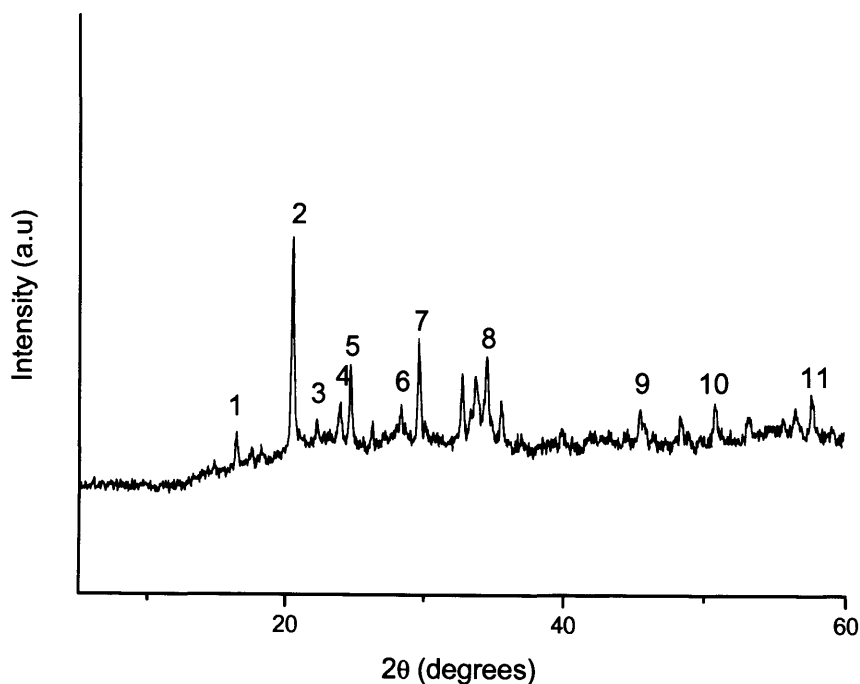
Fig. 4.15 The XRD pattern of POA.

Table 4.5 The XRD reflections of POA.

| Entry | Angle | Counts | d-space | Rel I | Standard | |
					d-space	Rel I
1	16.455	517	5.387	36	**4.79**	**10**
2	20.486	1442	4.335	100	**3.87**	**100**
3	22.255	579	3.995	40	**3.14**	**60**
4	23.966	661	3.713	46	**2.98**	**28**
5	24.662	839	3.61	58	**2.65**	**8**
6	28.345	650	3.149	45	**2.44**	**10**
7	29.621	964	3.016	67		
8	34.522	878	2.598	61		
9	45.542	632	1.992	44		
10	50.878	661	1.795	46		
11	57.693	704	1.598	49		

The XRD of the material (POA) was not comparable with standard [$(VO)_2P_2O_7$] in that the main intense peak was observed at 20.48° with d-space at 4.3. It can be assigned to α_I-$VOPO_4$, it is an intermediate before forming the final catalyst[5,11] and some other new peaks were also present with d-space 5.3, 3.6, 1.9 and 1.7. These are not related to $(VO)_2P_2O_7$ or $VOPO_4 \cdot 2H_2O$. Furthermore, peaks with small intensity are related to $(VO)_2P_2O_7$ with d-space at 3.9, 3.1, 3.0 and 2.59. According to the literature, $(VO)_2P_2O_7$ has more dominant peak at two theta 23 or 28 with d-space 3.87 or 3.1 respectively. It revealed that the DHOA was partially transformed to $(VO)_2P_2O_7$ consisting mainly of α_I-$VOPO_4$.[5,11]

The laser Raman spectrum of POA is shown in figure 4.16. SEM of POA is shown in figure 4.17.
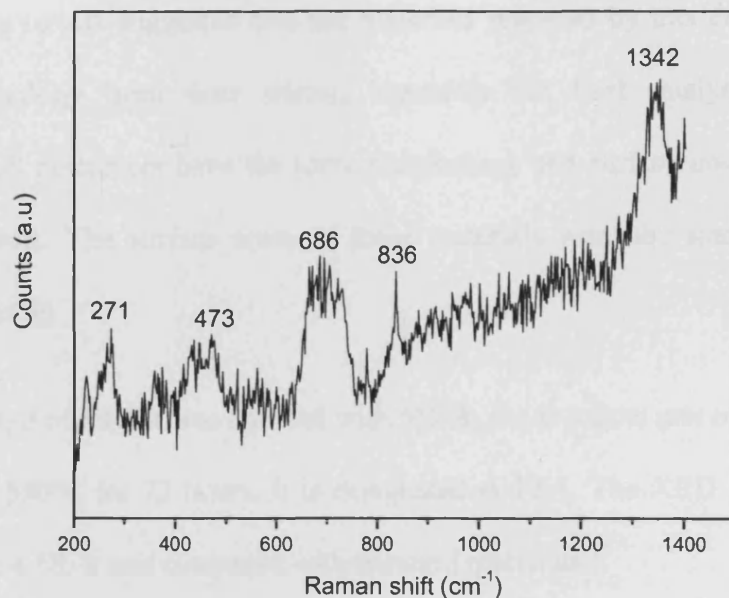
Fig. 4.16 The laser Raman spectrum of (POA)

The laser Raman peaks of POA (figure 4.16) cannot be assigned to $(VO)_2P_2O_7$. But two peaks (271 and 473 cm^{-1}) were related to $VOPO_4 \cdot 2H_2O$. It confirmed that DHOA was partially transformed to $(VO)_2P_2O_7$.
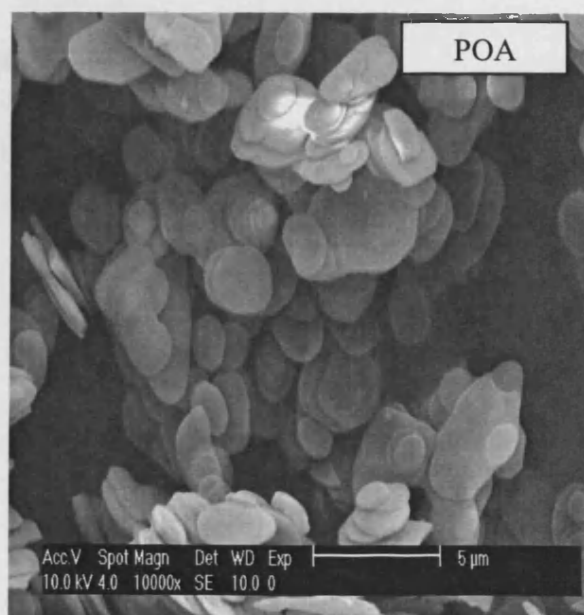

Fig. 4.17 The SEM of the materials prepared using direct route.

The SEM of POA (figure 4.17) was different from the starting materials (figure 4.3). The SEM of POA revealed that the plates were small when compared with the starting materials. These results suggested that the materials prepared by this direct route have a different morphology from their starting materials but final catalyst prepared from $VOHPO_4.0.5H_2O$ precursors have the same morphology and surface area of their starting catalyst precursors. The surface areas of these materials were the same as the starting materials (1-3 m^2/g)

The $VOPO_4·2H_2O$ of DHPA was reduced with 5% H_2/Ar at a flow rate of 50 ml/min and a temperature of 550°C for 72 hours. It is designated as PPA. The XRD pattern of PPA is shown in figure 4.18. It was compared with standard materials.[11]
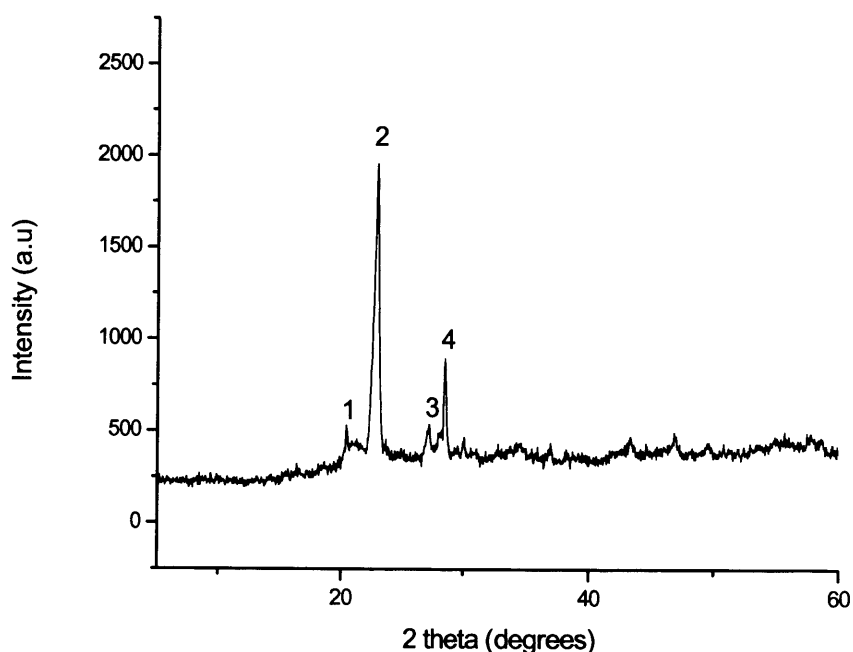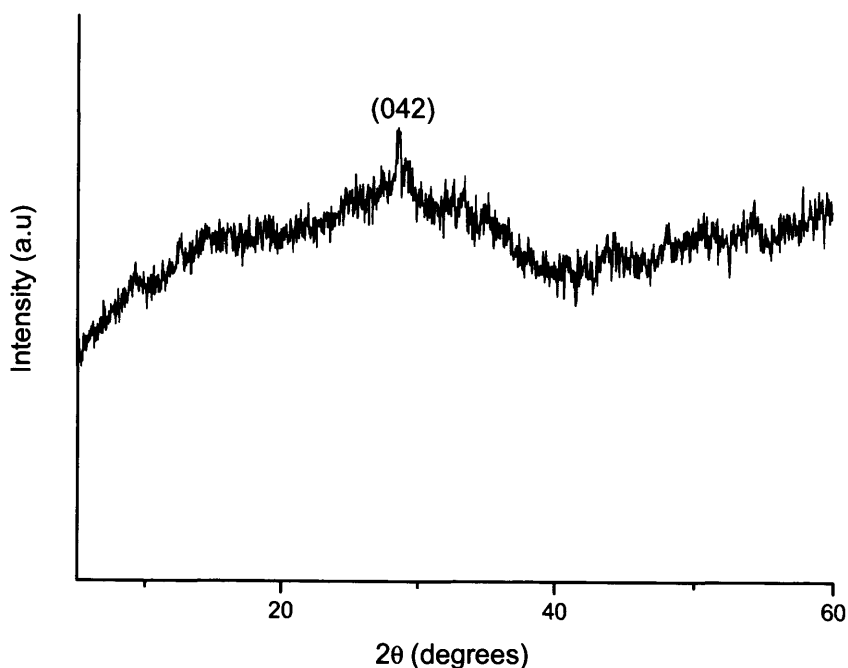

Fig. 4.18 The XRD pattern PPA.

Table 4.7 - The XRD reflections of PPA.

Entry	Angle	Counts	d-space	Rel I	Standard d-space	Rel I
1	20.428	530	4.347	27	4.79	10
2	22.98	1953	3.87	100	3.87	100
3	27.04	503	3.298	26	3.14	60
4	28.548	892	3.127	46	2.98	28
5					2.65	8
6					2.44	10

The XRD of PPA was not the same as with standard material [$(VO)_2P_2O_7$] (Table 4.7). However, most of these peaks were assigned to $(VO)_2P_2O_7$, with an intense peak observed at 22.98° with d-spacing of 3.87. Some other peaks were also present with d-space 4.3 and 3.2. These are not related to $(VO)_2P_2O_7$ or $VOPO_4 \cdot 2H_2O$. It can be assigned to α_I-$VOPO_4$. This indicated that materials were partially transformed to $(VO)_2P_2O_7$ phase.

The laser Raman spectrum and SEM of PPA are shown in figure 4.19 and 4.20 respectively. The laser Raman peak of PPA (figure 4.19) was observed at 918 cm^{-1} with a medium band. It was related to $(VO)_2P_2O_7$. The rest of these peaks were not related to $(VO)_2P_2O_7$. Some of these peaks are related to α_I-$VOPO_4$ (435 and 970 cm^{-1}) with a strong band. These results indicated that $VOPO_4 \cdot 2H_2O$ was not fully transformed to $(VO)_2P_2O_7$.
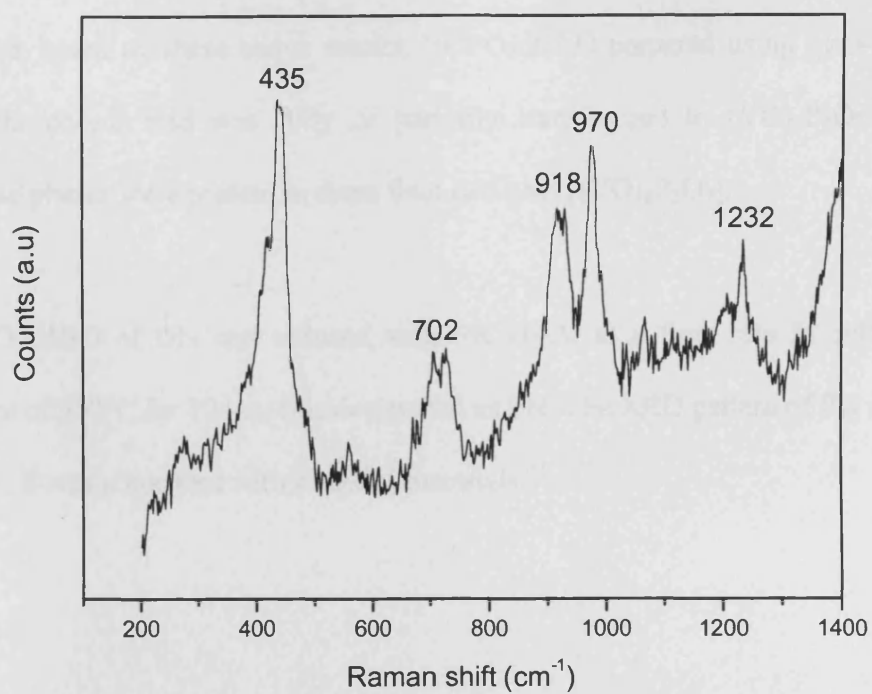
Fig. 4.19 The laser Raman spectrum of PPA.
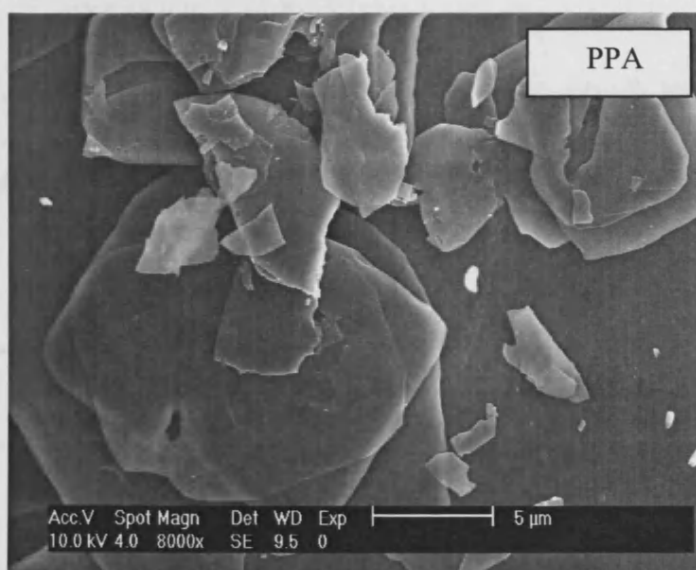
Fig. 4.20 The SEM of PPA.

The SEM of PPA (figure 4.20) indicated that materials were arranged with irregular fractured plates comparable to DHPA.

Furthermore, based on these above results, VOPO$_4$·2H$_2$O prepared using *pyro*-phosphoric

or *ortho*-phosphoric acid was fully or partially transformed to (VO)$_2$P$_2$O$_7$. However,

intermediate phases were present in these final catalysts [(VO)$_2$P$_2$O$_7$].

The VOPO$_4$·2H$_2$O of DN was reduced with 5% H$_2$/Ar at a flow rate 50 ml/min and a

temperature of 550°C for 72 hrs. It is designated as PN. The XRD pattern of PN is shown in

figure 4.21. It was compared with standard materials.[11]

Fig. 4.21 The XRD pattern of PN

Table 4.8 - The XRD reflections of PN.

Entry	Angle	Counts	Dspace	Rel I
1	28.432	941	3.139	100

The XRD of PN has only one peak with d-space at 3.1, it can be assigned to $(VO)_2P_2O_7$.

The crystallinity of these materials was lower as compared with POA and PPA. The surface

areas of these materials were the same as the surface area of DN (3 m^2/g)
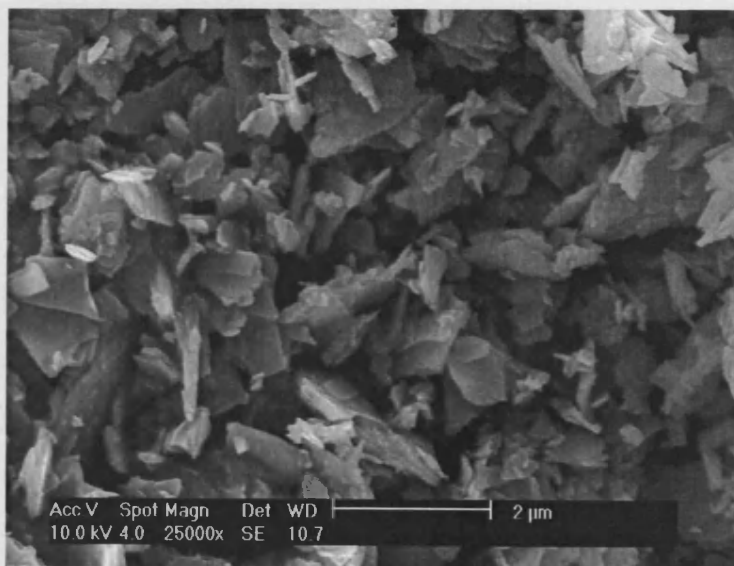
Fig. 4.22 The SEM of PN.

The morphology of PN was different from DN. PN was arranged with fractured irregular

plates.

4.4 Catalyst testing

The difference in the catalytic performance at 400°C of POA, PPA and PN catalysts prepared using new route is shown Table 4.9

Table 4.9 Catalyst performance of POA, PPA and PN for the oxidation of butane to maleic anhydride.[a]

Catalyst	Surface area (m^2/g) Catalyst	Conversion (%)	Selectivity (%) MA	CO	CO_2	Specific activity $(10^{-5}\ mol\ m^{-2}\ h^{-1})$
POA	3	56	13	9	78	3.10
PPA	3	23	24	27	49	2.36
PN	2	49	23	14	64	7.25

[a] Reaction conditions: 1.5% butane in air, 400°C, 1500 h^{-1}

The catalytic data for butane oxidation at 385°C of VPO and VPD catalysts prepared using isobutanol and a VPA catalyst has been reported by Hutchings et al.[12] The catalytic performance of standard VPA, VPO and VPD for butane oxidation is shown in Table 4.10

Table 4.10 Catalyst performance of VPA, VPO and VPD for the oxidation of butane to maleic anhydride.[12]

Catalyst	Surface area (m^2/g) Precursor	Catalyst	Conversion (%)	Selectivity (%) MA	CO	CO_2	Specific activity $(10^{-5}\ mol\ m^{-2}\ h^{-1})$
VPA	3	4	11	52	41	7	1.24
VPO	11	14	27	52	34	14	1.35
VPD	32	43	62	64	21	14	1.19

Based on the previous studies,[12] catalyst precursors with rosette structure (VPD) have much higher surface area than $VOHPO_4.0.5H_2O$ precursors prepared by the VPO or VPA route. The different catalysts have similar specific activities, so the surface area of the catalyst is the crucial factor in determining the final activity.

According to the present study (Table 4.9), the catalyst prepared via the direct route did not yield a higher activity for n-butane oxidation than the catalyst prepared from $VOHPO_4.0.5H_2O$ precursors.[12] Among these present results, catalysts POA, PPA and PN are less selective for maleic anhydride. However, specific activity of these catalysts is higher when compared to the conventional VPO and VPD catalyst.

4.5 Discussion

$VOPO_4\cdot2H_2O$ prepared using different phosphoric acids gave different XRD patterns. During the reaction the V_2O_5 dissolves in *pyro*-phosphoric acid very fast upon heating. In *ortho*-phosphoric acid, V_2O_5 only dissolves after the reaction has reached reflux conditions. As the V_2O_5 is not completely dissolved immediately in the *ortho*-phosphoric acid preparation, it is likely that there is a small amount of V_2O_5 impurity in the $VOPO_4\cdot2H_2O$ crystals. These impurities can cause defects in the structure, leading to a loss in crystallinity.[10]

Commonly, V_2O_5 dissolves in concentrated acid or alkali solution. In the standard preparation methods, initially V_2O_5 is not fully dissolved. Therefore, isobutanol was used as solvent to increase the solubility of V_2O_5 in the organic preparation route while water was

used as solvent in the standard preparation method. In the organic preparation route, the (001) and (200) reflections were considerably broadened when compared with standard $VOPO_4 \cdot 2H_2O$, it indicated that $VOPO_4 \cdot 2H_2O$ prepared using organic solvent method gave smaller crystallites as compared with standard methods.

The prepared catalyst materials via the new route were found to have d-spacing 3.8 as with the standard $(VO)_2P_2O_7$ but these materials are less selective for n-butane oxidation because α_I-$VOPO_4$ was formed with these catalyst materials. It has been reported that α_I-$VOPO_4$ is not selective for n-butane oxidation.[12] Therefore, the active site of $(VO)_2P_2O_7$ could be obstructed by other unselective sites. Hence, these materials exhibited less selectivity for butane to maleic anhydride oxidation. According to the previous results, the final catalyst prepared from $VOHPO_4 \cdot 0.5H_2O$ has the same surface area and morphology as the $VOHPO_4 \cdot 0.5H_2O$ precursors. The surface area of these precursors was high (Table 4.10). Therefore, these materials are more selective for butane oxidation (50% selectivity and 60% conversion). The final catalyst prepared from $VOPO_4 \cdot 2H_2O$ via the new route has a lower surface area, comparable to $VOPO_4 \cdot 2H_2O$. Therefore, these materials are less selective for butane oxidation. However, specific activity of the final catalyst prepared via direct route is better than the conventional catalyst due to the low surface area.

4.6 Conclusions

Same morphology of $VOPO_4 \cdot 2H_2O$ was obtained using different phosphoric acid while differing the size of the plate. The $VOPO_4 \cdot 2H_2O$ prepared using organic solvent gave smaller crystallite when compared with standard methods. $VOPO_4 \cdot 2H_2O$ was partially or fully transformed to $(VO)_2P_2O_7$ using this direct route. The selectivity of these final

catalysts for butane oxidation is less than the conventional catalysts (VPD and VPO). However, these materials exhibit a marked increases in specific activity compared to both the VPD and VPO.

4.7 References

(1)   F. Trifiro and F. Cavani, *Chemtech*, 1994, 18

(2)   Y. Zhang, R. P. A. Sneeden and J. C. Volta, *Catal. Today*, 1993, **16**, 39

(3)   J. Ziolkowski, E. bordes and P. Courtine, J. Catal, 1994, **16**, 126

(4)   J. R. Ebner, M. R. Thompson, *Catal. Today*, 1993, **16**, 51

(5)   E. Bordes, *Catal. Today*, 1987, **1**, 499

(6)   I. J. Ellison, G. J. Hutchings, M. T. Sananes , J. C. Volta and , J. *Chem. Soc., Chem. Comm,* 1994, 1093

(7)   C. J. Kiely, A. Burrows, S. Sajip, G. J. Hutchings, M. T. Sananés, A. Tuel and J. C. Volta, *J. Catal*, 1996, **162**, 31

(8)   G. J. Hutchings, A. Desmartin- Chomel, O. Oliver, J. C. Volta, *Nature*, 1994, **348**, 41

(9)   C. J. Kiely, A. Burrows, G.J. Hutchings, K. E. Bere, J. C. Volta, A. Tuel, M. Abon, *J. Chem. Soc, Faraday Discuss,* 1996, **105**, 103

(10)   J. W. Johnson, D. C. Johnston, A. J. Jacobson and J. F. Brody, *J. Am. Chem. Soc,* 1984, **106**, 8123

(11)   V .V. Guliants, J.B. Benziger, S. Sundaresan, I. E. Wachs, J. M. Jehng, J. E. Roberts, *Catal. Today*, 1996, **28**, 275

(12)   C. J. Kiely, A. Burrows, G.J. Hutchings, K.E. Bere, J.C. Volta, A. Tuel and M. Abon, *J. Chem. Soc., Faraday Disc.*, 1996, **105**, 103.

Chapter 5

Summary and Conclusions

5.1 Control the Morphology of Vanadium Phosphate Catalyst Precursors by Adding Alkane Solvents

Almost four decades have passed since Bergman and Frisch reported that VPO catalysts selectively oxidised n-butane to maleic anhydride. During this period, a number of synthesis approaches have been reported to control the morphology of vanadium phosphate catalyst precursors[1,2] because the catalytic properties of $(VO)_2P_2O_7$ are very dependent on its method of preparation and the best catalysts are prepared topotactically via $VOHPO_4.0.5H_2O$.[3-7]

(1) V_2O_5, phosphoric acid and alcohol were refluxed.

(2) $VOPO_4.2H_2O$ was reduced by various alcohols.

(3) $VOPO_4.2H_2O$ was intercalated, exfoliated and reduced by various alcohols and solvents.

However, addition of alkane solvents to this preparation has not been investigated in previous studies. Therefore, in this study the morphology of VPO catalyst precursors was controlled by adding alkane solvents into the VPD preparation method. $VOPO_4.2H_2O$ was reacted with alcohol and different amount of alkane solvents. Different morphology materials were obtained when adding of different amount of alkane solvent that B-0 materials shows the XRD pattern expected for a VPD sample with (220) as the main reflection. When small amounts of octane

are added into the preparation there is a decrease in the intensity of the (220) reflection and an increase in the intensity of the (001) reflection (B-25, B-50), indicating that there is a switch from a mixture of rosette and platelet type to platelet type morphology. This is shown in the SEM and TEM of the materials, with the B-25 sample showing both rosettes and platelets, whereas the sample B-50 consists only of thin platelets. The SEM shows that the platelets become thicker as more octane is added (B-100), leading to an increase in intensity of the side planes in the XRD pattern. As more octane is added to the preparation $VO(H_2PO_4)_2$ is formed instead of $VOHPO_4.0.5H_2O$ (B-400), which becomes more crystalline with increasing octane and the SEM and TEM show the characteristic of chunky morphology. When longer chain alkane solvents (hexadecane and dodecane) were used the same trend was observed. These changes occurred with smaller amounts of the longer chain alkane.

These phenomena can be explained in terms of the rate of reduction of V^{5+} to V^{4+}. The high concentration of the alcohol results in a fast reaction rate (between 1-butanol and $VOPO_4.2H_2O$) and a faster reduction rate (V^{5+} to V^{4+}). Therefore it can be suggested that $VOHPO_4.0.5H_2O$ is obtained whilst V^{4+}:P ratio kept at approximately 1:1 due to the fast reduction of V^{5+}

$VO(H_2PO_4)_2$ was obtained by using a low concentration of alcohol. The low concentration of alcohol results in a decreased reaction rate (between 1-butanol and $VOPO_4.2H_2O$) and a slower reduction rate (V^{5+} to V^{4+}). The slower reduction rate means that the V^{4+}:P ratio is 1:>>1 and the excess phosphorous favours the formation of $VO(H_2PO_4)_2$ which has a V:P ratio of 1:2.

Therefore, different materials will be obtained with respect to the different rate of material formation.

At high concentrations, $VOHPO_4.0.5H_2O$ with different morphology could be formed. It is thought that this is due to the rate changing the degree of supersaturation of the reaction product which has been shown previously to influence the morphology of precipitated materials.

Catalyst prepared from this route had comparable selectivity and conversion for n-butane oxidation. However, specific activity of these materials (B-100, 2.62×10^{-5} mol m^{-2} h^{-1}) is better than the conventional catalysts (VPO, 1.35×10^{-5} mol m^{-2} h^{-1}).

5.2 Catalyst Preparation Using New Preparation Route

To date researchers have been interested on the preparation of vanadyl pyrophosphate, $(VO)_2P_2O_7$ using $VOHPO_4{\cdot}0.5H_2O$ as the catalyst precursor. This has been activated in 1.5% butane in air at 400°C for 72 hours, therefore the preparation method of the hemihydrate, $(VOHPO_4{\cdot}0.5H_2O)$ is a crucial step to produce active catalyst. Here, the synthesis route is developed to prepare $(VO)_2P_2O_7$ using reducing environment. 50 ml/min, H_2/Ar was used for this transformation with different times (6, 24, 72 hours) at temperature 550°C. However, the results of the present work that material prepared using direct route is less selective for n-butane oxidation because α_I-$VOPO_4$ was formed with these catalyst materials. It has been reported that α_I-$VOPO_4$ is not selective for n-butane oxidation.[8] However, specific activity of these materials is higher than the conventional catalysts.

5.3 Future work

Different materials were obtained based on the relative reaction rates. Therefore, it is recommended that future work should involve detailed studies on the rates of the different material formation with mass balances for V and P. So, this information will be useful to design how to form high area rosettes which may lead to more active catalysts as activity directly correlates to conversion.

Furthermore, as it was shown that final catalyst obtained from $VOPO_4.2H_2O$ via direct route has less selective for n-butane oxidation because of its low surface area and morphology; it is recommended that the final catalyst should be prepared using different reducing agents and conditions.

Furthermore, a few unknown phases were obtained in this project. Additional characterisation techniques such as ^{31}P NMR and XPS should be carried out to assist with identification of these phases.

5.4 References

(1)   H. S. Horowitz, C. M. Blackstone, A. W. Sleight, G. Teufer, Appl. Catal, 1998, **38**, 193

(2)   J. W. Johnson, D. C. Johnston, A. J. Jacobson and J. F. Brody, *J. Am. Chem. Soc,* 1984, **106**, 8123

(3)   F. Javier Cabello Sanchez, R P. K. Wells, Colin Rhodes, J. K. Bartley, C. J. Kiely and G. J. Hutchings, *Phys. Chem. Chem. Phys.,* 2001, **3**, 4122

(4) V. V. Guliants, S. A. Holmes, J. B. Benziger, P. Heaney, D. Yates and I. E. Wachs, *J. Mol. Catal,* (2001), **172**, 265

(5) C. C. Torardi, Z. G. Li and H. S. Horowitz, *J. of. Solid State Chemistry,* 1995, **119**,349

(6) L. O. Mahony, T. Curtin, J. Henry, D. Zemlyanov, M. Mihov and B. K. Hodnet, *Applied Catalysis A: General,* 2005, **285**, 36

(7) S. Sajip, J. K. Bartley, A. Burrows, C. Rhodes, J. C. Volta, C. J. Kiely and G. J. Hutchings, *Phys. Chem. Chem. Phys.,* 2001, **3**, 2143

(8) C. J. Kiely, A. Burrows, G.J. Hutchings, K.E. Bere, J.C. Volta, A. Tuel and M. Abon, *J. Chem. Soc., Faraday Disc.,* 1996, **105**, 103.

6 Appendix

Characterisation of new materials prepared by reacting of VOPO4·2H₂O with 1-butanol and differing amount of heptane solvent

The XRD patterns of new materials prepared using different amount of (0, 25, 50, 100 ml) heptane solvents are shown in Appendix 3.1.
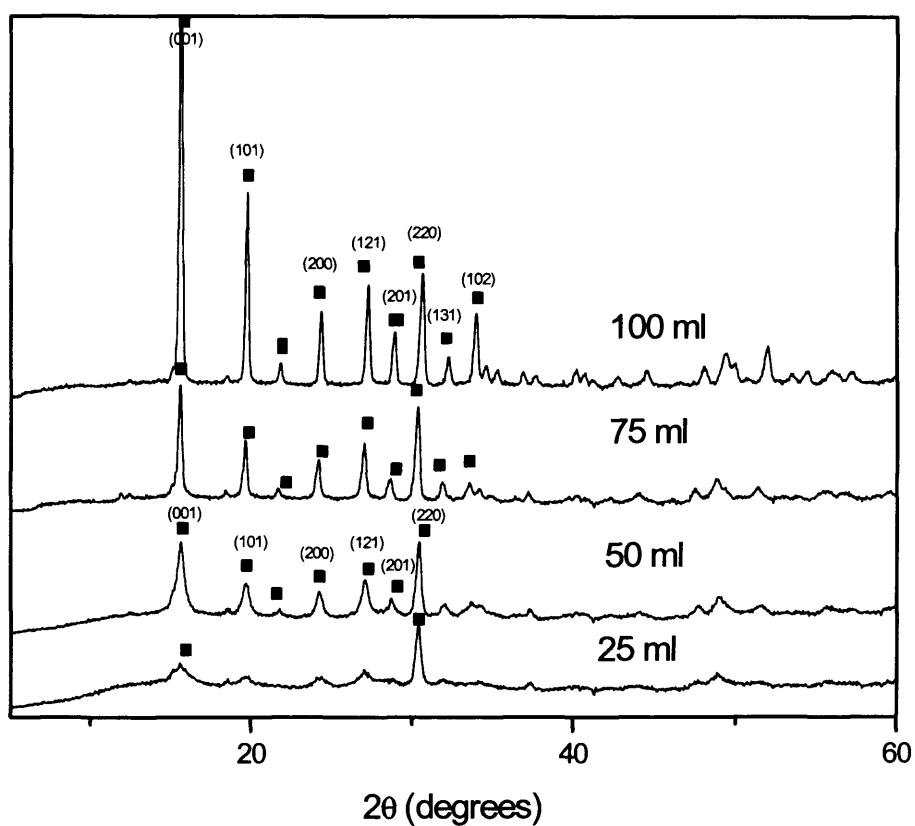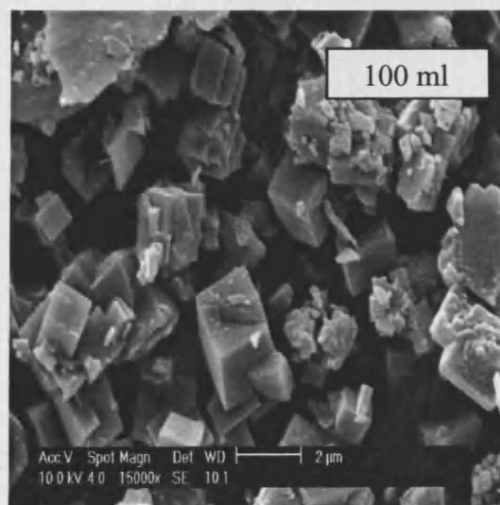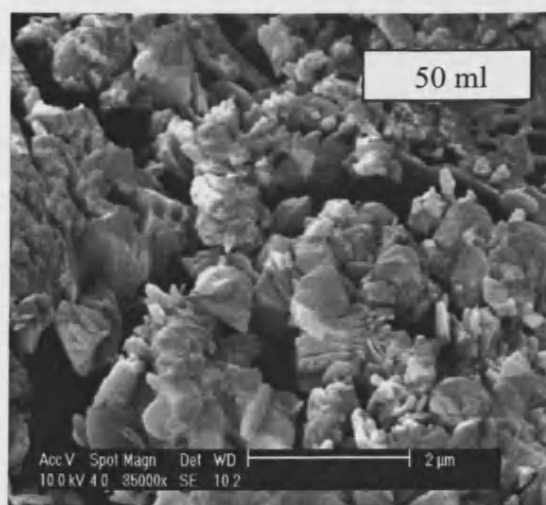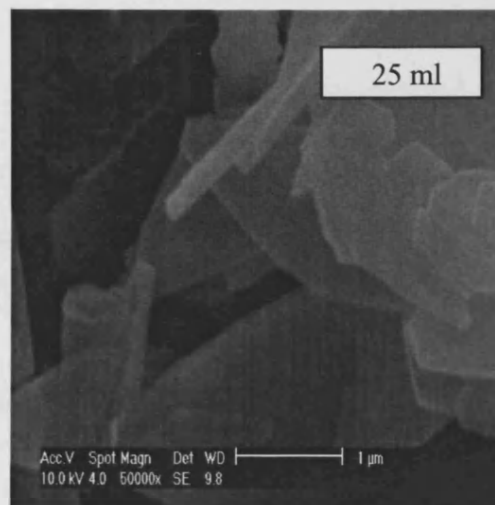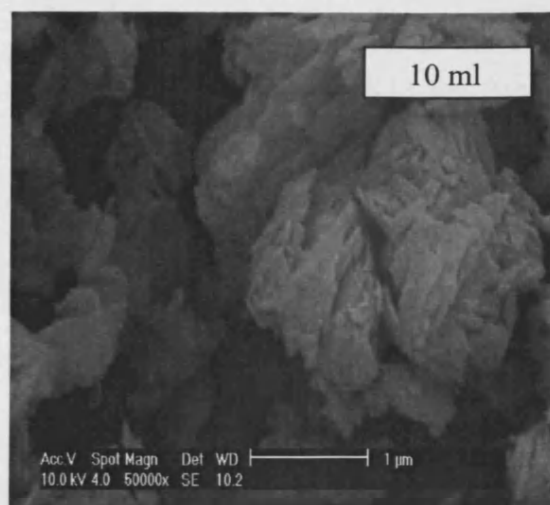

Appendix 3.1 Powder XRD patterns of the materials formed by reacting VOPO₄·2H₂O with 1-butanol and differing amounts of heptane. Key ■ = VOHPO₄.0.5H₂O

The laser Raman spectrum of new materials prepared using different amount of (0, 25, 50, 100 ml) heptane solvents are shown in Appendix 3.2.
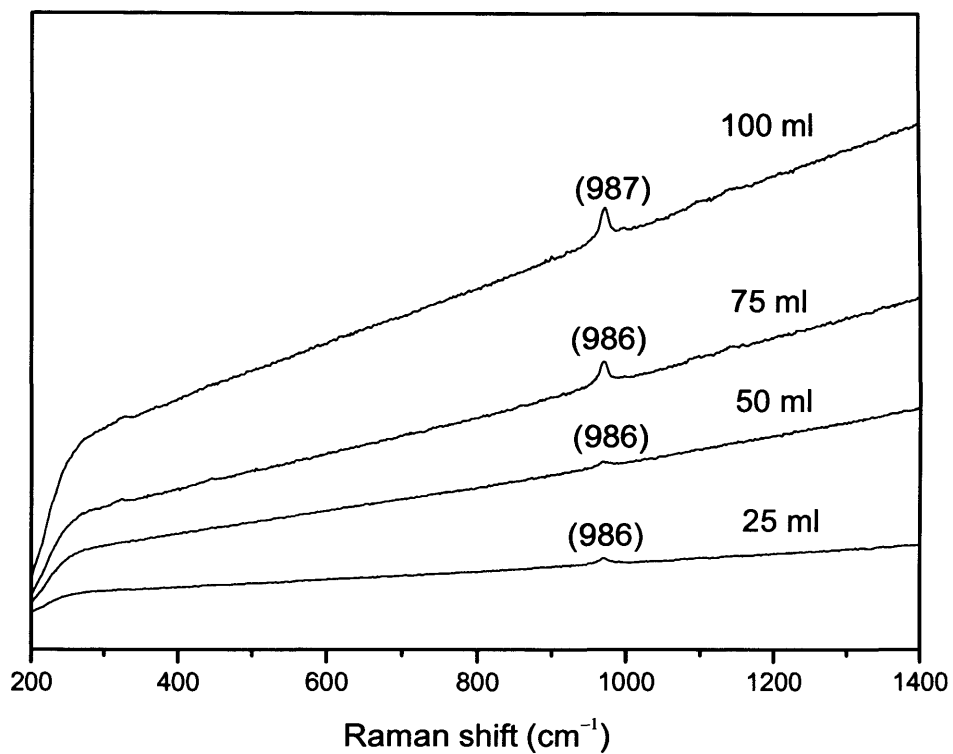
Appendix 3.2 Raman spectroscopy of the materials formed by reacting $VOPO_4 \cdot 2H_2O$ with 1-butanol and differing amounts of heptane.
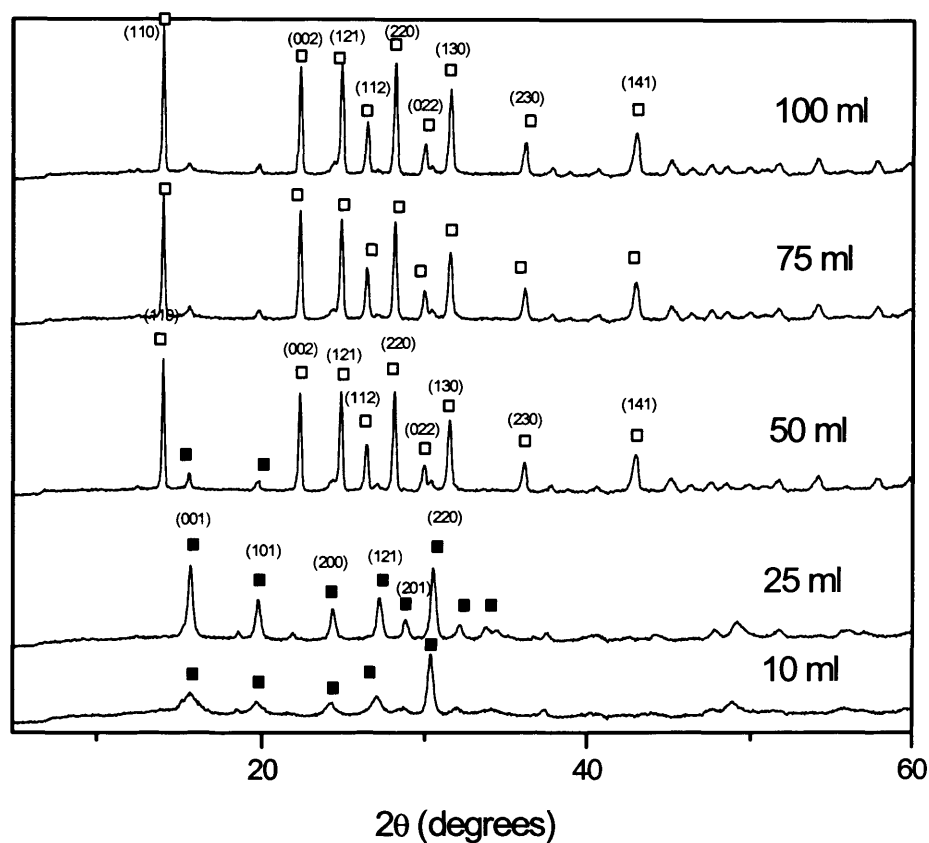
The SEM of new materials prepared using different amount of (0, 25, 50, 100 ml) heptane solvents are shown in Appendix 3.3.
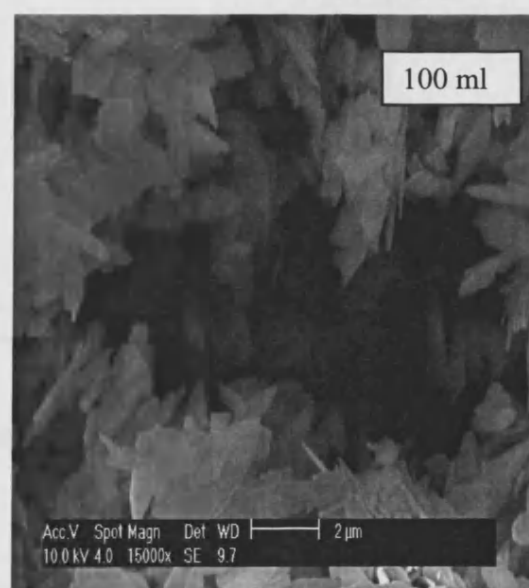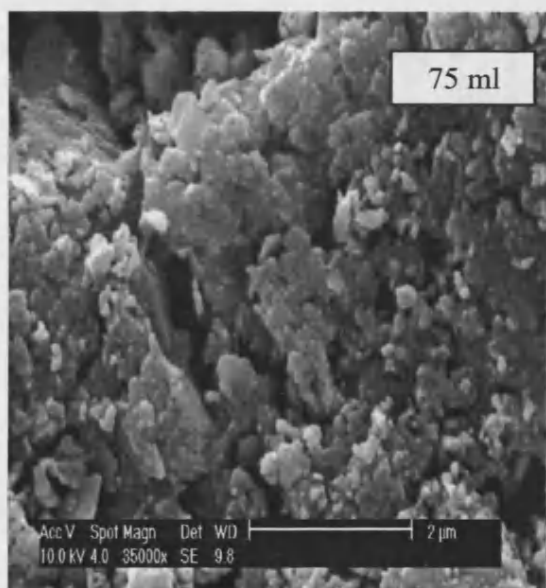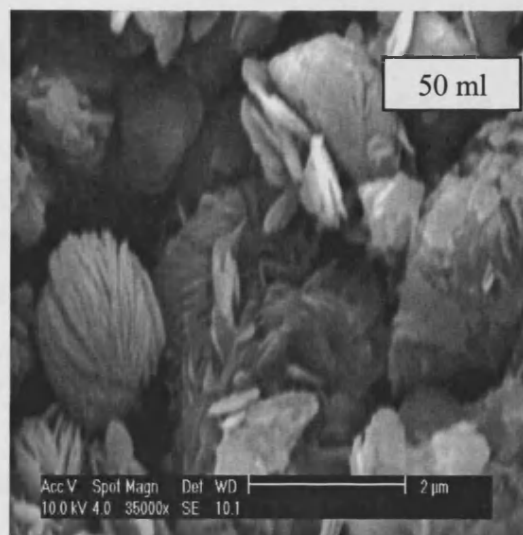
Appendix 3.3 - SEM of the materials formed by reacting $VOPO_4 \cdot 2H_2O$ with 1-butanol and differing amounts of heptane

Characterisation of new materials prepared by reacting of VOPO4·2H₂O with 1-butanol and differing amount of dodecane solvent

The XRD patterns of new materials prepared using different amount of (10, 25, 50, 100 ml) dodecane solvents are shown in Appendix 3.4.
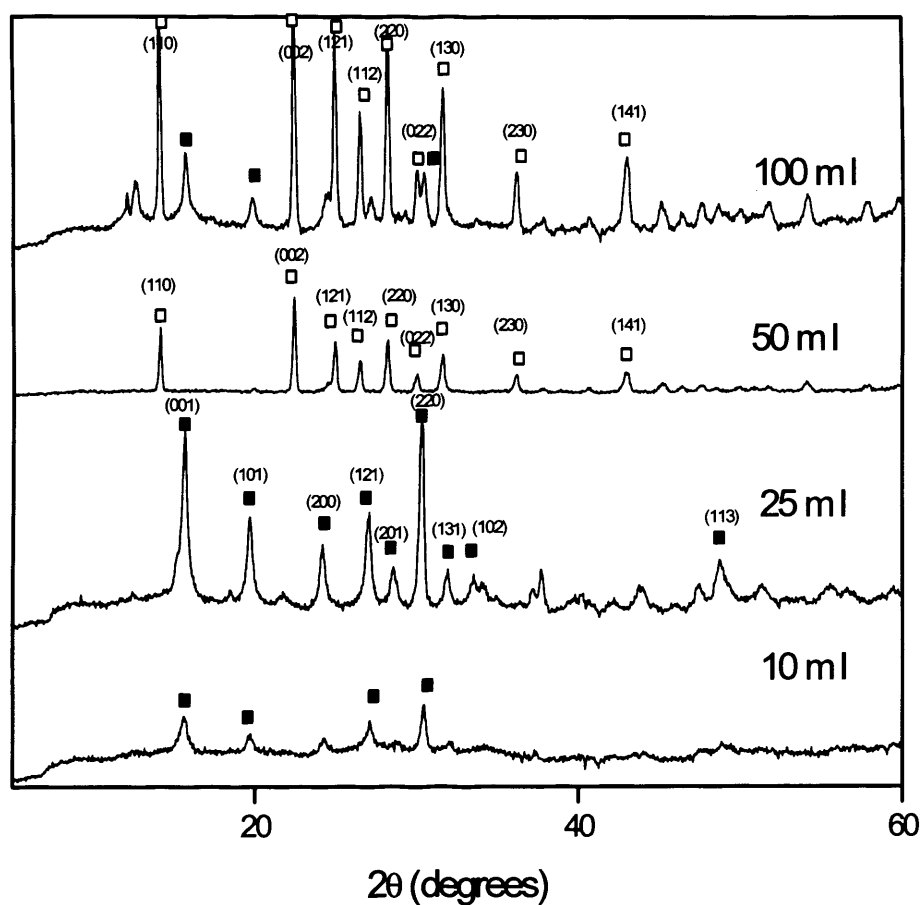
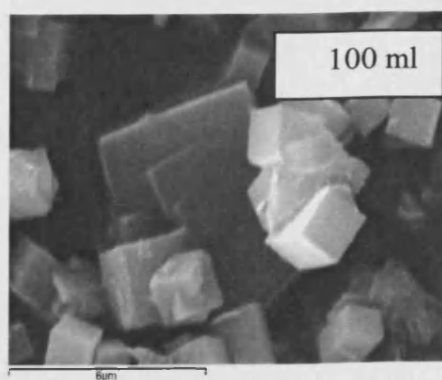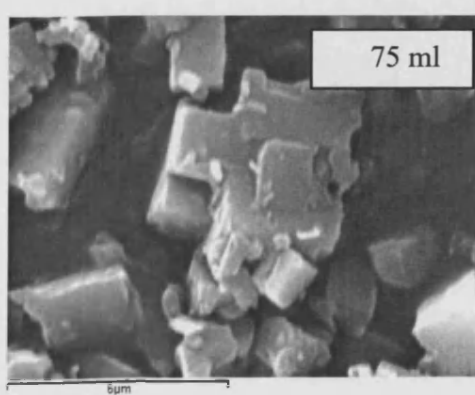Appendix 3.4 Powder XRD patterns of the materials formed by reacting $VOPO_4 \cdot 2H_2O$ with 1-butanol and differing amounts of dodecane. Key ■ = $VOHPO_4 \cdot 0.5H_2O$; □ = $VO(H_2PO_4)$

The laser Raman spectrum of new materials prepared using different amount of (10, 25, 50, 100 ml) dodecane solvents are shown in Appendix 3.5.
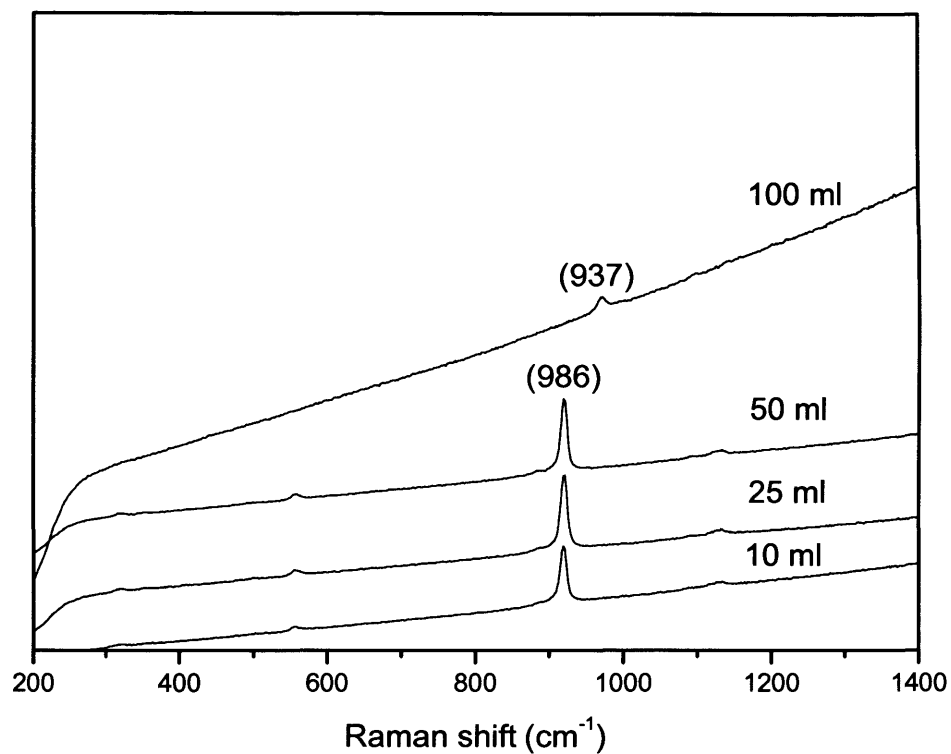
Appendix 3.5 Raman spectroscopy of the materials formed by reacting $VOPO_4 \cdot 2H_2O$ with 1-butanol and differing amounts of dodecane.

The SEM of new materials prepared using different amount of (10, 25, 50, 100 ml) dodecane solvents are shown in Appendix 3.6.

Appendix 3.6 SEM of the materials formed by reacting VOPO$_4$·2H$_2$O with 1-butanol and differing amounts of dodecane

Characterisation of new materials prepared by reacting of VOPO4·2H₂O with 1- butanol and differing amount of hexadecane solvent

The XRD patterns of new materials prepared using different amount of (10, 25, 50, 75, 100 ml) hexadecane solvents are shown in Appendix 3.7.
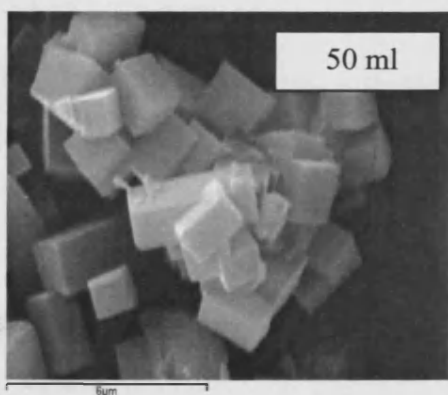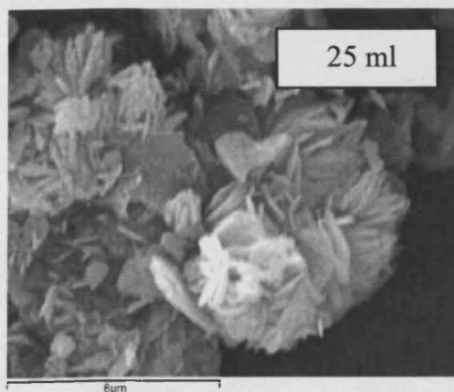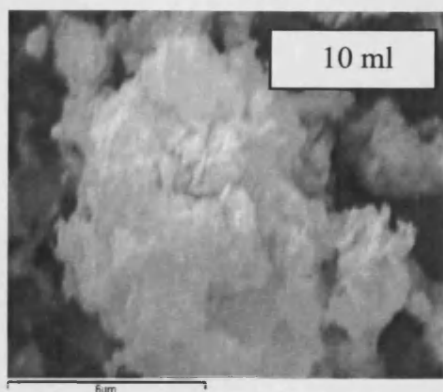

Appendix 3.7 Powder XRD patterns of the materials formed by reacting VOPO₄·2H₂O with 1-butanol and differing amounts of hexadecane. Key ■ = VOHPO₄·0.5H₂O; □ = VO(H₂PO₄)₂.

The laser Raman spectrum of new materials prepared using different amount of (10, 25,

50, 75, 100 ml) hexadecane solvents are shown in Appendix 3.8.
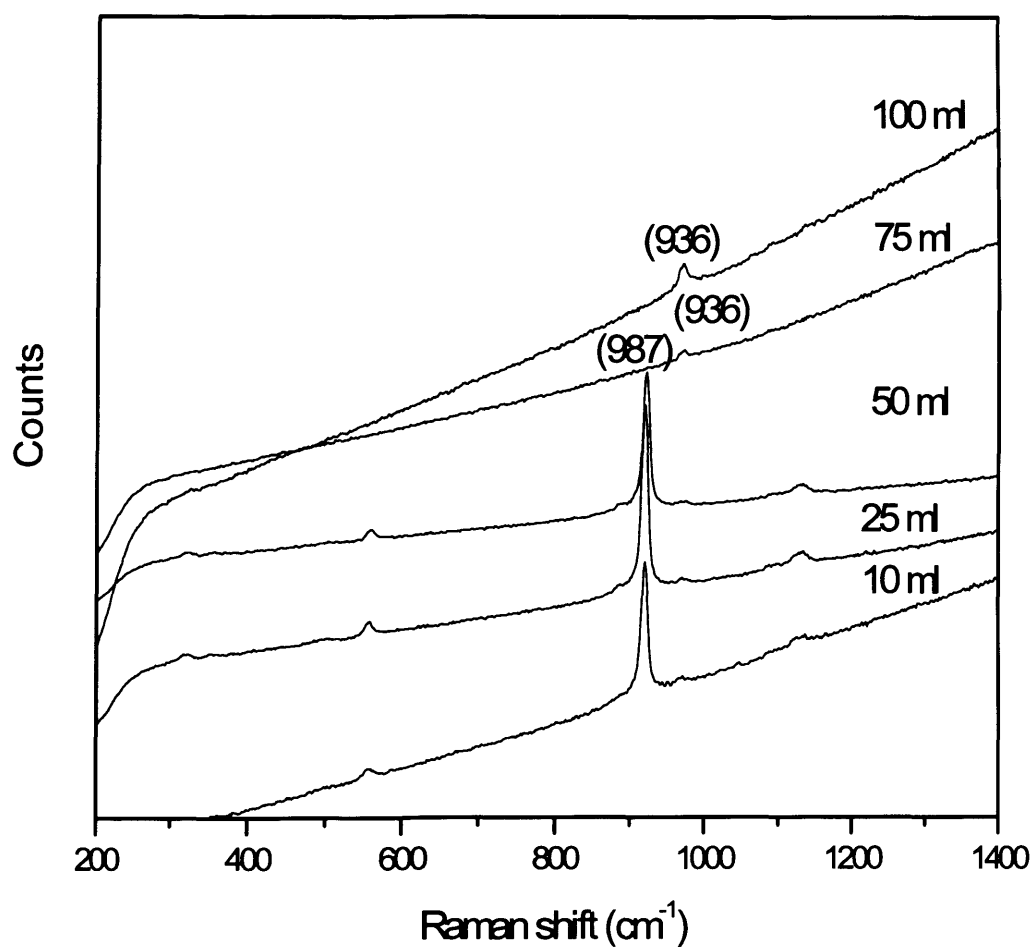
Appendix 3.8 Raman spectroscopy of the materials formed by reacting $VOPO_4 \cdot 2H_2O$

with 1-butanol and differing amounts of hexadecane.

The SEM of new materials prepared using different amount of (10, 25, 50, 75, 100 ml) hexadecane solvents are shown in Appendix 3.9.

Appendix 3.9 SEM of the materials formed by reacting $VOPO_4 \cdot 2H_2O$ with 1-butanol and differing amounts of hexadecane.